Mathematical Modelling of Glass Flow during a Pressing Operation

Carol Elizabeth Humphreys, B,Sc.

Thesis Presented for the

Degree of

Doctor of Philosophy

School of Materials

Department of Applied and Computational Mathematics

The University of Sheffield

October '91

Acknowledgements

I wish to thank my supervisors Dr. D.M. Burley and Professor M. Cable for their advice and encouragement. I am also indebted to S.E.R.C for financial support.

Summary

The aim of this project was to develop a mathematical model of the behaviour of molten glass during a pressing (hot forming) operation.

An outline of glass manufacturing is given in chapter 1, together with a discussion of the factors influencing the behaviour of the molten glass and the advantages of a mathematical model over direct experimentation.

Chapter 2 introduces the mathematical description of the glass behaviour. The molten glass was modelled by an imcompressible Newtonian liquid undergoing slow flow, it was also assumed that the finished article would be axisymmetric. The governing equations and boundary conditions were cast into the appropriate non-dimensional form.

Ways of solving the equations are considered in chapter 3. Initially the analytical solutions to simplified forms of the equations were considered, but these proved inadequate. Therefore numerical methods were used. An outline of the finite element method is given before details of its application to this problem.

The results of using the finite element method to solve the isothermal flow equations are presented in chapter 4. The model was able to cope with a range of parameters, though numerical instablities manifested themselves

at low Reynolds numbers.

Viscosity is strongly temperature dependent, hence the flow of heat in and around the glass is important. Temperature variations were introduced into the model in chapter 5. In molten glass a thin cooled 'skin' is formed, this physical phenomenon was exploited and an alternative boundary condition which encapsulated this effect was developed.

Results from the combined model are given in chapter 6. The predicted behaviour of the liquid is qualitatively correct.

Physical parameters for 'real life' glass forming operations are collated in chapter 7. Consideration is also given to the actual computing power needed to fully model a pressing operation.

Chapter 8 gives an overview of the work and includes suggestions for further study.

Contents

Chapter 1

Statement of Problem

1.1 Introduction

The aim of this project has been to use mathematical techniques to model a simple glass pressing operation. In this chapter, the advantages of a mathematical model are considered with a basic outline of the glass manufacturing process. Subsequent chapters deal with the governing equations and their approximate solution.

The manufacture of glass is a well established industry, with a long history, Douglas and Frank outline its development in their book[15]. In common with most industries, competitiveness is all important especially as new materials enter the marketplace. The modern large scale commercial

production of glass is an almost completely automated procedure, from the raw materials through to the finished article. Obviously, it is desirable to keep the wastage to a minimum as any glass failing the quality control test has to be recycled increasing production costs. Some systematic consideration as to the best range of forming parameters is useful to produce an article with the desired properties in the most efficient manner.

1.2 Glass Manufacture

1.2.1 Introduction

In many of the most modern factories there is a virtually continuous flow of glass from furnace to formation. The molten glass is formed by heating together the raw materials, it is then processed into the finished product.

1.2.2 Glass Formation

Most commerical glass is approximately 70% silica (SiO_2), the remainder is usually made up of a mixture of soda (Na_2O), lime (CaO), alumina (Al_2O_3), potash (K_2O), magnesia (MgO), lead oxide (PbO) boric oxide (B_2O_3) and small quantities of other oxides. Small changes in the chemical composition of the glass are reflected, sometimes disproportionately, by changes in the

physical properties. Therefore varying the ingredients gives some measure of control over the behaviour of the glass.

The raw materials are mixed with recycled glass known as cullet, which can make up as much as 75% of the batch, and introduced into the melting end of the furnace. They melt and react together. The molten glass is then heated to temperatures of approximately $1550°C$, to ensure good mixing and aid the release of trapped gas bubbles. The molten glass flows to the working end of the furnace, where it begins to cool, it is then distributed to the various forming machines.

1.2.3 Article Manufacture

The molten glass can be formed into a multitude of products, these can be divided as to their method of manufacture, this is shown in figure (1.2.1).

Continuous Formation

Continuous formation is where there is a continuous stream of glass which is manipulated to form an uninterrupted flow of finished product.

FLAT GLASS The production of flat glass is one of the largest sections of the glass industry. Originally flat glass was cast. Casting, first introduced in the 1680's, is now virtually obsolete, having been replaced by the float

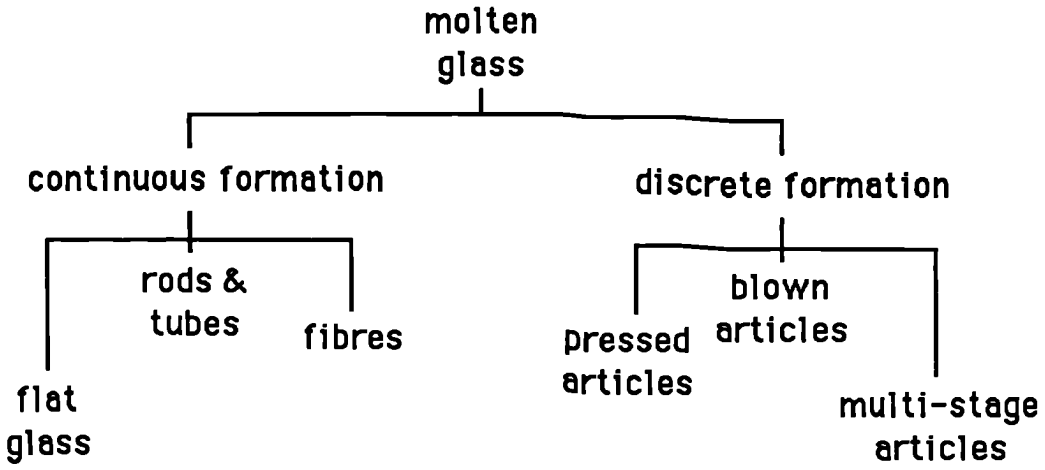

Figure 1.2.1

process. Another method used to produce flat glass is sheet drawing, introduced in the 1920's. This has been superseded by the float process in all but the most specialised of areas[1].

SHEET DRAWING A sheet of glass is pulled up from a bath of molten material. The sheet being pulled is unstable with a tendency to 'neck' and form a circular cross-section. This problem is controlled by cooling the sheet rapidly.

FLOAT PROCESS This process, developed in the 1950's, produces a continuous stream of high quality flat glass. A broad sheet of molten glass is

[1]e.g producing wire reinforced glass

floated on molten tin. It is cooled until almost rigid and then lifted off.

ROD AND TUBE DRAWING To make tubes and rods glass is drawn from a circular mandrel. For tubing the mandrel has a central hole through which air is blown.

FIBRE DRAWING Fibres have many uses[2] and their method of production differs depending on the length, thickness and quality desired. All the production methods consist of a thin jet of molten glass being ejected from a nozzle, how that jet is treated determines the properties of the fibre produced.

Discrete Formation

Discrete methods are where the molten glass is formed into separate 'lumps', called gobs, which are then processed. Glass flows from the furnace to the machines through shallow channels called forehearths. Whilst travelling it is conditioned so as to arrive at the desired viscosity; Carling[9] and Whiteman[44] have both considered mathematically modelling parts of this process. At the end of the forehearth there is a feeder mechanism, which forms the gobs. These gobs then fall under gravity into moulds in which

[2]From optical communications to low density insulation

the articles are formed. It is forced to take the shape of the mould by pressure supplied either by compressed air or by a metal plunger. Often, to achieve the desired shape more than one operation is used. For example, the production of bottles is a two stage process. First a parison is formed by pressing or blowing the gob. The parison is then transferred to another mould where it is blown into its final shape.

Once the article is formed there is the added complication that it must be 'set enough' so then when it is removed from the mould it does not deform or even collapse under gravity. A more detailed review of glass manufacturing proceedures can be found in a book such as [32] by Maloney.

The modelling of a blowing operation was considered by Graham, a previous student in the department [24]. Therefore, this project concentrates on pressed articles.

1.3 Glass Pressing

The glass pressing (or hot forming) process is restrictive as to the shapes it can produce but it also has some advantages. The most obvious is that it allows the shape of both surfaces to be controlled, unlike blowing into a mould which controls the outside shape but not the thickness or the inside

surface.

The pressing situation under consideration is shown schematically in figure (1.3.1). The gob of molten glass falls under gravity into a metal mould, it deforms on hitting the mould and is allowed to settle. It is then forced into its final shape by the application of a metal plunger.

1.4 Influences on the Glass Flow

In a pressing operation the processes involved are fluid and heat flow. The molten glass is a Newtonian viscous fluid, its flow being driven by gravity and the action of the plunger. The mould and plunger are not normally at the same temperature as the gob so there will be heat flow between the glass and its immediate surrounding as well as redistribution of heat within the glass. The temperature variations within the molten glass will affect its flow because the viscosity is strongly temperature dependent.

As noted previously, viscosity is dependent on composition, it is also strongly dependent on the temperature. Figure (1.4.1) taken from the book by Doremus[14] shows the viscosity temperature relationship for several commerical silicate glasses. An empirical formula can been fitted to the data.

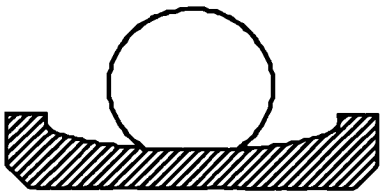

gob falls into metal mould

allowed to settle

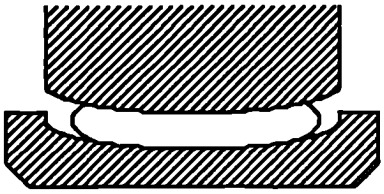

forced into final shape by plunger

Figure 1.3.1 Glass pressing

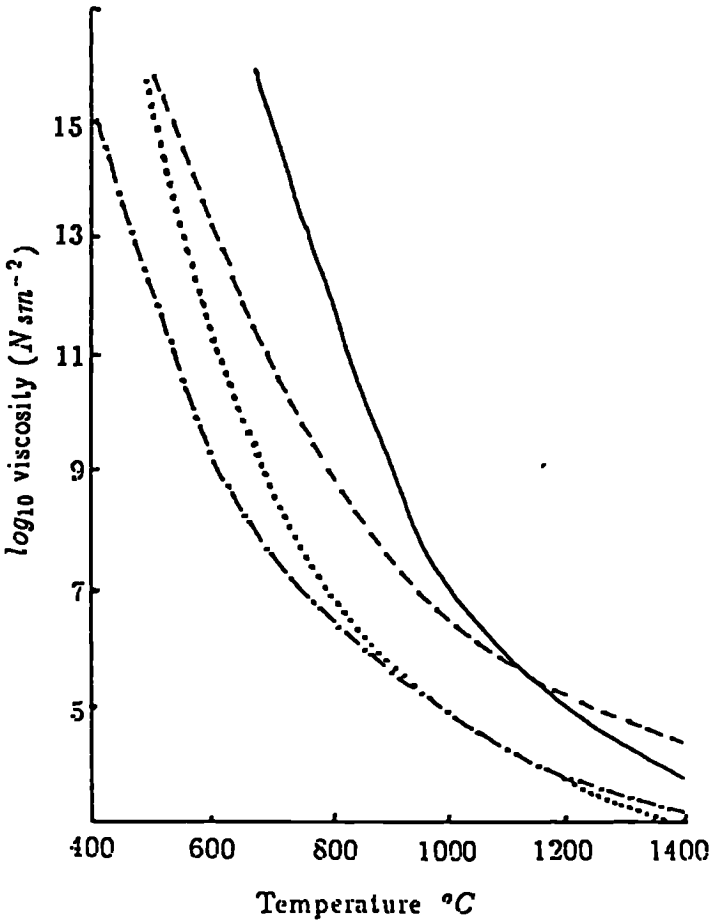

Figure 1.4.1 Temperature-Viscosity Relationships

The Fulcher equation

$$log_{10}\mu = A + \frac{B}{T - T_0} \tag{1.1}$$

The Fulcher equation (1.1), named after one of its proposers[20], contains three constants which allow it to be fitted to each particular curve. These constants can be found by careful experimentation or by using formulae that relate the constants to the concentrations of each particular oxide present in the glass.

Each glass operation has its ideal range of viscosities, some typical values are given below.

Operation	$\log_{10} \mu$ Nsm^{-2}
Melting	1.5 to 2.5
Forming gobs for containers	3.6 to 4.2
Pressing	4.0 to 4.4
Deform under gravity	11.3
Annealing	12.0 to 14.0

Hence, the temperature of the glass has to be accurately controlled to obtain the desired viscosity. This means that the heat flow in and around the glass is very important.

Within the glass, heat is transfered by conduction and radiation. Inter-

nal radiation is difficult to quantify as each small portion of glass absorbs and re-admits energy. The amount of internal radiation depends on many factors, such as the shape of the article, its opaqueness[3] or temperature. The overall effect of the internal radiation can be incorporated by using an effective conductivity which allows for the 'extra' transport of heat due to the internal radiation. Figure (1.4.2) shows typical effective thermal conductivities of colourless flint and green container glasses compared with the true conductivity over a range of temperatures, after Genzel[23].

Further discussion of the effect of internal radiation can be found in the two papers by Gardon[21] [22].

Heat can also be lost to (or gained from) the surroundings. Heat transfer from the glass surfaces is by conduction and/or radiation. It depends on the situation of each particular surface. For example metal is completely opaque, so no heat is lost from the glass to a metal mould by radiation.

In a pressing operation the temperature of the glass metal interface is important. The metal mould is initially cooler than the the glass so the glass is cooled. If there were perfect contact between the glass and iron mould

[3]slightly altering the colour of the glass can alter is adsorption spectrum

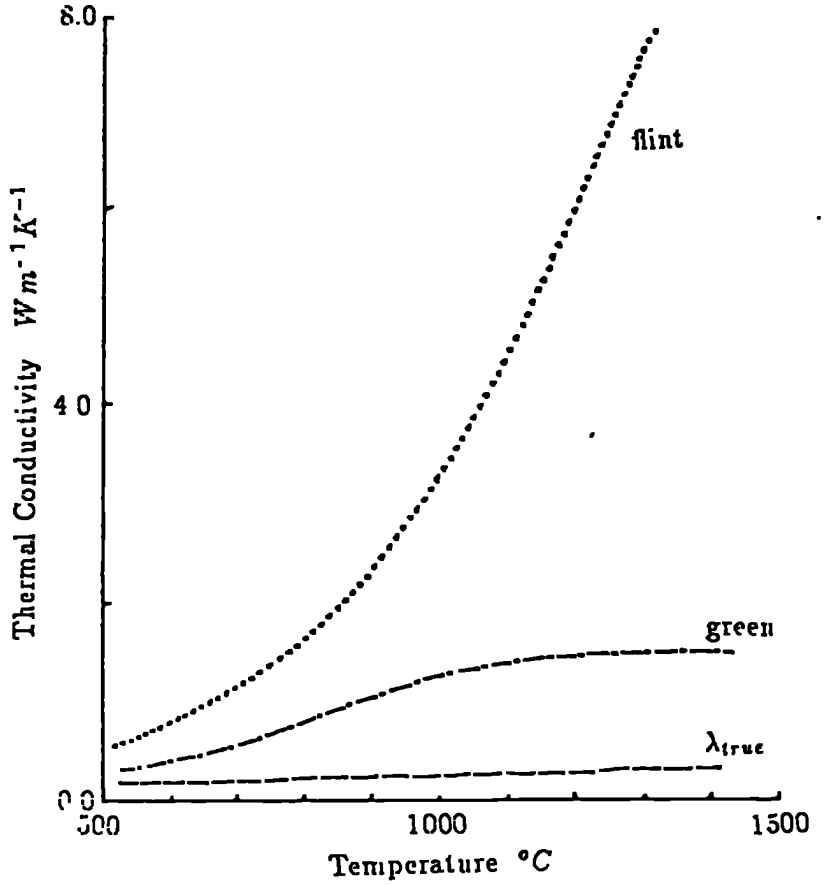

Figure 1.4.2 Thermal Conductivities

the the non-dimensional interfacial temperature, T*, would be given by

$$T^* = \sqrt{\left(\frac{\lambda_a \rho_a c_a}{\lambda_b \rho_b c_b}\right)}$$

where λ, ρ and c are the thermal conductivity, density and specific heat capacity respectively of the glass(a) and iron(b). For a typical glass at 1100^oC and mould at 550^oC, this interfacial temperature is $\approx 590^oC$. However, the contact between the glass and mould is not perfect. When the glass first touches the mould a good contact is formed and the glass is rapidly cooled. The cooling causes the glass to shrink away from the mould decreasing the contact, hence the glass/mould heat transfer coefficient is strongly time dependent. This process is vital, because it is this shrinkage which stops the glass sticking to the metal.

The complexities of the heat transfer make accurately controlling the glass viscosity difficult. If the glass is too hot the mould is heated too much and the glass sticks to it, if the glass is too cold it means that large stresses are needed to force it into the desired shape, these large stresses can lead to cracking.

1.5 Why a Mathematical Model?

Interrupting the continuous forming cycle to conduct a series of experiments would be disruptive, also factory floor experimentation is not always a viable option due to the very hostile environment. Large rates of change of temperature are envisaged so any instrumentation would need to be both sensitive and robust, also there is the added complication of the glass being inaccessible through much of the forming cycle. Rawson [38] considers some of these problems.

One option would be to conduct a series of small scale experiments in a laboratory. This method is likely to be hampered by the same sort of problems with measurements, as well as being relatively labour intensive.

The advantages of a mathematical model are that, once it has been verified by comparison to real life situations, it can deal with a large variety of situations and parameters with the minimum of further effort and there is no problem recovering variables for any section of the glass at any time during the pressing operation.

It must always be borne in mind that whichever of these methods is used there still needs to be some data input from the factory floor.

The appropriate mathematical description of this situation is developed

in the next chapter.

It is envisaged that an efficient computer model could be integrated into a modern industrial setting. Three of the possible uses are

- to assess the efficiency of a well established pressing operation with a view to saving time or energy, both commercially important resources.
- to help with the diagnosis of a problem with a pressing operation where a high proportion of the finished articles are flawed, and suggest possible cures.
- to help with the planning of new pressing operations.

It is not proposed that a computer model could ever replace a skilled production engineer, but would be a useful interactive tool.

Chapter 2

Mathematical Description of the Problem

2.1 Introduction

In this chapter, the partial differential equations that describe the temperature field and flow of a liquid are presented. These equations have been widely used, hence, no details of their derivation are included. Standard derivations are available in various texts, for example Batchelor[3] or Bird et al.[5].

A non-dimensionalization scheme and change of co-ordinates are intro-

duced to arrive at the form of the governing equations most suitable to this particular situation.

2.2 Flow Equations

In the derivation of the Navier-Stokes equations (2.1) the continuum hypothesis is assumed. This is the assumption that the physical properties associated with the fluid are distributed uniformly. This is not true on the microscopic level, but on the macroscopic scale it is valid for a well heated and mixed glass.

The assumption that the molten glass is incompressible is made, although this is not strictly true it introduces only slight errors over the practical range. This constraint is imposed via the continuity equation (2.2), which is a special case of mass conservation.

Navier-Stokes equations[1]

$$\rho\left(\frac{\partial u_i}{\partial t} + \mathbf{u}.\nabla u_i\right) = \frac{\partial \tau_{ij}}{\partial x_j} + f_i \tag{2.1}$$

Continuity equation

$$\frac{\partial u_i}{\partial x_i} = 0 \tag{2.2}$$

[1] the standard summing over a repeated suffix is used

These equations are expressed in cartesian co-ordinates $\mathbf{x} = (x_1, x_2, x_3)$ with $\mathbf{u} = (u_1, u_2, u_3)$ the corresponding velocities, ρ the density which is taken to be constant, τ the stress tenser and $\mathbf{F} = (f_1, f_2, f_3)$ the external body force.

The form of the stress tenser depends on assumptions made about the fluid. Here it is assumed that the fluid is Newtonian, albeit with a highly temperature dependent viscosity, i.e. that at any given temperature there is a linear relationship between stress and velocity gradient. There are many non-Newtonian liquids[2], but there is no evidence that slow moving molten glass is among them, further discussion of this point can be found in the chapter on viscosity in the book by Doremus[14].

The appropriate form of the stress tenser for an incompressible Newtonian fluid is

$$\tau_{ij} = -p\delta_{ij} + \mu\left(\frac{\partial u_i}{\partial x_j} + \frac{\partial u_j}{\partial x_i}\right) \tag{2.3}$$

where p is the pressure, μ is the viscosity and δ_{ij} the kronecker delta[3].

Solving the fully three dimensional equations is fiendishly complex, it is therefore convenient to assumed that the pressed article is axi-symmetric, this enables the use of ring elements, (see chapter 3) and gives a three-dimensional model whilst retaining the simplicity of a two-dimensional one.

[2] e.g. many suspensions, emulsions and liquids with long molecular chains
[3] $\delta_{ij} = 1$ if $i = j$ else $\delta_{ij} = 0$

Practically, this is not an unreasonable assumption as many pressed articles are roughly axi-symmetric.

To exploit the simplifications made by the axi-symmetric assumption the Navier-Stokes and continuity equations have to be transformed into cylindrical polar co-ordinates, (r, θ, z), the axi-symmetric nature is expressed by taking the azimuthal velocity as zero and the changes in that direction as zero i.e. $\frac{\partial}{\partial \theta} = 0$. The transformed equations are

$$\rho\left(\frac{\partial u}{\partial t} + u\frac{\partial u}{\partial r} + w\frac{\partial u}{\partial z}\right) = \frac{1}{r}\frac{\partial \tau_{rr}}{\partial r} - \frac{\tau_{\theta\theta}}{r} + \frac{\partial \tau_{rz}}{\partial z} + f_r \qquad (2.4)$$

$$\rho\left(\frac{\partial w}{\partial t} + u\frac{\partial w}{\partial r} + w\frac{\partial w}{\partial z}\right) = \frac{1}{r}\frac{\partial \tau_{rz}}{\partial r} + \frac{\partial \tau_{zz}}{\partial z} + f_z \qquad (2.5)$$

where u, w are the velocities in the r, z directions. $(f_r, 0, f_z)$ is the body force. The case of gravity acting downwards, i.e. the minus z direction, is expressed by

$$f_z = -\rho g, f_r = 0$$

where g is the acceleration due to gravity taken as $9.8ms^{-2}$. The stresses are also expressed in cylindrical polars, the non-zero stress components are

$$\begin{aligned} \tau_{rr} &= -p + 2\mu\frac{\partial u}{\partial r} \\ \tau_{rz} &= \mu\left(\frac{\partial u}{\partial z} + \frac{\partial w}{\partial r}\right) \\ \tau_{\theta\theta} &= -p + 2\mu\frac{u}{r} \end{aligned}$$

$$\begin{aligned} \tau_{zr} &= \mu\left(\frac{\partial u}{\partial z}+\frac{\partial w}{\partial r}\right) \\ \tau_{zz} &= -p+2\mu\frac{\partial w}{\partial z} \end{aligned} \tag{2.6}$$

The transformed continuity equation is

$$\frac{\partial u}{\partial r}+\frac{u}{r}+\frac{\partial w}{\partial z}=0 \tag{2.7}$$

2.2.1 Non-Dimensionalization

Here the variables are scaled to group the physical parameters into non-dimensional groups. This is a technique with several advantages, it minimizes the parameters involved, enables the relative importance of each of the terms to be assessed and allows for the direct comparison of different situations via the characteristic non-dimensional numbers[4].

The new variables introduced are u^*, x^*, t^*, p^* given by

$$u^*=\frac{u}{U_0}, x^*=\frac{x}{L}, t^*=\frac{tU_0}{L}, p^*=\frac{p}{\rho U_0^2} \tag{2.8}$$

where U_0, L are a reference velocity and length respectively. These can be substituted into (2.4) and (2.5), noting that U_0, L, ρ are constants so as can be removed from the differentials, for example

$$\frac{\partial u}{\partial t}=\frac{\partial(U_0u^*)}{\partial(\frac{L}{U_0}t^*)}=\frac{U_0^2}{L}\frac{\partial u^*}{\partial t^*}$$

[4]sometimes called dimensionless numbers

The physical parameters can then be grouped together giving

$$\frac{\partial u^*}{\partial t^*} + u^*\frac{\partial u^*}{\partial r^*} + w^*\frac{\partial u^*}{\partial z^*} = \frac{1}{r^*}\frac{\partial r^*\tau^*_{rr}}{\partial r^*} - \frac{\tau^*_{\theta\theta}}{r^*} + \frac{\partial \tau^*_{rz}}{\partial z^*} \quad (2.9)$$

$$\frac{\partial w^*}{\partial t^*} + u^*\frac{\partial w^*}{\partial r^*} + w^*\frac{\partial w^*}{\partial z^*} = \frac{1}{r^*}\frac{\partial r^*\tau^*_{rz}}{\partial r^*} + \frac{\partial \tau^*_{zz}}{\partial z^*} + \frac{1}{Fr} \quad (2.10)$$

Where the non-dimensional stress components are given by

$$\begin{aligned}
\tau^*_{rr} &= -p^* + 2\frac{1}{Re}\frac{\partial u^*}{\partial r^*} \\
\tau^*_{rz} &= \frac{1}{Re}\left(\frac{\partial u^*}{\partial z^*} + \frac{\partial w^*}{\partial r^*}\right) \\
\tau^*_{\theta\theta} &= -p^* + 2\frac{1}{Re}\frac{u^*}{r^*} \\
\tau^*_{zr} &= \frac{1}{Re}\left(\frac{\partial u^*}{\partial z^*} + \frac{\partial w^*}{\partial r^*}\right) \\
\tau^*_{zz} &= -p^* + 2\frac{1}{Re}\frac{\partial w^*}{\partial z^*}
\end{aligned} \quad (2.11)$$

The non-dimensional groups introduced are the Reynolds and Froude numbers, Re & Fr, given by

$$\begin{aligned}
Re &= \frac{\rho U_0 L}{\mu} \\
Fr &= \frac{U_0^2}{gL}
\end{aligned} \quad (2.12)$$

The Reynolds number represents the ratio of the inertia forces to the viscous forces. When the Reynolds number is small viscous forces dominate. The inertia forces are most important when the Reynolds number is large, these flows tend to be turbulent. In the mid-range, $1 < Re < 100$, neither type

of forces dominates. The flows considered here are characterized by a small Reynolds number, this is mostly due to the high viscosities of molten glass. This type of flow regime, where the viscous forces dominate, is commonly called slow or creeping, and the non-linear inertia forces,

$$u^* \frac{\partial u^*}{\partial r^*} + w^* \frac{\partial u^*}{\partial z^*} \text{ and } u^* \frac{\partial w^*}{\partial r^*} + w^* \frac{\partial w^*}{\partial z^*}$$

can be neglected.

The non-dimensionalized continuity equation is

$$\frac{\partial u^*}{\partial r^*} + \frac{u^*}{r^*} + \frac{\partial w^*}{\partial z^*} = 0 \tag{2.13}$$

2.3 Temperature Equations

The temperature varies according to the energy equation (2.14) this is derived from application of conservation of energy to the fluid.

$$\rho c \frac{DT}{Dt} = \frac{\partial}{\partial x_j} \left(\lambda_{true} \frac{\partial T}{\partial x_j} \right) + \Phi + q_v \tag{2.14}$$

Here T is temperature, c specific heat, λ_{true} the true thermal conductivity, q_v internal heat generation and Φ heat generated by viscous dissipation. Φ is given by

$$\Phi = \frac{2\mu}{\rho} \left(e_{ij} e_{ij} - \frac{1}{3} \Delta^2 \right) \tag{2.15}$$

where

$$e_{ij} = \frac{1}{2}\left(\frac{\partial u_i}{\partial x_j} + \frac{\partial u_j}{\partial x_i}\right) \tag{2.16}$$

and

$$\Delta = e_{ii} \tag{2.17}$$

q_v is associated with the internal radiation in the glass. For large bulks internal radiation has the effect of increasing the effective conductivity, but the proximity of solid boundaries lessens this effect. The temperature and hence the viscosities near the surfaces have a much greater effect on the behaviour of the glass during the shaping process and the internal radiation has only a minor role in determining the temperature distribution and heat flux close to a glass/metal interface, this is discussed by Rawson[37]. McGraw[33] asserts that the thinner the glass becomes the less the effects of radiation within, for a thickness of 1cm the heat distribution is nearly 100% conduction.

Radiation effects are important during the reheating stage when the article is removed from the mould, but during the actual forming operation it is reasonable to assume that the effect of internal radiation is adequately described by replacing the true thermal conductivity, λ_{true}, by the effective

thermal conductivity[5], λ.

Viscous dissipation contributes little to the temperature calculation, hence Φ can be neglected.

2.3.1 Non-Dimensionalization

The energy equation can be cast in the appropriate axi-symmetric non-dimensional form. The non-dimensionalizing scheme is as in section (2.2.1), with the extra variables being

$$T^* = \frac{T - T_0}{T_{max} - T_{min}}$$
$$\lambda^* = \frac{\lambda}{\lambda_0} \tag{2.18}$$

where λ_0 is the thermal conductivity measured at the reference temperature T_0. T_{max} and T_{min} are the maximum and minimum temperatures associated with the flow.

When viscous dissipation is neglected and there is no internal heat generation (2.14) takes the form

$$\frac{\partial T^*}{\partial t^*} + u^*\frac{\partial T^*}{\partial r^*} + w^*\frac{\partial T^*}{\partial z^*} = \frac{1}{Pe}\left(\frac{\partial}{\partial r^*}\left[\lambda^*\frac{\partial T^*}{\partial r^*}\right] + \frac{\lambda^*}{r^*}\frac{\partial T^*}{\partial r^*} + \frac{\partial}{\partial z^*}\left[\lambda^*\frac{\partial T^*}{\partial z^*}\right]\right) \tag{2.19}$$

[5]hereafter just refered to as the thermal conductivity

The extra non-dimensional number introduced is the Peclet number, Pe, given by

$$Pe = \frac{LU_0\rho c}{\lambda_0} \tag{2.20}$$

This number represents the ratio of the heat transfer by convection to heat transfer by conduction within the fluid.

If the thermal conductivity, λ, is assumed constant, i.e. $\lambda_0 = \lambda$ making $\lambda^* = 1$, the energy equation (2.18) further simplifies to

$$\frac{\partial T^*}{\partial t^*} + u^*\frac{\partial T^*}{\partial r^*} + w^*\frac{\partial T^*}{\partial z^*} = \frac{1}{Pe}\left(\frac{\partial^2 T^*}{\partial r^{*2}} + \frac{1}{r^*}\frac{\partial T^*}{\partial r^*} + \frac{\partial^2 T^*}{\partial z^{*2}}\right) \tag{2.21}$$

2.3.2 The Temperature Viscosity Relationship

The viscosity, μ, is not a constant, it depends strongly on temperature, as well as being affected by the particular glass composition. Therefore the temperature field has a direct effect on the flow field.

A number of empirical formulae have been suggested to fit the available data. One such is the Fulcher equation (2.22).

The Fulcher Equation

$$log_{10}\mu = A + \frac{B}{T - T_0} \tag{2.22}$$

The constants, A, B, T_0, vary according to the actual composition of the glass.

Combining equations (2.12) and (2.22) gives the relationship between the Reynolds number and the temperature.

$$Re = \frac{\rho U_0 L}{exp\left(A + \frac{B}{T^*(T_{max} - T_{min})}\right)} \tag{2.23}$$

2.4 Boundary Conditions

2.4.1 Fluid

There are two distinct types of interface that have to be considered, the glass-mould (or plunger) interface and the glass-air interface.

The Glass-Mould Interface It is assumed that the glass sticks to the mould so the velocity of the glass immediately next to the solid surface is the same as that of the surface.

There is much debate[6] as to the actual mechanism of the moving contact point in a spreading liquid. Here the contact point is assumed to advance purely as a result of a 'rolling motion' rather than any 'slip' occurring along the surface.

[6] see the work of Dussan[16] [17] or Huh and Scriven[29] for further discussion

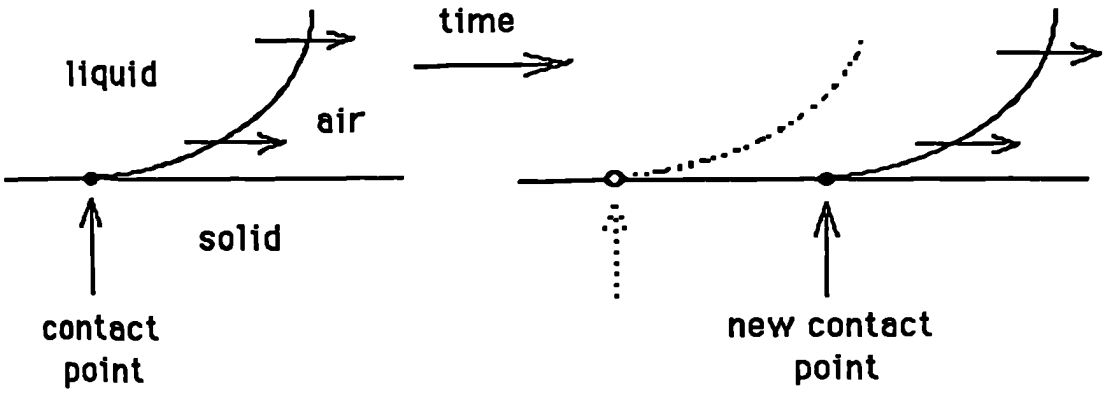

figure 2.4.1 The Contact Point

The Glass-Air Interface The free-surface boundary conditions can be expressed in terms of the stresses, Hirt et al.[27] give such a formulation.

The tangential stress is continuous across the surface, and any discontinuity in the normal stress is a result of the surface tension and the ambient pressure. These conditions can be expressed symbolically as

$$\tau_{ij} s_i n_j = 0 \tag{2.24}$$

$$\tau_{ij} n_i n_j = -p_0 + \sigma \left(\frac{1}{R_1} + \frac{1}{R_2} \right) \tag{2.25}$$

Where n,s are the normal and tangent to the surface, σ is the coefficient of surface tension, R_1 and R_2 are the principal radii of curvature. When using non-dimensional variables σ is replaced by $\frac{\sigma}{\rho U_0^2 L}$ this is sometimes called the Weber number abbreviated to Wb.

For a general 3-D surface $F(x, y, z) = 0$

$$\frac{1}{R_1} + \frac{1}{R_2} = -\frac{\partial}{\partial x}\left(\frac{1}{D}\frac{\partial F}{\partial x}\right) - \frac{\partial}{\partial y}\left(\frac{1}{D}\frac{\partial F}{\partial y}\right) - \frac{\partial}{\partial z}\left(\frac{1}{D}\frac{\partial F}{\partial z}\right) \tag{2.26}$$

with

$$D^2 = \left(\frac{\partial F}{\partial x}\right)^2 + \left(\frac{\partial F}{\partial y}\right)^2 + \left(\frac{\partial F}{\partial z}\right)^2 \tag{2.27}$$

In an axi-symmetric system with a surface independent of θ, so that it has the form $F = F(r, z)$ equations (2.25) and (2.26) become

$$\frac{1}{R_1} + \frac{1}{R_2} = -\frac{1}{r}\frac{\partial}{\partial r}\left(\frac{r}{D}\frac{\partial F}{\partial r}\right) - \frac{\partial}{\partial z}\left(\frac{1}{D}\frac{\partial F}{\partial z}\right) \tag{2.28}$$

with

$$D^2 = \left(\frac{\partial F}{\partial r}\right)^2 + \left(\frac{\partial F}{\partial z}\right)^2 \tag{2.29}$$

If it is taken that $F = z - f(r)$ then this equation yields

$$R_1 = -\frac{\left(1 + \left(\frac{\partial f}{\partial r}\right)^2\right)^{\frac{3}{2}}}{\frac{\partial^2 f}{\partial r^2}} \tag{2.30}$$

$$R_2 = -r\frac{\left(1 + \left(\frac{\partial f}{\partial r}\right)^2\right)^{\frac{1}{2}}}{\frac{\partial f}{\partial r}} \tag{2.31}$$

Note that R_1 is the 2-D radius of curvature.

2.4.2 Temperature

The heat is lost from the surface of the glass by conduction and radiation.

Conduction The rate of conduction is proportional to the temperature drop across the surface.

$$\lambda \frac{\partial T}{\partial n} = H(T - T_{am}) \tag{2.32}$$

where H is the heat transfer co-efficient and T_{am} is the temperature of the adjacent media. H will differ depending on the surface, for example heat transfer to the metal mould is usually faster than into the surrounding air.

Radiation Radiation from the surface of the hot glass is governed by

$$\lambda \frac{\partial T}{\partial n} = \epsilon \sigma_s([T + 273]^4 - [T_{am} + 273]^4) \tag{2.33}$$

where ϵ is the emissivity (less than 1) and σ_s is the Stefan constant. The radiation depends on the absolute temperature hence the conversion to Kelvin.

At a glass metal interface conduction is the major method of heat transport from the glass to the mould because metal is opaque to radiation, whereas radiation plays an important role at a free surface.

Both these boundary conditions can be expressed in non-dimensional forms.

$$\frac{\partial T^*}{\partial n^*} = H^*(T^* - T^*_{am}) \tag{2.34}$$

$$\frac{\partial T^*}{\partial n^*} = \epsilon^*([T^* + \frac{T_0 + 273}{T_{max} - T_{min}}]^4 - [T^*_{am} + \frac{T_0 + 273}{T_{max} - T_{min}}]^4) \tag{2.35}$$

Introducing two more non-dimensional groups. The non-dimensional Heat transfer co-efficient.

$$H^* = \frac{HL}{\lambda} \tag{2.36}$$

and the non-dimensional emmissivity

$$\epsilon^* = \frac{\sigma_s \epsilon (T_{max} - T_{min})^3}{\lambda} \tag{2.37}$$

2.5 Summary

2.5.1 Flow Equations

Navier-Stokes' Equations

$$\frac{\partial u^*}{\partial t^*} = \frac{1}{r^*}\frac{\partial r^* \tau^*_{rr}}{\partial r^*} - \frac{\tau^*_{\theta\theta}}{r^*} + \frac{\partial \tau^*_{rz}}{\partial z^*} \tag{2.38}$$

$$\frac{\partial w^*}{\partial t^*} = \frac{1}{r^*}\frac{\partial r^* \tau^*_{rz}}{\partial r^*} + \frac{\partial \tau^*_{zz}}{\partial z^*} + \frac{1}{Fr} \tag{2.39}$$

Where the stress components are given by

$$\begin{aligned}
\tau^*_{rr} &= -p^* + 2\frac{1}{Re}\frac{\partial u^*}{\partial r^*} \\
\tau^*_{rz} &= \frac{1}{Re}\left(\frac{\partial u^*}{\partial z^*} + \frac{\partial w^*}{\partial r^*}\right) \\
\tau^*_{\theta\theta} &= -p^* + 2\frac{1}{Re}\frac{u^*}{r^*} \\
\tau^*_{zr} &= \frac{1}{Re}\left(\frac{\partial u^*}{\partial z^*} + \frac{\partial w^*}{\partial r^*}\right) \\
\tau^*_{zz} &= -p^* + 2\frac{1}{Re}\frac{\partial w^*}{\partial z^*}
\end{aligned} \tag{2.40}$$

Continuity Equation

$$\frac{\partial u^*}{\partial r^*} + \frac{u^*}{r^*} + \frac{\partial w^*}{\partial z^*} = 0 \tag{2.41}$$

2.5.2 Flow Boundary Conditions

Glass-Mould Interface

No-slip

Glass-Air Interface

$$\tau^*_{ij} s_i n_j = 0 \tag{2.42}$$

$$\tau^*_{ij} n_i n_j = -p_0 + Wb\left(\frac{1}{R_1} + \frac{1}{R_2}\right) \tag{2.43}$$

2.5.3 Temperature Equation

$$\frac{\partial T^*}{\partial t^*} + u^*\frac{\partial T^*}{\partial r^*} + w^*\frac{\partial T^*}{\partial z^*} = \frac{1}{Pe}\left(\frac{\partial^2 T^*}{\partial r^{*2}} + \frac{1}{r^*}\frac{\partial T^*}{\partial r^*} + \frac{\partial^2 T^*}{\partial z^{*2}}\right) \tag{2.44}$$

2.5.4 Temperature-Viscosity Relationship

$$log_{10}\mu = A + \frac{B}{T - T_0} \tag{2.45}$$

2.5.5 Temperature Boundary Conditions

Glass-Mould Interface

$$\frac{\partial T^*}{\partial n^*} = H^*_m(T^* - T^*_{am}) \tag{2.46}$$

Glass-Air Interface

$$\begin{aligned}\frac{\partial T^*}{\partial n^*} &= H_a^*(T^* - T_{am}^*) \\ &+ \epsilon^* \left([T^* + \frac{T_0 + 273}{T_{max} - T_{min}}]^4 - [T_{am}^* + \frac{T_0 + 273}{T_{max} - T_{min}}]^4\right) \quad (2.47)\end{aligned}$$

2.5.6 Non-Dimensional Groups

Reynolds Number

$$Re = \frac{\rho U_0 L}{\mu}$$

Froude Number

$$Fr = \frac{U_0^2}{gL}$$

Weber Number

$$Wb = \frac{\sigma}{\rho U_0^2 L}$$

Peclet Number

$$Pe = \frac{L U_0 \rho c}{\lambda}$$

n.d.Heat Transfer Co-efficient

$$H^* = \frac{HL}{\lambda}$$

n.d.Emmissivity

$$\epsilon^* = \frac{\sigma_s \epsilon (T_{max} - T_{min})^3}{\lambda}$$

Chapter 3

Mathematical Approximations

3.1 Introduction

This chapter looks at the mathematics involved in calculating the isothermal flow field.

Before any numerical methods are used, existing solutions for a simplified situation or portions of the field are considered. These solutions can then be used in conjunction with or to validate a more numerical approach.

The equations developed in chapter 2, are then written in a numerical

form and solved using the finite element (f.e) method.

3.2 Analytical Solutions

The main difficulty is the complicated free surface boundary condition (2.25). In a steady state, $\frac{\partial}{\partial t} = 0$, two dimensional cartesian, $(x, y, 0)$, case the Navier-Stokes equations simplify to

$$\frac{\partial p}{\partial x} = 0 \tag{3.1}$$

$$\frac{\partial p}{\partial y} + g\rho = 0 \tag{3.2}$$

with the free surface boundary condition (2.25) becoming

$$\Delta p = \sigma \frac{\varsigma''}{(1+\varsigma'^2)^{\frac{3}{2}}} \tag{3.3}$$

where Δp is the change of pressure across the free surface which is given by $x = \varsigma(y)$. This set of equations can be solved to give solutions of the form

$$\frac{y}{d} = \cosh^{-1}\frac{2d}{\varsigma} - \cosh^{-1}\frac{2d}{h} + C \tag{3.4}$$

where C is a constant determined by the situation, and

$$d^2 = \frac{\sigma}{\rho g}$$

$$h^2 = 2\frac{\sigma}{\rho g}(1 - \sin\theta)$$

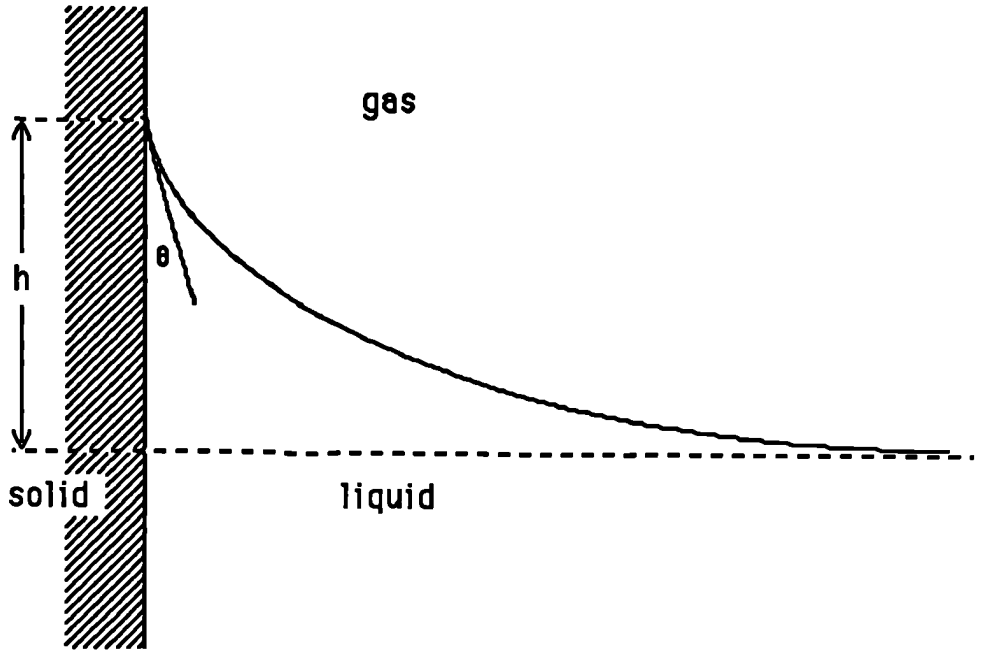

Figure 3.2.1 A Liquid Surface Meeting a Vertical Wall

θ is the contact angle. This method is used by Batchelor[3] to calculate the shape of a meniscus[1] and the capillary rise of liquid in a small tube.

This result is of little use for the present problem because it only applies to the stationary situation and the contact angle is not necessarily a known constant; studies by workers such as Bartell[2] and Elliot[2] show the difficulty of accurately measuring the contact angle and cast doubt on its independence of other conditions.

[1]figure (3.2.1) shows the geometry for this case

The condition for equilibrium at any point at the interface for the three dimensional situation is

$$\rho g z - \sigma \left(\frac{1}{R_1} + \frac{1}{R_2} \right) = const. \tag{3.5}$$

This is difficult to solve for the surface shape but is useful in showing that $\sqrt{\frac{\sigma}{\rho g}}$ is the only relevant parameter with the dimensions of length.

The solution which describes the surface shape of a 2-d stationary fluid is the limit of the analytical method. However, some appoximate methods are useful, in particular lubrication theory.

If the glass is being pressed in a (relatively) thin film between two parallel plates, as in figure (3.2.2), then lubrication theory can be applied and a squeeze film approximation used for the portion of fluid well away[2] from the free surface. This approach gives the approximate velocity field of

$$\left.\begin{aligned} u &= \tfrac{-6}{h^3} x y (y-h) \\ v &= \tfrac{6}{h^3} y^2 \left(\tfrac{y}{3} - \tfrac{h}{2} \right) \end{aligned}\right\} \text{ for 2-d case} \tag{3.6}$$

$$\left.\begin{aligned} u &= \tfrac{-3}{h^3} r z (z-h) \\ w &= \tfrac{6}{h^3} z^2 \left(\tfrac{z}{3} - \tfrac{h}{2} \right) \end{aligned}\right\} \text{ for 3-d axisymmetric case} \tag{3.7}$$

[2] of the order of the exit length, given by $\frac{0.2h^2 U_0 \rho}{\mu}$ where h is the distance between the plates.

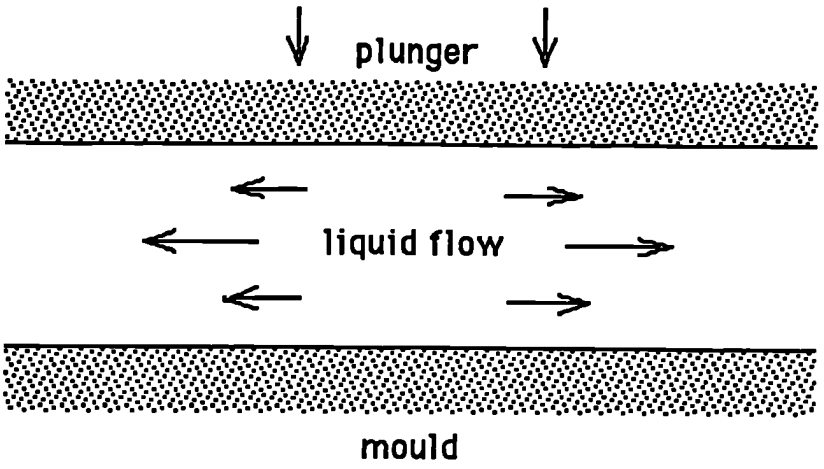

Figure 3.2.2 A Squeeze Film

Further information on the assumptions used in lubrication theory can be found in various texts such as those by Cameron[8] or Taylor[42].

If a mathematical model is to be used to predict the behaviour of molten glass during the pressing of a disc, then the possibility arises of using an approximation of the form given in equation (3.7) for the central portion of the flow[3].

However, neither of these solutions provides any information about the movement of the free surface, hence the need to resort to a finite element method.

[3]this idea is picked up in section (4.5)

3.3 The Finite Element Method (f.e.m)

3.3.1 Introduction

The use of finite elements is a well established versatile method that allows the calculation of approximate numerical solutions to systems governed by partial differential equations.

The finite element method has its roots in engineering, originally used as a way of solving stress related problems in networks, it was developed independently by various mathematicians and physicists. The term finite element appeared first in work by Clough[13] in 1960. Numerical solutions of this nature became more practical with the development of powerful computers. This technique was first applied to the solution of fluid mechanics problems in the 70s, by workers such as Meissner[34] and Ikegawa[30]. The method has progressed and is currently used for very complicated situations, for example, calculating the flow of air round an aircraft which involves working with millions of variables on very powerful computers.

There are many commercial finite element and finite difference software packages available, but in this project all the computer programs were written from scratch. Working in this way ensures full understanding of the methods involved, as well as being able to tailor the package to fit the prob-

lem.

There are many books solely devoted to the f.e.method, for example, the text by Zienkiewiez[47], so only a basic outline is given before a more detailed description of the application to this particular problem.

3.3.2 Common Steps

There are various steps that all implementations of the f.e method share. First the domain of interest is discretized into elements, these can take various forms. The most used 2-d shapes are the triangle, either 3 or 6 node and the quadrilateral 4 or 9 node. In 3-d tetrahedron or cuboid elements can be used. Also there are special elements that can exploit any known symmetry, for example the ring element which is used for axi-symmetric cases, makes use of the fact that there are no changes in the direction of the azimuthal angle.

The unknowns are then assumed to have a prescribed form, eg linear or quadratic polynomial, within each element. The behaviour of an unknown in any given element can then be described by a finite number of values, stored at nodes at the corners and/or within each element, and the chosen interpolation function. The choice of suitable interpolation functions for the elements is not arbitrary, there are certain requirements that have to

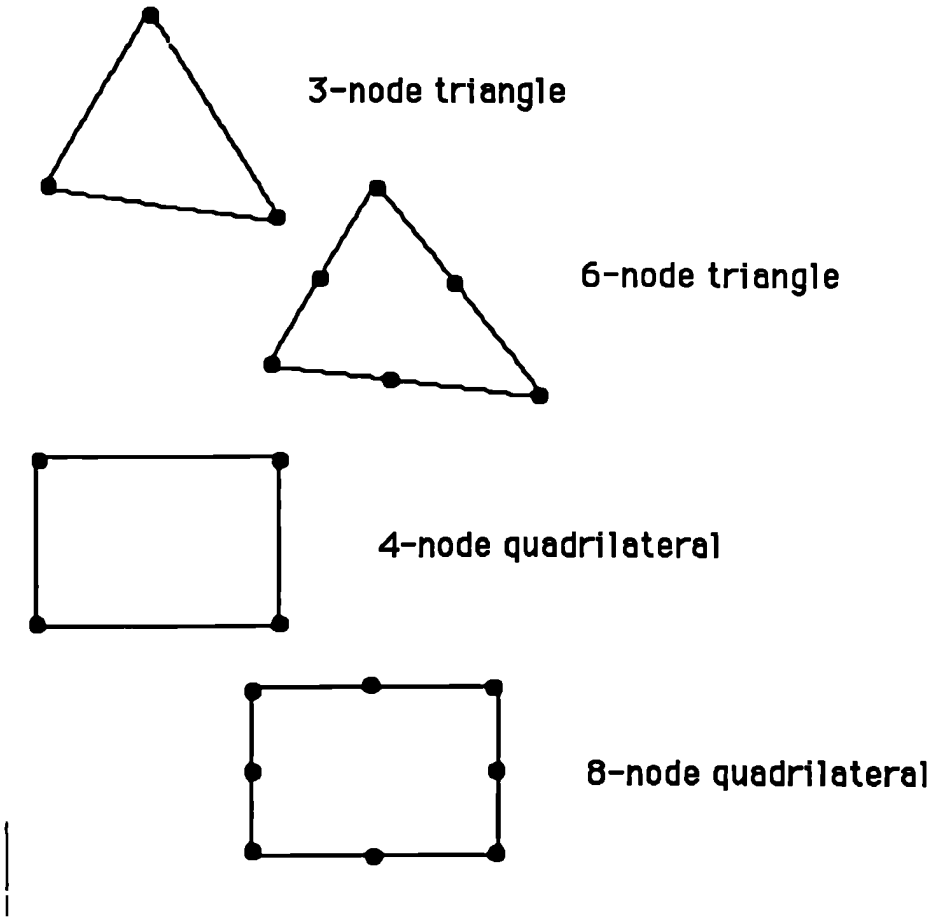

Figure 3.3.1 Common Element Types

be met to ensure inter element continuity. These conditions are imposed so that approximate values obtained for these field variables converge towards the exact solutions as the elements become smaller. In general the two conditions to be satisfied are

- At element interfaces the field variables and any of its partial derivatives up to one order less than the highest derivative appearing in the final form of the integral governing equations, must be continuous.
- All states of the unknowns and its partial derivatives up to the highest order appearing should have a representation in the approximate form which becomes exact when in the limit the element size shrinks to zero.

The first is known as the compatibility requirement and is necessary for the successful application of the assembly procedure. The second is the completeness requirement. This process reduces the number of unknowns from an infinite number to a finite one.

The partial differential equations governing the problem have to be cast into an integral formulation. Various methods to achieve this are available the most popular amongst them are the variational and weighted residuals methods. The variational method relies on the differential equations having

an equivalent variational formulation. There are however only a limited number of problems for which a variational statement has been found. In the absence of a variational statement a more general method for deriving the element equations must be applied, and the method of weighted residuals is often used.

This method proceeds directly from the differential equations governing the problem. Taking the governing equations to be of the form

$$D(u) - G = 0 \tag{3.8}$$

where D is a differential operator, u is a field variable and G a given function applied in a solution domain V bounded by a surface S. If an approximate solution u^* is assumed to have the form

$$u^* = \sum_{i=1}^{n} \phi_i^e u_i^e \tag{3.9}$$

where u_i^e are the unknown values at the i^{th} node in the e^{th} element and ϕ_i^e are chosen to satisfy the boundary conditions applied on S. As u^* is only an approximate solution it will not satisfy the equation exactly, there will be a residual error r.

$$D(u^*) - G = r \tag{3.10}$$

Although it will not be possible to force the error to vanish, a weighted

integral incorporating the residual performed over the entire solution domain can be made to vanish. Hence if ψ^e are suitable weighting functions

$$\sum_{e=1}^{m} \int_V \psi^e (D(u^*) - G) dV^e = \sum_{e=1}^{m} \int_V \psi^e r dV^e = 0 \qquad (3.11)$$

for a solution domain containing m elements. The choice of the ψ depend on the residual method being employed. The most popular method is the Galerkin method, where $\psi = \phi$.

Once a form of the governing equations has been found it can be manipulated into the most useful form, often the order of derivatives can be reduced via an application of Stokes' or Green's Theorem. This reduction is advantageous as it allows for a simpler interpolation function to be used.

Each element is required to satisfy these integral equations producing a set of algebraic equations, the integrations having been performed exactly or numerically. These algebraic equations are then assembled into a matrix or several matrix equations. Boundary conditions are usually incorporated at this stage. These matrix equations can then be solved by any convenient algorithm. Any further calculations can be performed to recover the desired variables. If the problem is a steady state one only one such calculation need be undertaken, however if the problem is time dependent many such calculations have to be performed to obtain the progression of solutions

with time. The calculations to obtain this progression of solutions can be explicit or implicit. An explicit scheme is where the motion at the present timestep is assumed to depend only on the past history whereas an implicit scheme assumes that the present motion depends on the present and past history. An implicit scheme normally involves iterative solutions and is more difficult to program than the corresponding explicit method. However, explicit methods tend to be numerically less stable. The grid formed by the node points can either be fixed or moving. A moving grid is useful when a free surface needs to be tracked accurately, this device was introduced by Hirt et al.[28]. The node points are moved a small distance indicated by $\delta t\mathbf{u}$ before the next calculation is performed.

3.3.3 Present Usage

Now follows a more detailed description of the f.e method as applied in this case.

The Elements

The model is axi-symmetric hence ring elements were used. Originally three node triangular cross sectional ones were experimented with but these were found to be very restrictive. The final model utilized ring elements with a

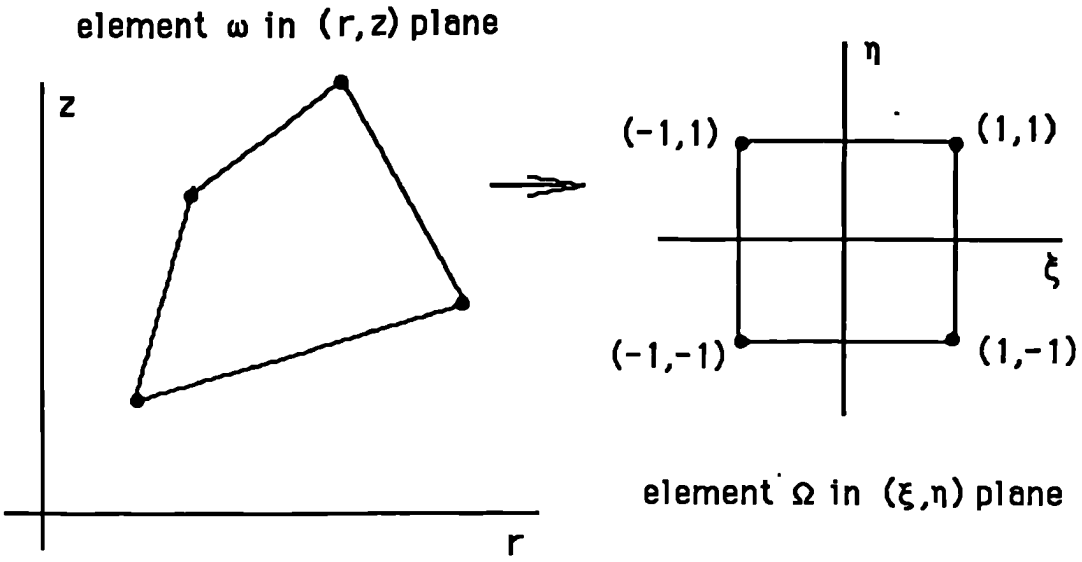

Figure 3.3.2 4-Node Isoparametric Elements

four node isoparametric cross section.

The interpolation for velocity and acceleration was bi-linear across these elements with pressure constant within.

Each of the irregular quadrilaterals in the (r, z) field can be transformed to a square in the (ξ, η) field, this process which makes subsequent calculations much easier to perform, is shown schematically in figure(3.3.2). The original element has interpolations functions of

$$\phi_1 = \frac{F_{23}(r,x)F_{34}(r,z)}{F_{23}(r_1,z_1)F_{34}(r_1,z_1)} \tag{3.12}$$

where

$$F_{ij}(r,z) = z(r_j - r_i) + r(z_i - z_j) + (r_i z_j - r_j z_i) \tag{3.13}$$

ϕ_2, ϕ_3, ϕ_4 can be obtained by cyclic permutations of suffixes. The new co-ordinates introduced are given by

$$\begin{aligned} \xi &= -\phi_1 - \phi_2 + \phi_3 + \phi_4 \\ \eta &= -\phi_1 + \phi_2 + \phi_3 - \phi_4 \end{aligned} \tag{3.14}$$

The transformed element has interpolation functions of

$$\begin{aligned} \Phi_1 &= \frac{1}{4}(1-\xi)(1-\eta) \\ \Phi_2 &= \frac{1}{4}(1+\xi)(1-\eta) \\ \Phi_3 &= \frac{1}{4}(1+\xi)(1+\eta) \\ \Phi_4 &= \frac{1}{4}(1-\xi)(1+\eta) \end{aligned} \tag{3.15}$$

All the field variables can now be expressed in terms of ξ and η, and the integrations can be transformed using the Jacobian, J, its modulus $|J|$, or inverse, J^{-1}.

$$J = \begin{pmatrix} \frac{\partial r}{\partial \xi} & \frac{\partial z}{\partial \xi} \\ \frac{\partial r}{\partial \eta} & \frac{\partial z}{\partial \eta} \end{pmatrix} \tag{3.16}$$

that is

$$J = \begin{pmatrix} \Sigma_{i=1}^{4} r_i \frac{\partial \Phi_i}{\partial \xi} & \Sigma_{i=1}^{4} z_i \frac{\partial \Phi_i}{\partial \xi} \\ \Sigma_{i=1}^{4} r_i \frac{\partial \Phi_i}{\partial \eta} & \Sigma_{i=1}^{4} z_i \frac{\partial \Phi_i}{\partial \eta} \end{pmatrix} \tag{3.17}$$

$$|J| = j_{11}j_{22} - j_{12}j_{21}$$

$$J^{-1} = \frac{1}{|J|} \begin{pmatrix} j_{22} & -j_{12} \\ -j_{21} & j_{11} \end{pmatrix} \tag{3.18}$$

these equations provide the necessary relations to transform integral expressions on any element ω in the (r, z) plane to the associated element Ω in the (ξ, η) plane. For example, the integral

$$k = \int_{\omega} \left(a \frac{\partial \Psi_i}{\partial x} \frac{\partial \Psi_j}{\partial y} + b \Psi_j \right) dx dy \tag{3.19}$$

where a and b are functions of x and y, becomes

$$k = \int_{\Omega} \left(A \left(j_{11}^{*} \frac{\partial \Psi_i}{\partial \eta} + j_{12}^{*} \frac{\partial \Psi_i}{\partial \xi} \right) \left(j_{21}^{*} \frac{\partial \Psi_j}{\partial \eta} + j_{22}^{*} \frac{\partial \Psi_j}{\partial \xi} \right) + B \Psi_j \right) |J| d\eta d\xi \tag{3.20}$$

where A and B are functions expressed in terms of ξ and η, $j^{*}$are the elements of the inverse Jacobian.

Integral Equations

The axi-symmetric form of the Navier Stokes equations given in chapter 2 can be written in the alternative form[4].

$$\begin{aligned}\frac{\partial u}{\partial t} &= \frac{1}{r}\frac{\partial}{\partial r}(r\tau_{rr}) + \frac{1}{r}\frac{\partial}{\partial z}(r\tau_{rz}) - \frac{\tau_{\theta\theta}}{r} \\ \frac{\partial w}{\partial t} &= \frac{1}{r}\frac{\partial}{\partial r}(r\tau_{zr}) + \frac{1}{r}\frac{\partial}{\partial z}(r\tau_{zz}) + \frac{1}{Fr}\end{aligned} \tag{3.21}$$

where

$$\begin{aligned}\tau_{rr} &= -p + \frac{2}{Re}\frac{\partial u}{\partial r} \\ \tau_{rz} &= \frac{1}{Re}\left(\frac{\partial u}{\partial z} + \frac{\partial w}{\partial r}\right) \\ \tau_{\theta\theta} &= -p + \frac{2}{Re}\frac{u}{r} \\ \tau_{zr} &= \frac{1}{Re}\left(\frac{\partial u}{\partial z} + \frac{\partial w}{\partial r}\right) \\ \tau_{zz} &= -p + \frac{2}{Re}\frac{\partial w}{\partial z}\end{aligned} \tag{3.22}$$

This form does not assume that the Reynolds number is constant so is applicable to the non-isothermal case. The straight forward application of Galerkin's method gives

$$\int_\omega \phi\frac{\partial u}{\partial t} = \int_\omega \phi\left(\frac{1}{r}\frac{\partial}{\partial r}(r\tau_{rr}) + \frac{1}{r}\frac{\partial}{\partial z}(r\tau_{rz}) - \frac{\tau_{\theta\theta}}{r}\right)d\omega \tag{3.23}$$

[4]all field variables are dimensionless but the starred notation used in chapter 2 has been dropped for clarity

This can be rewritten as

$$\begin{aligned}\int_\omega \phi\frac{\partial u}{\partial t} &= \int_\omega \nabla.(\phi\tau_{rr}, 0, \phi\tau_{rz})\, d\omega \\ &- \int_\omega \left(\tau_{rr}\frac{\partial \phi}{\partial r} + \tau_{rz}\frac{\partial \phi}{\partial z} + \phi\frac{\tau_{\theta\theta}}{r}\right) d\omega \end{aligned} \tag{3.24}$$

Application of the Gauss theorem to the second order derivatives present gives

$$\begin{aligned}\int_\omega \phi\frac{\partial u}{\partial t} d\omega &= \int_s \phi(\tau_{rr}, 0, \tau_{rz}).d\mathbf{S} \\ &- \int_\omega (\tau_{rr}\frac{\partial \phi}{\partial r} + \tau_{rz}\frac{\partial \phi}{\partial z} + \phi\frac{\tau_{\theta\theta}}{r}) d\omega \end{aligned} \tag{3.25}$$

where s refers to the boundary of the solution domain containing the free surface[5]. This surface integral can be written in a more useful form. If the surface has equation $F(r,z) = 0$ then

$$\mathbf{n} = \frac{1}{\sqrt{\left(\frac{\partial F}{\partial r}\right)^2 + \left(\frac{\partial F}{\partial z}\right)^2}} \left(\frac{\partial F}{\partial r}, 0, \frac{\partial F}{\partial z}\right) \tag{3.26}$$

and

$$d\mathbf{S} = \mathbf{n} r\, ds\, d\theta \tag{3.27}$$

so the surface integral can be written as

$$\int_s \phi \left(\tau_{rr}\frac{\partial F}{\partial r} + \tau_{rz}\frac{\partial F}{\partial z}\right) \frac{r}{\sqrt{\left(\frac{\partial F}{\partial r}\right)^2 + \left(\frac{\partial F}{\partial z}\right)^2}} dr\, d\theta \tag{3.28}$$

[5]the contributions from internal element boundaries cancel out, also it is zero along the solid boundaries so effectively the only contribution is from the free surface

Now since

$$\frac{ds}{dz} = \frac{\sqrt{\left(\frac{\partial F}{\partial r}\right)^2 + \left(\frac{\partial F}{\partial z}\right)^2}}{\frac{\partial F}{\partial r}} \tag{3.29}$$

and recalling the natural boundary condition

$$\left[-p_0 + \sigma\left(\frac{1}{R_1} + \frac{1}{R_2}\right)\right]\frac{\partial F}{\partial r} = \tau_{rr}\frac{\partial F}{\partial r} + \tau_{rz}\frac{\partial F}{\partial z} \tag{3.30}$$

this can be substituted in to equation (3.28) giving

$$\int_s \phi\left[-p_0 + \sigma\left(\frac{1}{R_1} + \frac{1}{R_2}\right)\right] r dz d\theta \tag{3.31}$$

As there is no dependence on θ this variable can be integrated out, giving 2π which immediately cancels.

The final integral formulation of the equation is

$$\begin{aligned}\int_v \phi\frac{\partial u}{\partial t} r dr dz = \int_s \phi\left(-p_0 + \sigma\left(\frac{1}{R_1} + \frac{1}{R_2}\right)\right) r dz \\ - \int_v \left(-p + \frac{2}{Re}\frac{\partial u}{\partial r}\right)\frac{\partial \phi}{\partial r} + \frac{1}{Re}\left(\frac{\partial u}{\partial z} + \frac{\partial w}{\partial r}\right)\frac{\partial \phi}{\partial z} \\ + \frac{\phi}{r}\left(-p + \frac{2}{Re}\frac{u}{r}\right) r dr dz\end{aligned} \tag{3.32}$$

A similar process can be used to obtain the z component equation.

$$\begin{aligned}\int_v \phi\frac{\partial w}{\partial t} r dr dz = \int_s \phi\left(-p_0 + \sigma\left(\frac{1}{R_1} + \frac{1}{R_2}\right)\right) r dz \\ - \int_v \left(-p + \frac{2}{Re}\frac{\partial w}{\partial r}\right)\frac{\partial \phi}{\partial z} + \frac{1}{Re}\left(\frac{\partial w}{\partial r} + \frac{\partial u}{\partial z}\right)\frac{\partial \phi}{\partial z} \\ + \left(\frac{\phi}{Fr}\right) r dr dz\end{aligned} \tag{3.33}$$

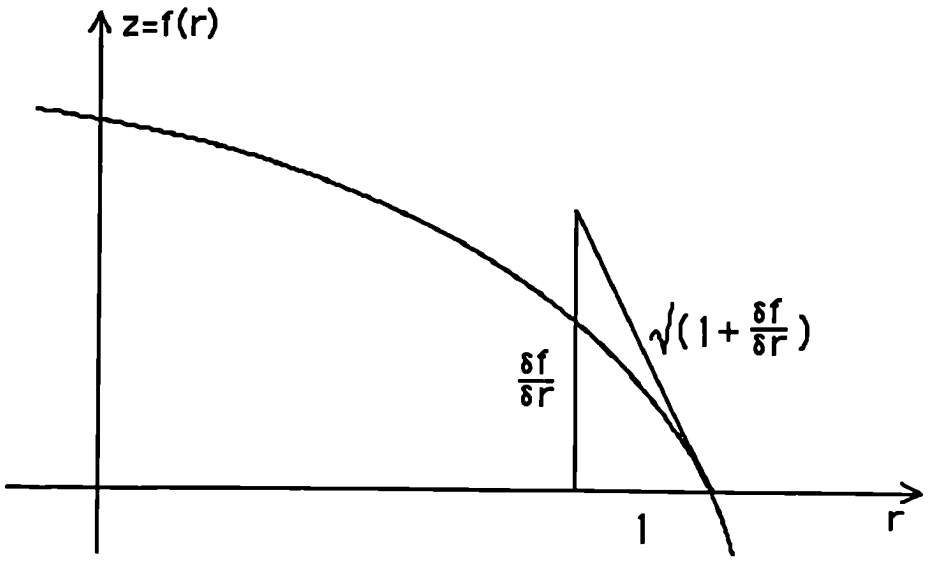

Figure 3.3.3 Calculating R_2

The continuity condition (2.41) is replaced by a volume constraint, i.e. the volume of each element in the grid remains constant; more details are given in the section describing the grid.

Radii of Curvature

As the radii of curvature have been introduced into the equation there has to be a recipe for calculating them.

An approximation for R_1 can be obtained by fitting a circle through

three adjacent surface nodes and finding its radius.

R_2 is easily calculated once it has been noted that for a surface $z = f(r)$

$$sin\alpha = \frac{\frac{\partial f}{\partial r}}{\sqrt{1 + \left(\frac{\partial f}{\partial r}\right)^2}} \tag{3.34}$$

where α is the angle between the tangent and the horizontal. Then

$$\frac{1}{R_2} = \frac{-sin\alpha}{r} \tag{3.35}$$

obviously this has a singularity on the axis $r = 0$ but this is the axis of symmetry so here $R_1 = R_2$.

The Implementation

Now approximations for the field variables can be substituted into equations (3.32) and (3.33). Due to the quite complicated nature of the integrals, numerical integration was used.

The integrals written in terms of the transformed co-ordinates (ξ, η) can be evaluated by the use of four Gauss points, given in figure (3.3.4).

η	ξ	weight
-0.577	-0.577	1.0
-0.577	0.577	1.0
0.577	-0.577	1.0
0.577	0.577	1.0

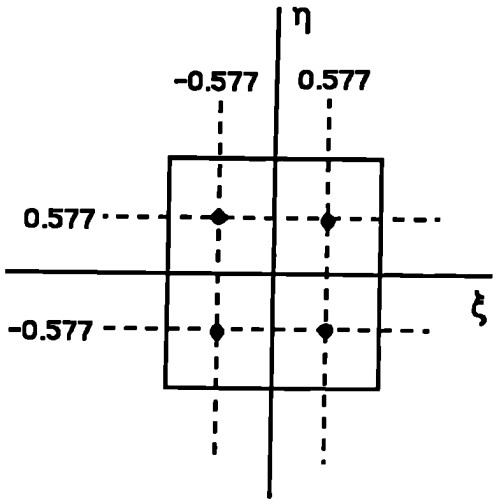

$$\int h(\xi,\eta)d\eta d\xi = h(0.577,0.577) + h(0.577,-0.577)$$
$$+h(-0.577,0.577) + h(-0.577,-0.577) \quad (3.36)$$

Figure 3.3.4 4-Gauss Points

An n-point Gaussian quadrature integrates polynomials of order 2n-1, or less, exactly. Therefore the 2-point quadrature used here integrates polynomials upto and including order 3 exactly.

This form of numerical integration has the useful by-product of avoiding evaluating anything on the $r = 0$ axis, hence the presence of the $\frac{1}{r}$ term in equation (3.32) does not prove a difficulty.

The Grid

A moving grid is used so that the boundary can be followed. After each calculation the node points are moved in accordance with the newly calculated velocities and accelerations. The continuity condition is replaced by a volume constraint, that is, the volume of each ring remains constant over each grid movement. The volume of a ring element is given by

$$V(r,z) = \int 2\pi r dr dz = \frac{\pi}{3}\left[(r_1^2 - r_3^2)(z_2 - z_4) + (r_2^2 - r_4^2)(z_3 - z_1)\right.$$
$$\left. +(r_2 - r_4)(r_3 z_3 - r_1 z_1) + (r_1 - r_3)(r_2 z_2 - r_4 z_4)\right] \quad (3.37)$$

Therefore the conservation of volume is expressed as

$$V(r^N, z^N) = V(r^{N+1}, z^{N+1}) \quad (3.38)$$

where r^{N+1} and z^{N+1} depend on the accelerations, velocities and the step length δt. This condition involves powers of δt up to 4, δt is small therefore the terms in δt^3 and δt^4 are neglected.

Assembly

Within an element the field variable are approximated using the nodal values of the variable and the interpolation function. For example

$$u^e = u_1^e \phi_1^e + u_2^e \phi_2^e + u_3^e \phi_3^e + u_4^e \phi_4^e$$

These approximations are substituted into equations (3.32), (3.33) and (3.37). The integrals are then expressed in terms of ξ and η. They can then be evaluated numerically by summing over the Gauss points[6].

For example

$$\int_v \phi \frac{\partial u}{\partial t} r dr dz$$

is approximated in each element by

$$\int_e \phi_i^e [\phi^e] \mathbf{a}^e [\phi^e] \mathbf{r}^e dr dz$$

where $a_i = \frac{\partial u}{\partial t}$ evaluated at the i^{th} node, $i = 1..4$. It is then transformed into the (ξ, η) plane to give

$$\int_e \Phi_i^e [\Phi^e] \mathbf{a}^e [\Phi^e] \mathbf{r}^e |J| d\xi d\eta$$

and evaluated

$$\sum_{G=1}^{4} \left(\sum_{i=1}^{4} \Phi_i^e r_i^e \right)_G |J|_G \begin{bmatrix} \Phi_1^e\Phi_1^e & \Phi_1^e\Phi_2^e & \Phi_1^e\Phi_3^e & \Phi_1^e\Phi_4^e \\ \Phi_2^e\Phi_1^e & \Phi_2^e\Phi_2^e & \Phi_2^e\Phi_3^e & \Phi_2^e\Phi_4^e \\ \Phi_3^e\Phi_1^e & \Phi_3^e\Phi_2^e & \Phi_3^e\Phi_3^e & \Phi_3^e\Phi_4^e \\ \Phi_4^e\Phi_1^e & \Phi_4^e\Phi_2^e & \Phi_4^e\Phi_3^e & \Phi_4^e\Phi_4^e \end{bmatrix}_G \begin{pmatrix} a_1^e \\ a_2^e \\ a_3^e \\ a_4^e \end{pmatrix}$$

to give

$$[K]^e(\mathbf{a}) \tag{3.39}$$

[6] the volume constraint is evaluated slightly differently

Where G are the four Gauss points. The other terms of the integral equations are treated similarly.

$$\int_s \phi(-p_0 + \sigma\left(\frac{1}{R_1}+\frac{1}{R_2}\right))\,r\,dz - \int_v \frac{2}{Re}\frac{\partial u}{\partial r}\frac{\partial \phi}{\partial r} + \frac{1}{Re}\left(\frac{\partial u}{\partial z}+\frac{\partial w}{\partial r}\right)\frac{\partial \phi}{\partial z} + \frac{\phi}{r}\left(-p+\frac{2}{Re}\frac{u}{r}\right) r\,dr\,dz \text{ gives } [Ur]^e(\mathbf{u},\mathbf{w})^T \tag{3.40}$$

and

$$\int_v p\frac{\partial \phi}{\partial z}\,dr\,dz \text{ gives } [Pr]^e(\mathbf{p}) \tag{3.41}$$

The matrix equation which expresses the volume conservation is a rearrangement of equations (3.36) and (3.37). In this way three equations for each element are obtained, one each for the r and z direction nodal accelerations in terms of the pressures and velocities, and one which expresses the volume conservation, i.e.

$$\begin{aligned} [K]^e(\mathbf{a}) &= [Pr]^e(\mathbf{p}) + [Ur]^e(\mathbf{u},\mathbf{w})^T \\ [K]^e(\mathbf{b}) &= [Pz]^e(\mathbf{p}) + [Uz]^e(\mathbf{u},\mathbf{w})^T \\ [VM]^e(\mathbf{a},\mathbf{b})^T &= [fv]^e(\mathbf{u},\mathbf{w})^T \end{aligned} \tag{3.42}$$

These element equations are assembled so that three large matrix equations, representing the movement of the whole volume, are formed.

$$\text{i, } [K](\mathbf{a}) = [Pr](\mathbf{p}) + [Ur](\mathbf{u},\mathbf{w})^T$$

$$\text{ii, } [K](\mathbf{b}) = [Pz](\mathbf{p}) + [Uz](\mathbf{u},\mathbf{w})^T$$

$$\text{iii, } [VM](\mathbf{a},\mathbf{b})^T = [fv](\mathbf{u},\mathbf{w})^T \tag{3.43}$$

Solution

It is possible to solve these equations using various methods. A direct explicit method was chosen. That is the velocities,$(\mathbf{u},\mathbf{w})$, are assumed known so that the pressures, $(\mathbf{p})$, and accelerations, $(\mathbf{a},\mathbf{b})$, are the only unknown variables i.e. 2n+m unknowns 2n+m equations. Equations i and ii can be used to eliminate the accelerations from equation iii which can then be solved for pressure. These are then substituted back to give the nodal accelerations.

Direct solution was chosen because of the existence of fast efficient solving packages. The one used here was Nag F04ATS based on the Crout factorisation method[7].

Now new velocities can be calculated using

$$u^{N+1} = u^N + \delta t a^{N+1}$$

$$v^{N+1} = v^N + \delta t b^{N+1} \tag{3.44}$$

[7]for further details see the handbook by Wilkinson and Reinsch[45]

and the grid moved according to

$$r^{N+1} = r^N + \delta t u^{N+1}$$

$$z^{N+1} = z^N + \delta t v^{N+1} \tag{3.45}$$

where the superscripts denote the time and δt is the length of the N+1th step. More complicated expressions could be used instead of (3.44) and (3.45), but in practice the step length δt is short, i.e. $\delta t \leq 0.01$, making terms of $O(\delta t^2)$ and above small.

Node Crossing

Before moving the nodes, it has to be checked that none of the new positions are outside the fixed boundaries. If moving a node according to (3.45) takes that node across a solid boundary then the time step has to be shortened so that the node just touches the boundary.

Grid Distortion

Moving the grid nodes means that the elements are constantly changing shape. This distortion of the grid can create problems as the interpolation functions are only valid for convex elements. Non-convex elements also introduce the possibility of non-positive Jacobians leading to various numer-

ical difficulties. The deformation of the grid can be successfully combatted by the introduction of a suitable remeshing scheme that redraws the grid periodically; further discussion of the point can be found in section (4.4) and appendix B.

Chapter 4

Isothermal Results

4.1 Introduction

This chapter contains results obtained when the computer model was used to predict the flow of a viscous liquid in various simple isothermal situations. They are used to illustrate the effects of the various parameters involved and some of the problems encountered.

4.1.1 The Parameters

The non-dimensionalization scheme, introduced in chapter 2, allows the flow to be characterized by three non-dimensional numbers, recalled here.

$$\begin{aligned} \text{Reynolds number} = \text{Re} &= \frac{\rho U_0 L}{\mu} \\ \text{Froude number} = \text{Fr} &= \frac{U_0^2}{gL} \\ \text{Weber number} = \text{Wb} &= \frac{\sigma}{L\rho U_0^2} \end{aligned} \tag{4.1}$$

It is also useful to recall the relationship between time, pressure and their non-dimensional equivalents.

$$t^* = \frac{U_0}{L}t, p^* = \frac{p}{\rho U_0^2} \tag{4.2}$$

4.2 Effect of Changing Viscosity

Here the computer model was used to predict the behaviour of liquids of different viscosities, when they were pressed under identical circumstances.

It was assumed that the portion of liquid was dropped onto a flat plate, hence the liquid was assumed to have a uniform downward velocity of magnitude $0.9U_0$ at $t = 0$. It was then pressed by a flat plunger moving at a uniform downward speed, U_0. The difference in viscosities was expressed via the Reynolds number. All other parameters are constant, hence the non-

dimensional time (n.d.t) and non-dimensional pressures (n.d.p) are directly comparable between the three cases presented. A grid made up of twenty ring elements was used to represent the fluid. The step size, δt, was limited by the need for numerical stability. Figures (4.2.1)-(4.2.3) show snapshots of the grid positions and pressure contours at particular times. All calculations assume that the situation is axi-symmetric so the grid represents a cross-section through the axis of symmetry.

figure	Re[a]	δt	number of steps
4.2.1	1.0	0.05	25
4.2.2	0.1	0.005	250
4.2.3	0.01	0.0005	2500

[a]An increase in viscosity corresponds to a decrease in Reynolds number

The most obvious difference between the three flows considered is that as the viscosity increases larger pressures and pressure gradients are produced. This is not unexpected, because the downward velocity of the plunger, which drives the flow, was chosen to be a fixed constant, hence larger forces, i.e. pressure gradients, are needed to force the more viscous liquid to move. The increase in internal pressure would be important if it became large enough to influence the movement of the plunger, how large depends on the power

available in the particular machine. In practice a glass of very high viscosity and too high an internal pressure can fracture as if it were an elastic solid.

There are other more subtle differences, these are most noticable at the free surface. Along the free surface the downward velocity is different in each of the three cases. At n.d.time=0.25 the average downward velocities are 1.32, 2.45 and 2.59 for Re=1.0, 0.1 and 0.01 respectively. The actual velocity profiles are shown in figure (4.2.4). In the more viscous flows more of the plunger's downward velocity is directly transfered to the fluid, rather than being converted to a mixture of outward and downward motion. There is a smaller difference between the Re=0.1 and Re=0.01 flows than between the Re=1.0 and Re=0.1 flows suggesting that there is a limit as the Reynolds number decreases. The larger downward velocity means that the first free surface node touches the bottom plate sooner, i.e. the gob spreads quicker. As time progresses this effect is masked because nodes are lost from the free surface making it more angular. The problem of losing nodes from the free surface is addressed in section (4.4). However, these examples do illustrate that the viscosity doesn't only influence the internal pressures, an expected effect, but also has more subtle effects on the motion of the liquid.

Computationally, the most striking feature is the decrease in numerical

stability. This is consistent with the condition quoted by Hirt et al.[28]

$$\delta t < c \times Re \tag{4.3}$$

where c is dependent on the grid. This is important because as the step size is decreased the CPU time is consequently increased. The situation illustrated in (4.2.1) where twenty-five steps were used took only a couple of minutes on an IBM 3018 Mainframe, whereas the situation in (4.2.3) with two thousand five hundred steps to cover the same amount of n.d.time took over three hours. This has obvious ramifications for the usability of the model in very low Reynolds number situations.

The numerical instabilities first manifest themselves in pressure oscillations. Figure (4.2.5) shows a comparison of the pressure history in one of the internal elements[1], the black line clearly shows the oscillations in the unstable case; these values were taken from a run with $Re = 0.1$ $\delta t = 0.01$ the red line shows the pressures from the same internal element from a run with a decreased time step $\delta t = 0.005$. If unchecked these oscillations grow until they cause the program to crash, an example of this growth is shown in figure (4.2.6) which is the internal pressure from a run with $Re = 0.01$ $\delta t = 0.001$.

More discussion of numerical instabilities can be found in appendix A.

[1]A similar pressure behaviour is observed in all the elements, an internal element was chosen as a representative example.

FIGURE 4.2.1 REYNOLDS NUMBER = 1.0

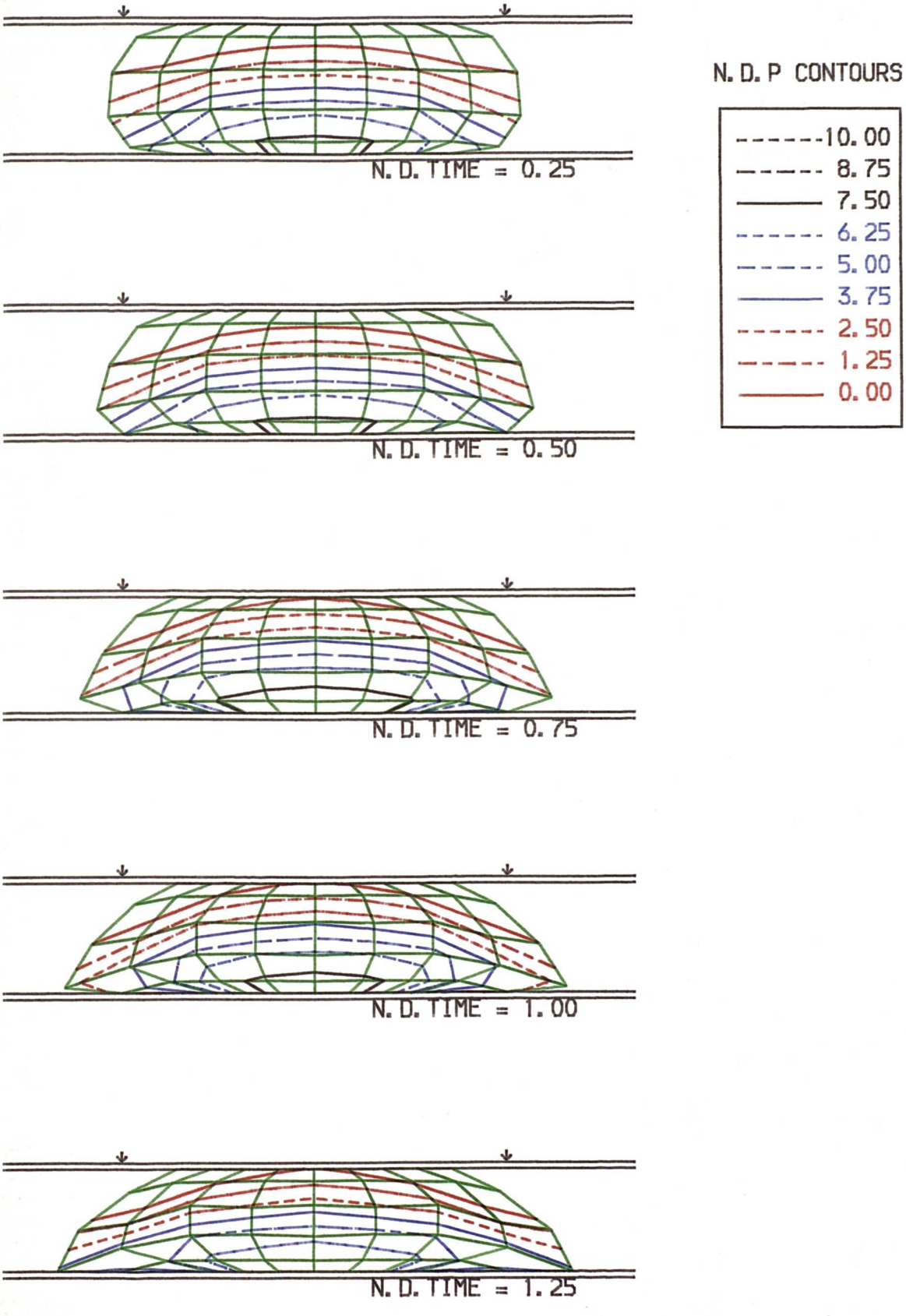

FIGURE 4.2.2 REYNOLDS NUMBER = 0.1

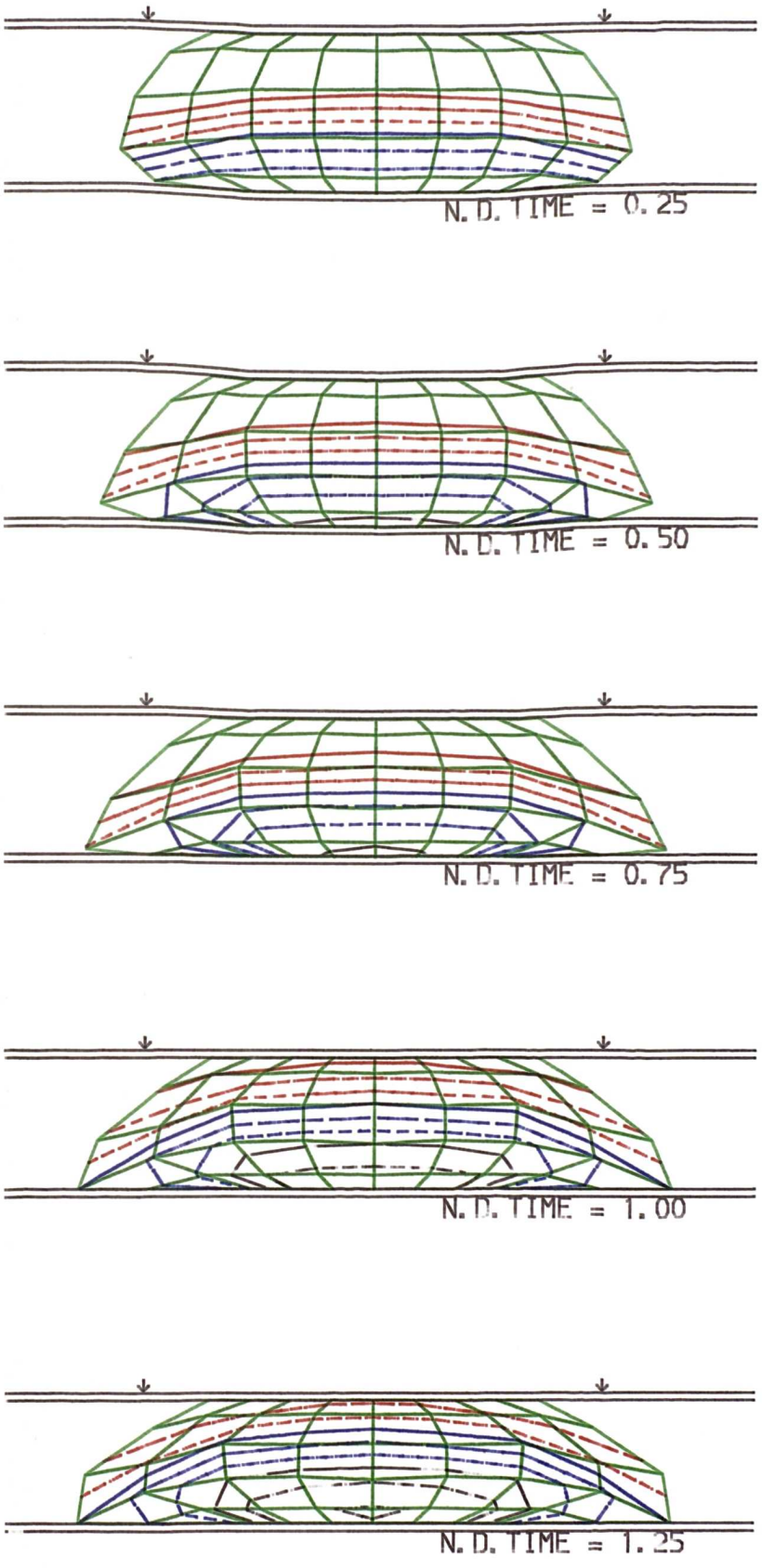

N. D. P CONTOURS

-80.00
-70.00
-60.00
-50.00
-40.00
-30.00
-20.00
-10.00
0.00

FIGURE 4.2.3 REYNOLDS NUMBER = 0.01

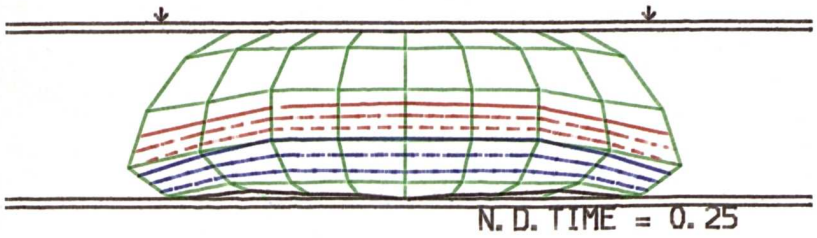

N. D. TIME = 0.25

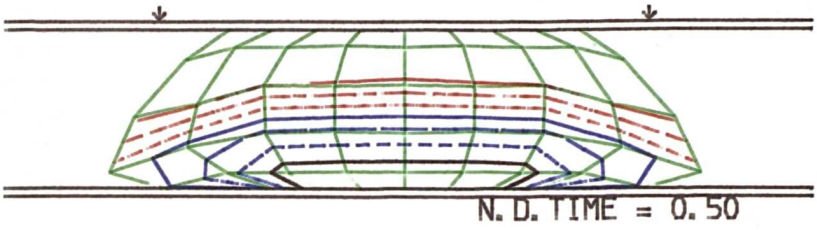

N. D. TIME = 0.50

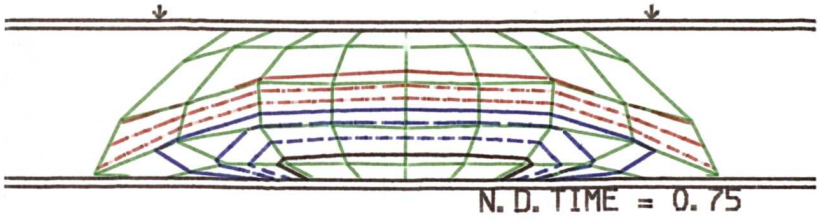

N. D. TIME = 0.75

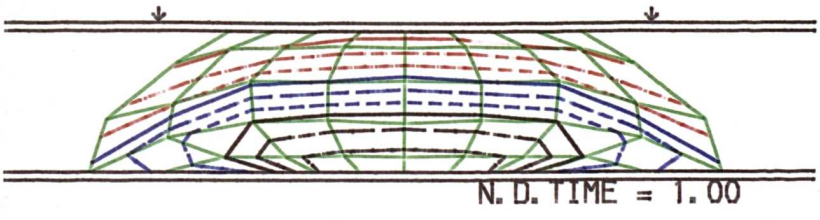

N. D. TIME = 1.00

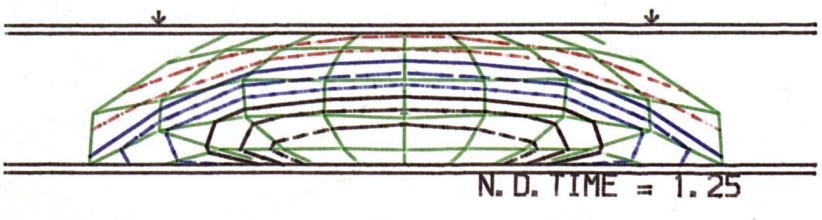

N. D. TIME = 1.25

N. D. P CONTOURS

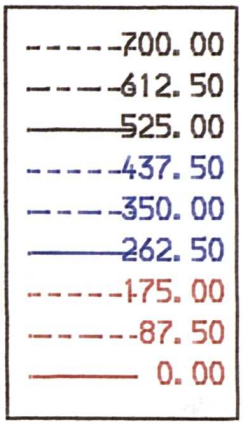

Figure 4.2.4 Downward Velocity along Free Surface

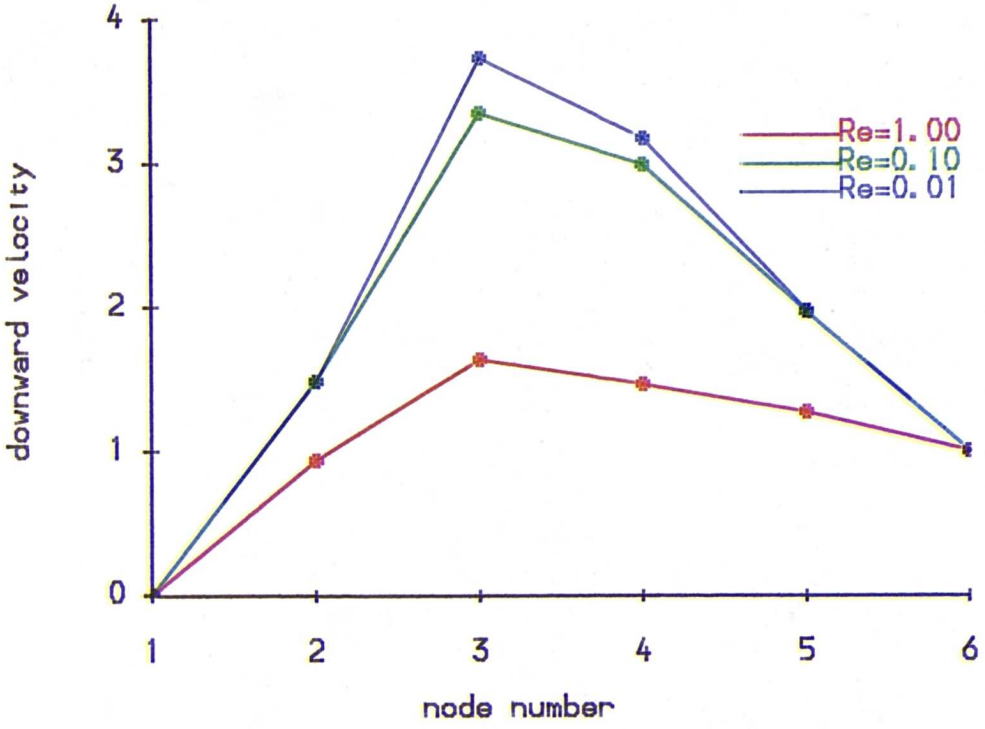

Node Numbering

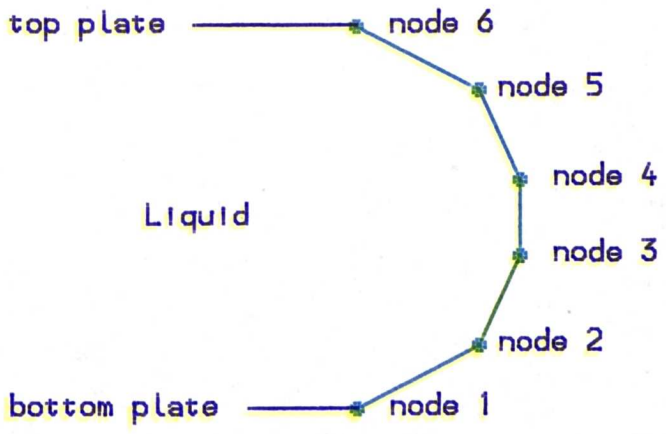

Figure 4.2.5 Pressure in 13th Element

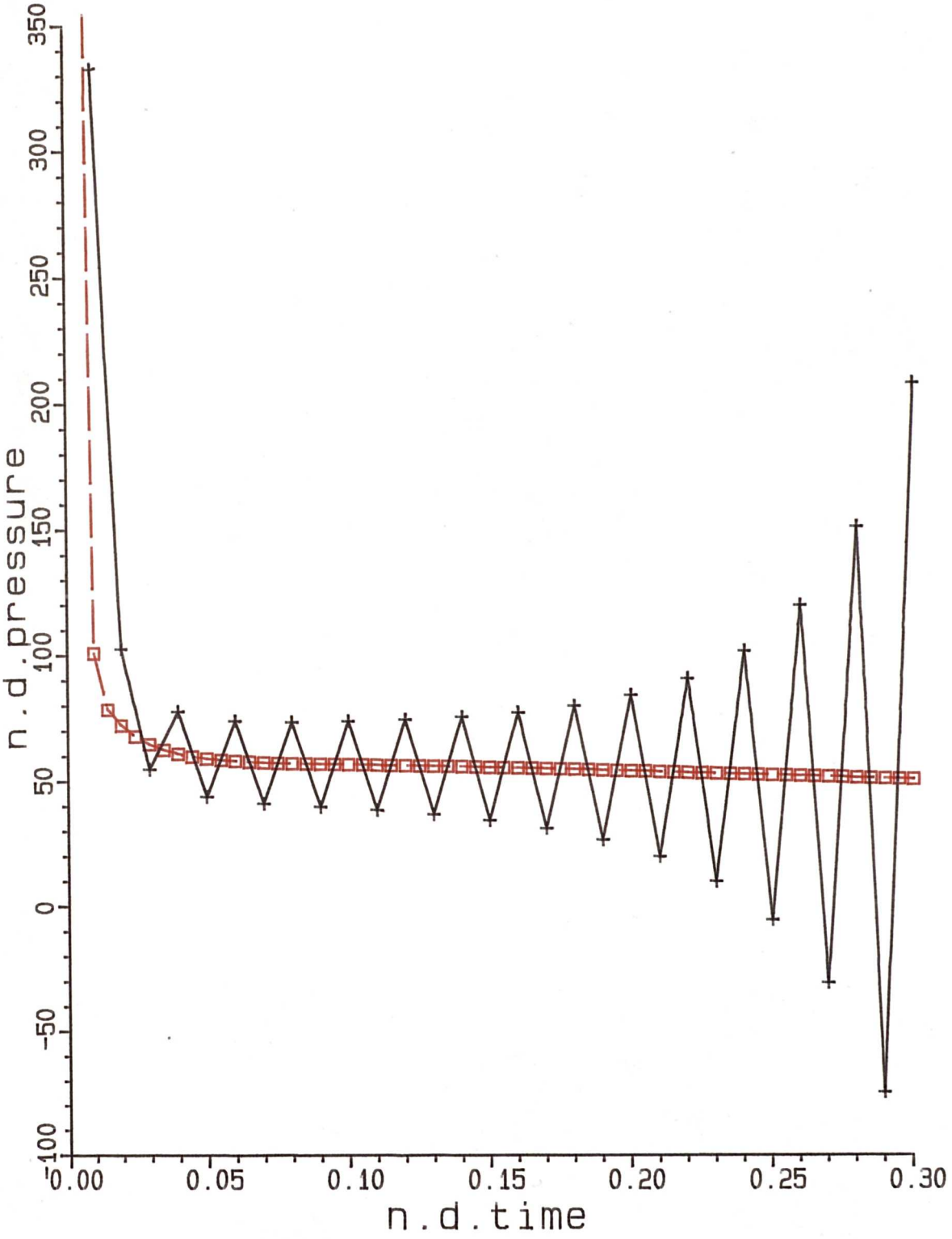

Figure 4.2.6 Pressure in 13th Element

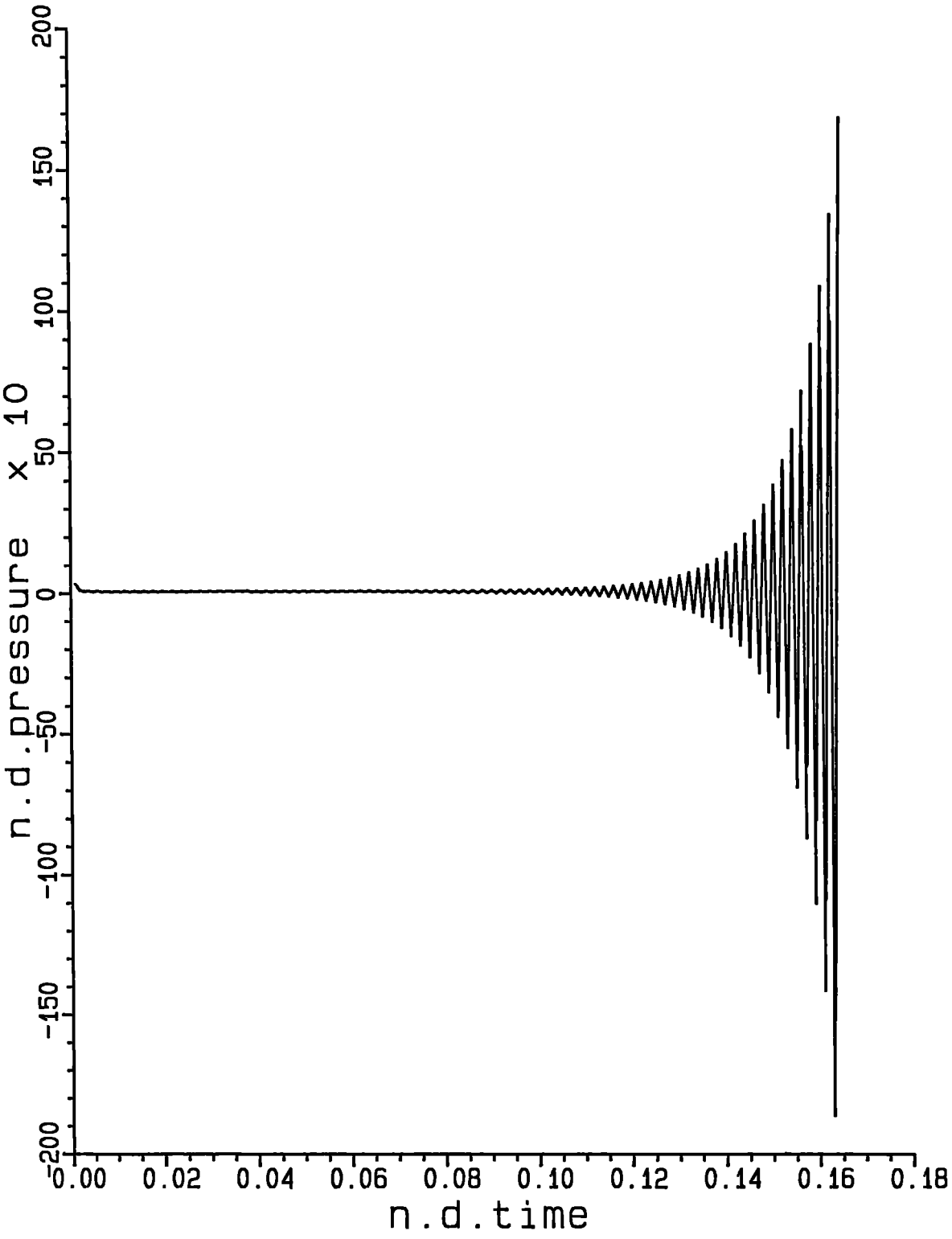

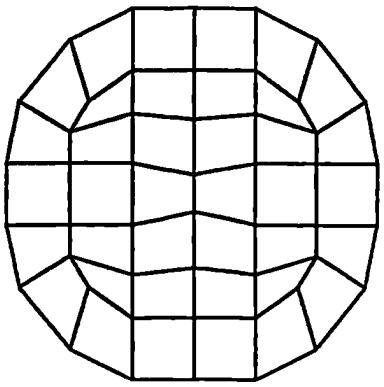

Grid used in section 4.3

4.3 Effect of Surface Tension and Weight

In this section the model is used to predict the steady-state shape of a blob of molten glass placed on a flat plate. The equilibrium heights reflect the altered surface tension to weight balance. To model such a situation requires a slightly different grid configuration from that used in the previous case, also, care has to be taken when applying the free surface boundary conditions at the axis of symmetry.

The roughly spherical gob of glass is assumed to have been placed on a plate and to have no initial velocity.

Wb	$\frac{1}{Fr}$	$Wb \times Fr$	equilibrium height
0.5	0.3	1.67	2.67
1.0	0.3	3.33	3.13
2.5	0.4	6.25	3.50
2.0	0.2	10.00	3.96
3.0	0.2	15.00	4.11
1.0	0.0	∞	5.26

The final height of the droplet will depend on the balance between the surface tension which is 'holding the liquid up' and the weight which is 'pulling the liquid down'. It is assumed that there is no interaction between the liquid and the plate it is resting upon.

The relevant parameter[2]is $\frac{\sigma}{\rho g}$; $\frac{\sigma}{\rho g} \rightarrow \infty$ represents a very light material, a low gravity situation or large surface tension and in this case the shape will be approximately spherical; $\frac{\sigma}{\rho g} \rightarrow 0$ represents a situation with low surface tension or a very heavy fluid and the droplet should spread to form a thin film.

Figure (4.3.1) shows in outline the final static positions of the grid in

[2]see chapter 2 section 2

the first five cases from the table above, figure (4.3.2) shows the relationship between the equilibrium heights and Weber× Froude for the same cases. The parameter Wb×Fr is chosen because

$$\frac{\sigma}{\rho g} \propto \frac{\sigma}{L\rho U_0^2}\frac{U_0^2}{gL} = Wb \times Fr$$

The graph suggests that the height is an increasing function of Wb×Fr. The calculated height 5.26 for Wb×Fr=∞ gives an upper bound for the function. Wb×Fr=∞ represents the gravity free situation, i.e. where $\frac{1}{Fr} = 0$ here the liquid should take up a position as near to a sphere as is possible[3]. In the gravity free situation the equilibrium height can be calculated analytically, this height of 5.48 compares reasonably with that of 5.26 from the grid calculation. Theoretically, when Wb×Fr=0 the liquid should spread to form a infinitely thin film, however calculations for small values of Wb×Fr are difficult because the grid becomes very distorted.

These results have been useful in confirming the effects of altering the Weber and Froude numbers. Experimentally the equilibrium of a droplet of liquid on a plate is important because it provides a method of calculating the surface tension. Details of this procedure called the 'sessile drop method', can be found in a book edited by Bockris et al.[6].

[3]Given a fixed finite contact area with the plate.

FIGURE 4.3.1 EQUILIBRIUM PROFILES

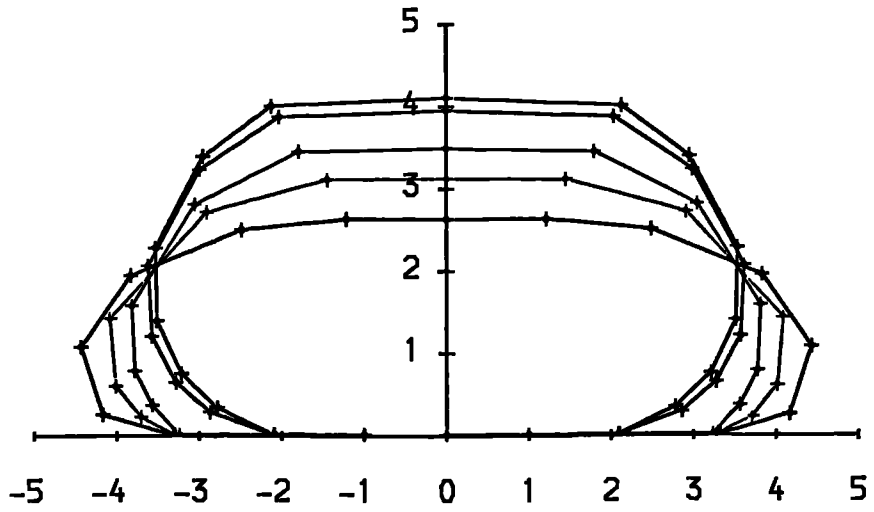

FIGURE 4.3.2 EQUILIBRIUM HEIGHT AGAINST WEBER X FROUDE

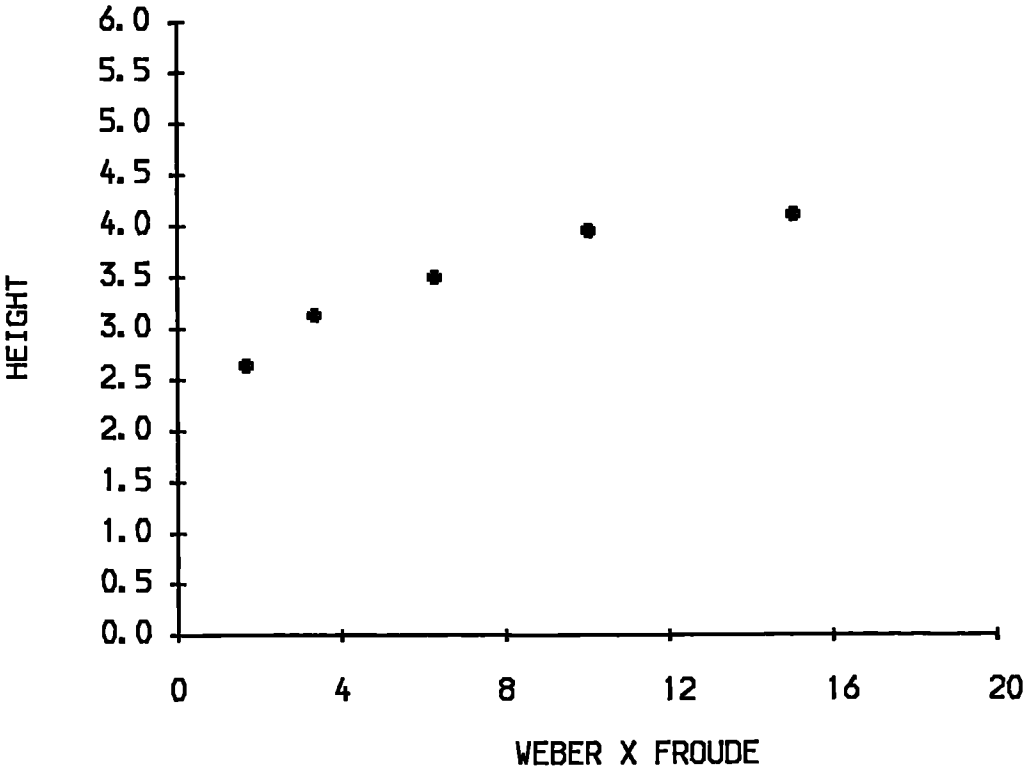

4.4 Remeshing

As each surface node touches a solid boundary it sticks to that boundary, hence as time progresses nodes are lost from the free surface. The smaller the number of nodes on the free surface the worse the piecewise linear approximation is to the actual curve. If this process is allowed to continue as in figure (4.4.1) the boundary becomes increasingly angular and a less acceptable approximation to the liquid being modelled. The free surface was initially described by five straight line segments, when the n.d.time=1.8 the surface is approximated by three segments, by n.d.time=2.5 only two segments are used. Eventually a singular matrix for the volume conservation becomes inevitable. This situation can be prevented by introducing a remeshing procedure. Remeshing is also used to combat grid distortion, the interpolation functions used are only appropriate for convex elements, non-convex elements such as those in figure (4.4.2) have non-positive Jacobians and must be avoided. The remeshing process redraws the grid and interpolates to find the new nodal velocities. Figure (4.4.3) shows the effect of using a model incorporating a simple remeshing scheme, which is triggered by a surface node touching the boundary, to model the same situation. It can be seen that thoughout the calculation five line segments are used to

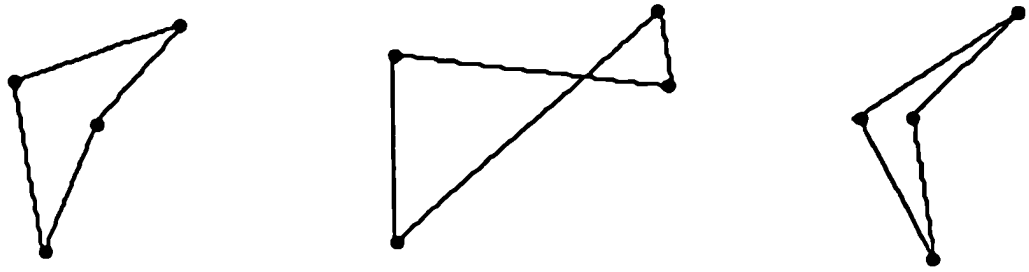

Figure 4.4.2 Non-Convex elements

describe the free surface giving a far more realistic approximation.

Many remeshing schemes are available, the one used here places the nodes equidistant along the surfaces and then calculates the new positions of the internal nodes. More details of the remeshing procedure can by found in appendix B.

FIGURE 4.4.1 GRID DISTORTION

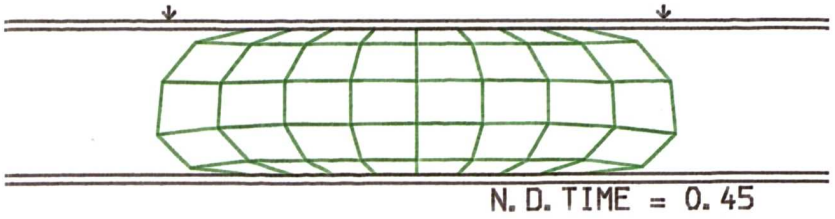

N. D. TIME = 0.45

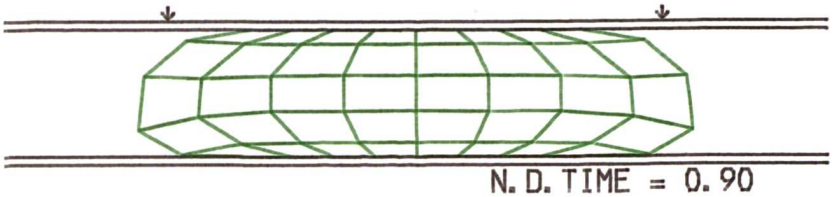

N. D. TIME = 0.90

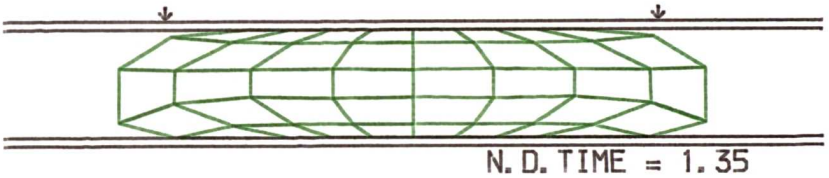

N. D. TIME = 1.35

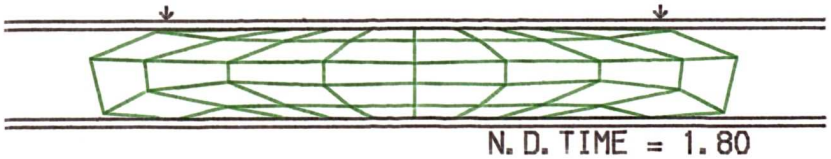

N. D. TIME = 1.80

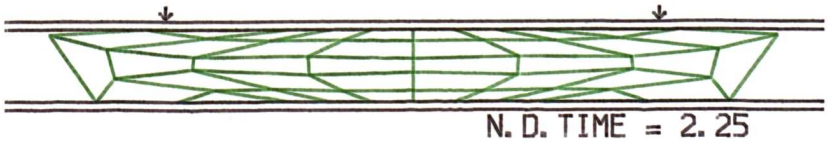

N. D. TIME = 2.25

FIGURE 4.4.3 CALCULATION WITH REMESHING

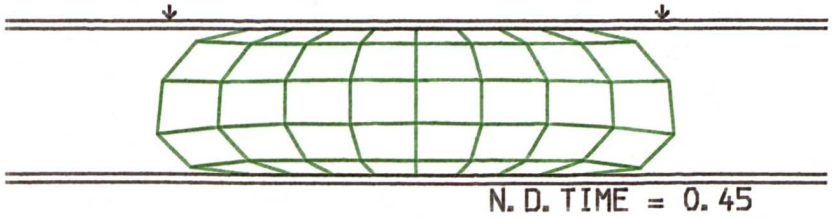

N. D. TIME = 0.45

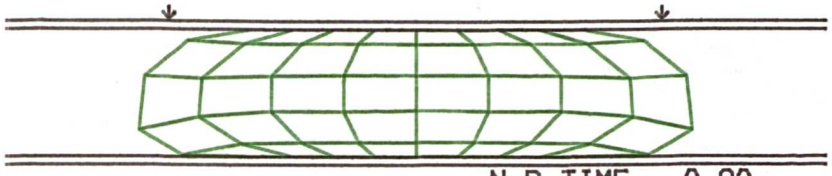

N. D. TIME = 0.90

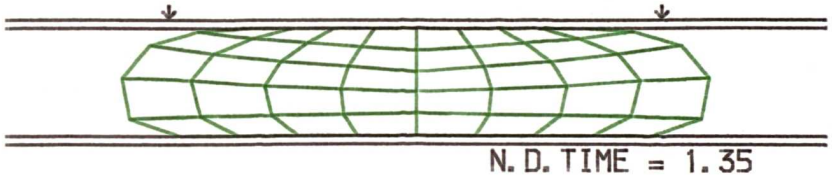

N. D. TIME = 1.35

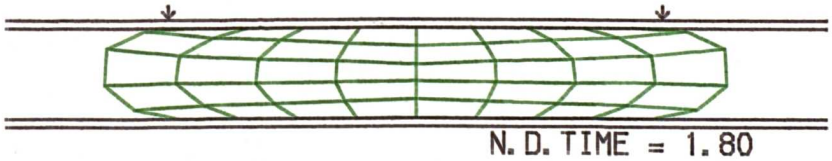

N. D. TIME = 1.80

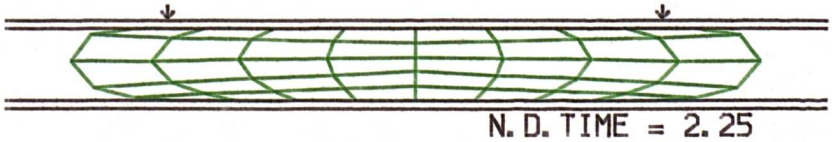

N. D. TIME = 2.25

4.5 Central Approximations

Once a suitable remeshing procedure has been introduced there is no theoretical reason why the model representing a gob of glass being pressed between two flat plates, such as the situation described in section (4.2), cannot be continued until a large very thin plate is produced. The disadvantage is that a large number of elements would be needed; increasing the computer time used. However, there exists a model for the flow of glass at the centre of a disc, it is provided by the 'squeeze film' approximation, described in chapter 3. This approximation can be used as the boundary condition on the interior of a hollow cylinder of elements, reducing the CPU time needed and allowing the computational effort to be concentrated on the area of interest.

For example, figure (4.5.1) shows the result of using a forty-five element grid to model a simple pressing operation[4]. The model was run for a short time until a reasonably stable velocity field was set up within the glass. This velocity field is very regular in the central portion of the grid. Figure (4.5.2) shows the results obtained when a twenty element hollow grid with a central 'squeeze film' approximation was used to model the same situation. Figures (4.5.3) and (4.5.4) show comparisons of the r and z velocities from

[4]The plunger moving at a constant downward velocity U_0, $Re = 1.0$, $Fr = 10.0$, $Wb = 1.0$.

along the free surfaces in the case where a central approximation is used, shown in red, and the case where the predictions are obtained on a full grid, shown in green. The maximum variation[5] between the two calculated cases is 13% with an average value of 3%. Figure (4.5.5) shows the non-linear relationship[6]between the number of elements used and the CPU time for a single step[7]. The CPU time for the twenty elements used in (4.5.2) was $\approx$ 10% of that needed by the forty-five elements used in (4.5.1). This is a substantial saving making the 'patching together' of any suitable analytical solutions with the numerical model computationally economical, though not as accurate.

[5]variation between u_1 and u_2 is taken as

$$\frac{absolute(u_1 - u_2)}{maximum(u_1, u_2)} \times 100\%$$

[6]time $\approx$ constant (number of elements)^3

[7]The times depend to some extent on the proportion of the nodes on the free surface, the times show are the average taken over ten successive steps using roughly 'square' grids.

FIGURE 4.5.1 CALCULATION WITH FULL GRID

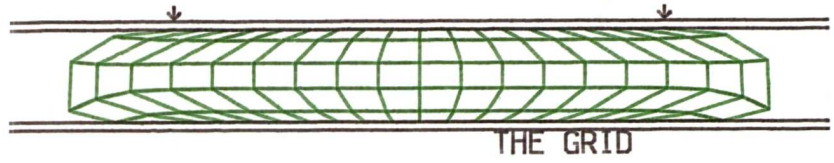

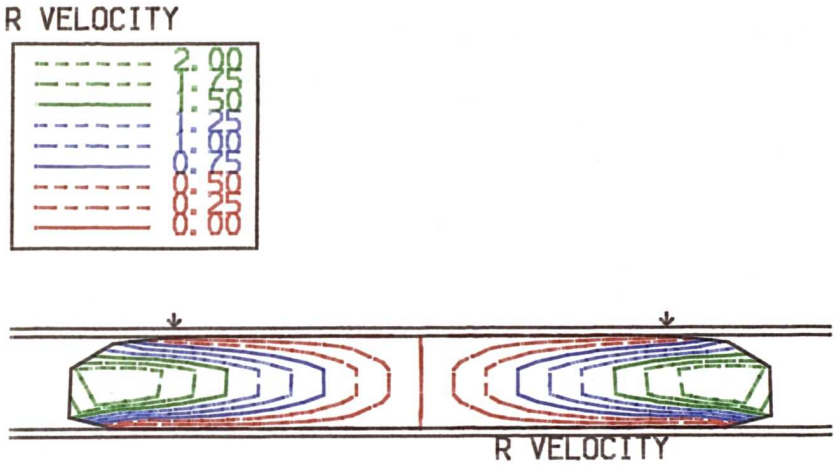

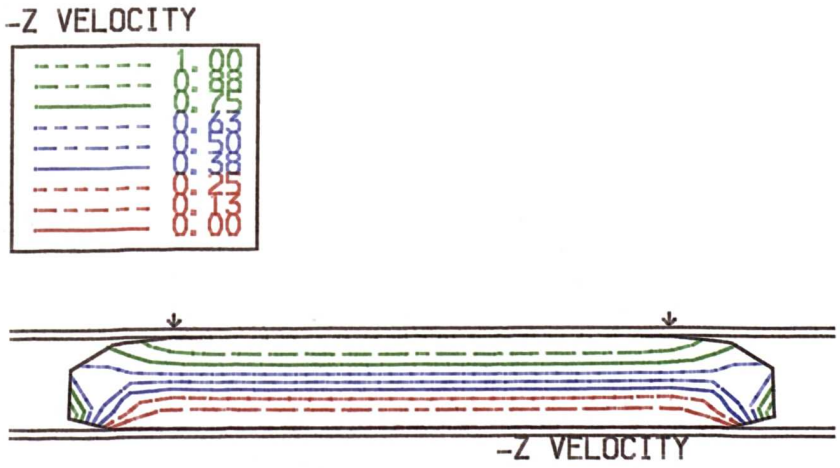

FIGURE 4.5.2 CALCULATION WITH CENTRAL APPROX.

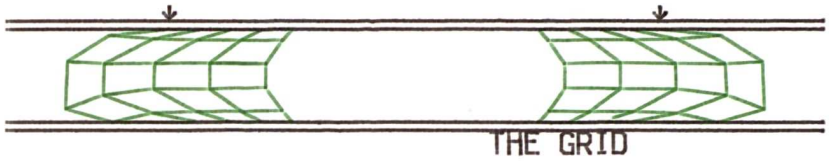

THE GRID

R VELOCITY

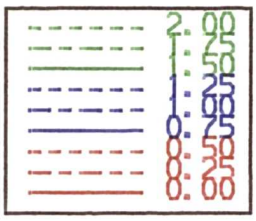

R VELOCITY

-Z VELOCITY

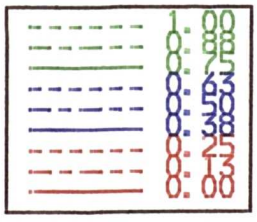

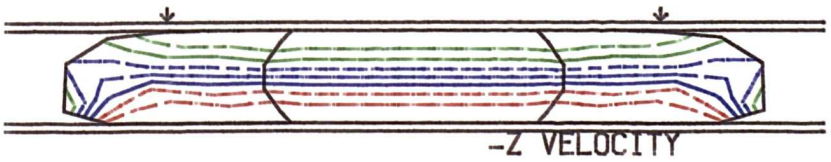

-Z VELOCITY

Figure 4.5.3 Outward velocities

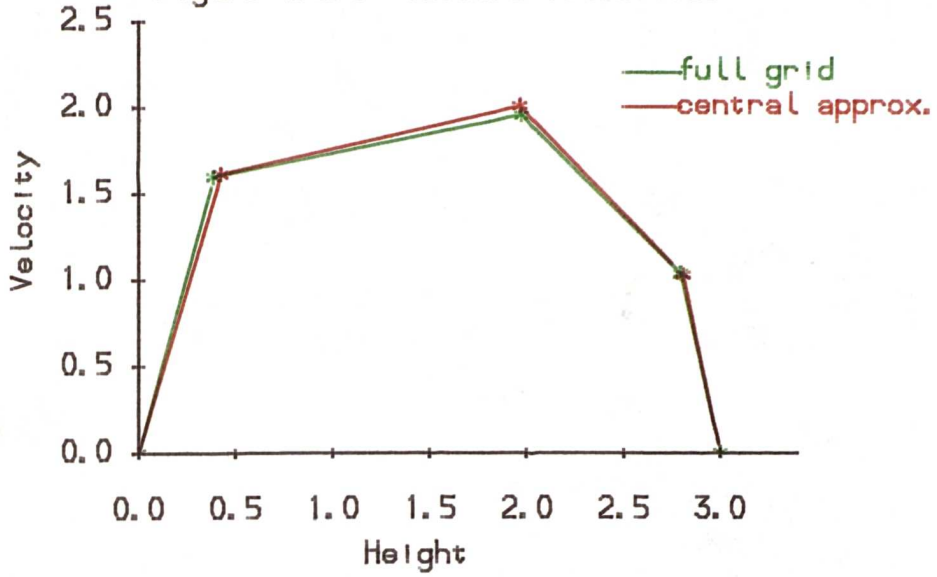

Figure 4.5.4 Downward velocities

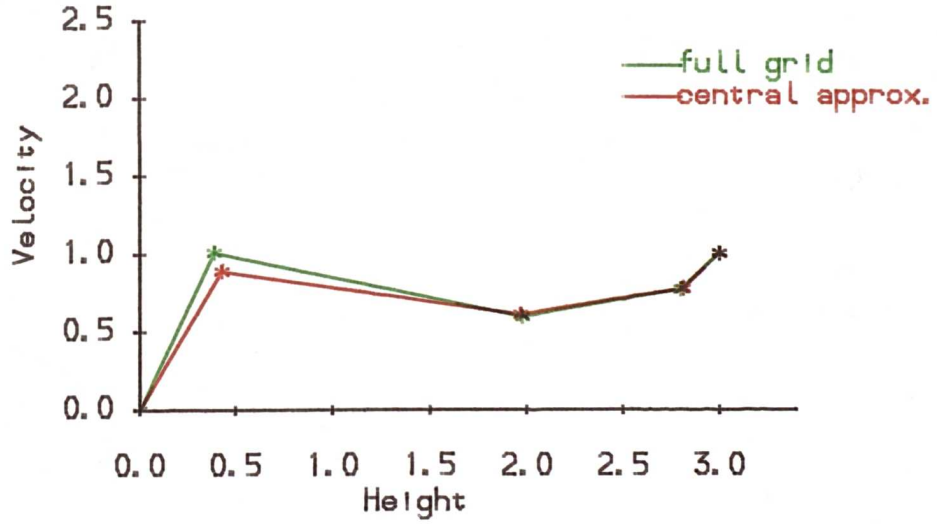

Figure 4.5.5 CPU time v Number of Elements

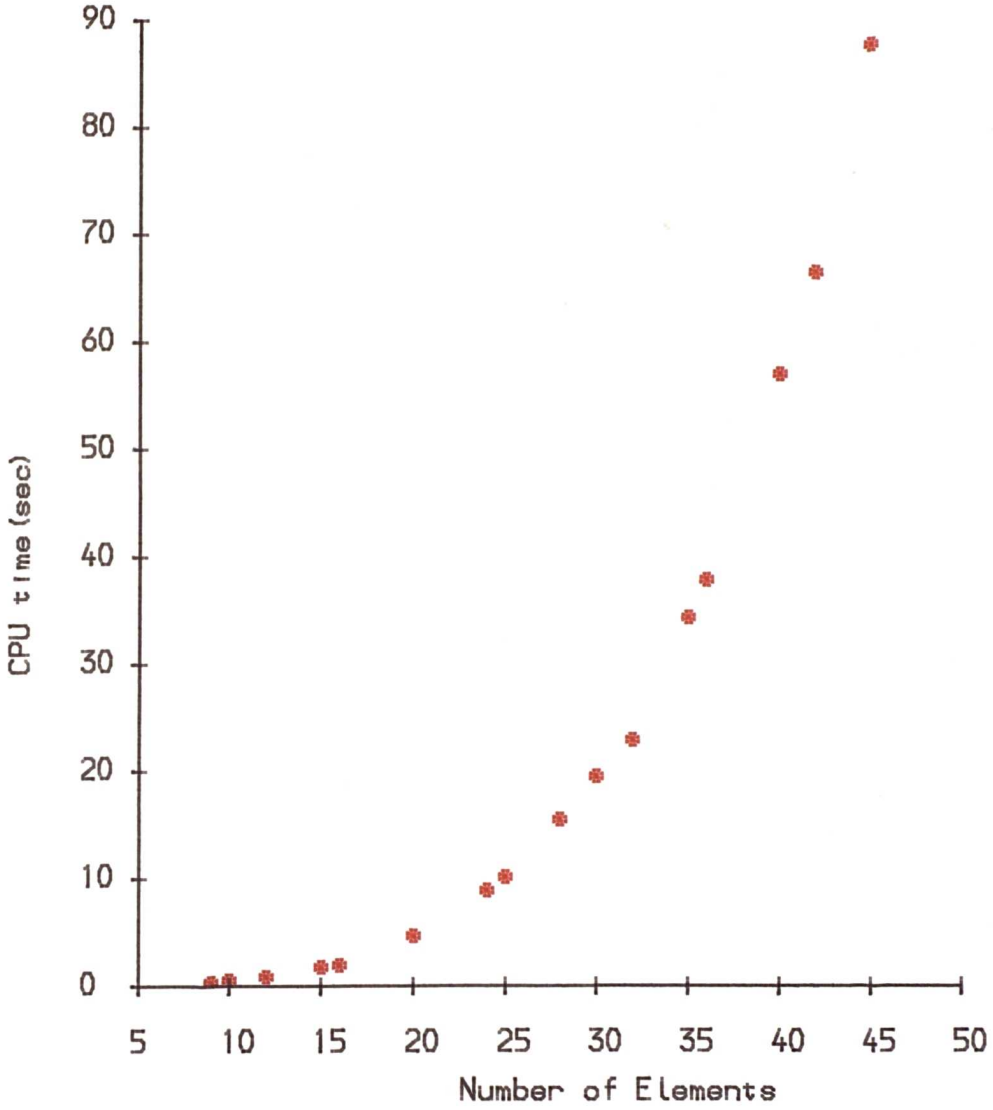

4.6 Different Mould Shapes

In reality glass is rarely pressed between two parallel flat plates, it is more likely that both the mould and plunger will be shaped. Figure (4.6.1) shows the result of the model being used to represent a gob of glass settling into a bowl shaped mould. The glass is given an initial downward velocity of $0.9U_0$ to represent the fact that the gob would have fallen into the mould rather than been placed on it, the other parameters are Re = 1.0, Fr=10.0, Wb=1.0. Figure (4.6.2) shows its deformation when pressed by a shaped plunger moving at a constant downward velocity, U_0. Different shapings can easily be accommodated. However, the grid can only form a piecewise linear approximation to the desired shape. Hence, the accuracy of the fit depends on the size of the elements and the rates of change in gradient of the solid surfaces. Sharp angular corners of a mould will always prove a difficulty for a moving grid model as there is no guarantee that a node will coincide exactly with the corner. These considerations need to be borne in mind when the number and size of the elements is chosen. In practice the mould and plunger shapes are restricted by the need to remove the finished article and tend to be smoothly curved.

FIGURE 4.6.1 GOB SETTLING INTO A SHAPED MOULD

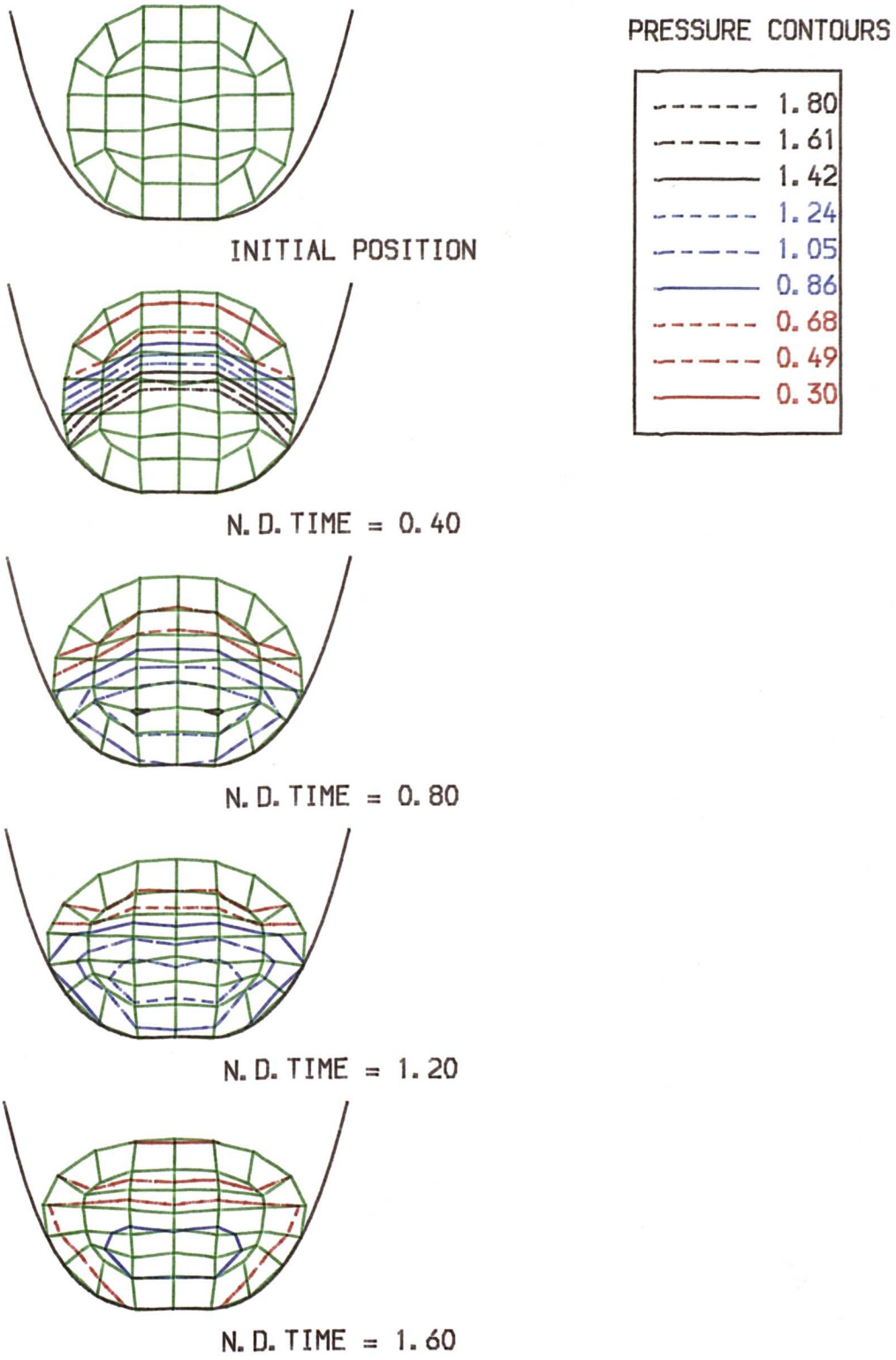

FIGURE 4.6.2 PRESSING OF GOB

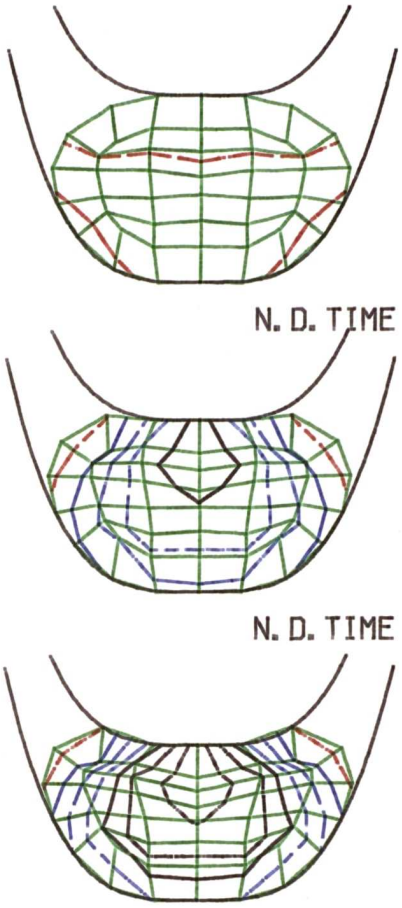

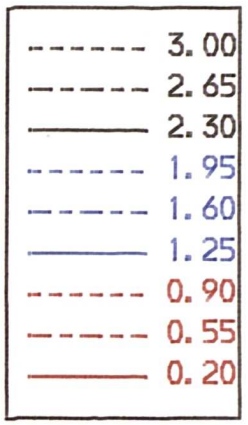

Chapter 5

Temperature Dependence

5.1 Introduction

Up to this point the model has only dealt with isothermal cases, that is ones in which the temperature is constant throughout the fluid. The existence of a non-uniform temperature field cannot be ignored because the temperature and flow fields are coupled via the temperature-viscosity relationship. In this chapter consideration is given to the appropriate form of the temperature field and how its effect can be built into the finite element flow model developed previously.

The temperature field satisfies the energy equation, the axi-symmetric non-dimensional form of this equation was given in chapter two and is re-

called here.

The Energy Equation

$$\frac{\partial T}{\partial t} + u\frac{\partial T}{\partial r} + w\frac{\partial T}{\partial z} = \frac{1}{Pe}\left(\frac{\partial^2 T}{\partial r^2} + \frac{1}{r}\frac{\partial T}{\partial r} + \frac{\partial^2 T}{\partial z^2}\right) \tag{5.1}$$

with

$$Pe = \text{Peclet number} = \frac{LU_0\rho c}{\lambda} \tag{5.2}$$

where all the symbols have their usual meaning[1]. As with the Navier-Stokes equation, there are analytical solutions to the energy equation under certain conditions, for example Carslaw[10] gives solutions when the fluid is stationary, but none of the available analytic solutions accurately fit this dynamic situation. Therefore, numerical methods have to be used.

5.2 Form of the Temperature Field

There are no analytical solutions to the energy equation suitable for calculating a dynamic axi-symmetric temperature field, but information about the role of the Peclet number and the form of the temperature field can be gleaned from consideration of a one dimensional situation, which has an

[1] the starred notation has been dropped

analytic solution. The system governed by

$$\frac{\partial T}{\partial t} = \frac{1}{Pe}\frac{\partial^2 T}{\partial x^2} \text{ for } x > 0 \tag{5.3}$$

with boundary conditions of[2]

$$T = 1 \text{ at } t = 0$$

$$T = 0 \text{ at } x = 0 \text{ for } t > 0 \tag{5.4}$$

has solution

$$T = erf\left(\frac{x}{2}\sqrt{\frac{Pe}{t}}\right) \tag{5.5}$$

Figure (5.2.1)[3] shows this function plotted for various values of $K = \frac{1}{2}\sqrt{\frac{Pe}{t}}$, it can be seen that for large values of this parameter, temperature field consists of a small region near $x = 0$ with rapid temperature changes and a larger region with $T \approx 1$. The Peclet number for molten glass is very large and the times involved in a pressing operation are small, this implies that the majority of the cooling will be confined to a thin boundary skin, with very little temperature variation in the interior.

[2]the condition $T = 0$ at $x = 0$ is the most extreme case of Newton cooling $H \to \infty$
[3]generated using the NAG routine S15AEF

Figure 5.2.1 The Error Function

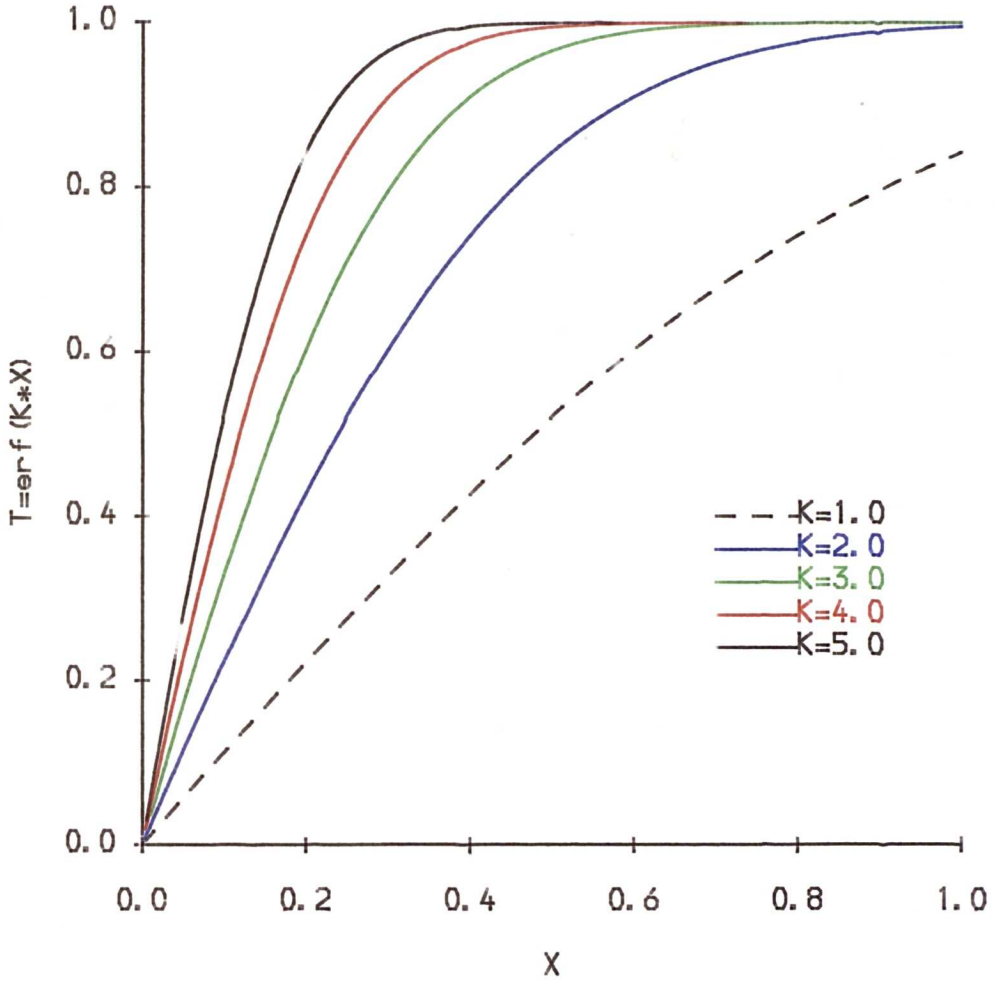

5.3 Finite Element Implementation

When the finite element flow model was constructed the Reynolds number was not assumed to be a constant. Therefore, the existing flow model can accommodate a variable viscosity. Once the temperature field has been calculated no further alterations are needed.

It is relatively straightforward, following the procedure outlined in Chapter 3, to calculate the temperature field using a finite element method. It can be based on the same grid as that used in the flow calculation with the temperature varying bilinearly across each element. However, this is computationally very time consuming. In view of the form of the temperature field it is also inefficient and inaccurate. A full finite element calculation will be inefficient since the temperature changes in the internal elements will be negligible. Unless the size of the boundary elements is comparable with that of the cooled skin, i.e. very small, then the linear approximation for the temperature will greatly over estimate the cooling. This over estimation as well as being inaccurate would exacerbate the instability problems noted in Chapter 4.

If the computing time was unimportant a f.e model for the temperature based on a smaller grid with a quadratic or even cubic interpolation function

for temperature could be used. However, it was decided to capitalize on the information as to the nature of the temperature field and look for an alternative approach.

5.4 Boundary Approximation

5.4.1 Introduction

The physical situation is such that the changes in temperature at the centre of the gob of glass are negligible compared with the temperature changes near the glass/metal or glass/air interface. The aim, in this section, is to use this information to simplify the system allowing all the effects of the temperature variations at the boundaries to be encapsulated in an augmented boundary condition.

Firstly, a simple one dimensional system is considered.

5.4.2 1-d System

If a very simple 1-d system is considered where there is a semi-infinite liquid (liquid A), coated with a thin film of another liquid (liquid B) that has a different viscosity. If there are no body forces present, and the viscosities of each liquid are constant but different, then the Navier-Stokes equations

simplify to give

for liquid B, $-\ell < x < 0$

$$\frac{\partial \tau_B}{\partial x} = \frac{\partial u_B}{\partial t} \tag{5.6}$$

for liquid A, $0 < x$

$$\frac{\partial \tau_A}{\partial x} = \frac{\partial u_A}{\partial t} \tag{5.7}$$

the stress boundary conditions are

$$u_B(0,t) = u_A(0,t)\ ,\ \tau_B(0,t) = \tau_A(0,t) \tag{5.8}$$

$$\tau_B(-\ell,t) = F \tag{5.9}$$

where F is a known function of x and the surface tension, τ is the stress. If the pressure is taken to be constant, the stresses are then dependent only on velocity and viscosity, and the system becomes

$$\frac{2}{Re_B}\frac{\partial^2 u_B}{\partial x^2} = \frac{\partial u_B}{\partial t} \text{ for } -\ell < x < 0 \tag{5.10}$$

$$\frac{2}{Re_A}\frac{\partial^2 u_A}{\partial x^2} = \frac{\partial u_A}{\partial t} \text{ for } 0 < x \tag{5.11}$$

with

$$u_A(0,t) = u_B(0,t)\ ,\ \frac{1}{Re_A}\frac{\partial u_A(0,t)}{\partial x} = \frac{1}{Re_B}\frac{\partial u_B(0,t)}{\partial x} \tag{5.12}$$

$$\frac{2}{Re_B}\frac{\partial u_B(-\ell,t)}{\partial x} = F \tag{5.13}$$

Laplace Transform method If the extra boundary condition of

$$\frac{\partial u_A(x,t)}{\partial x} \to 0 \text{ as } x \to \infty \tag{5.14}$$

is introduced the system can be solved by using Laplace transforms to eliminate the time dependence[4]. The solution obtained by this method is

$$\overline{u_A} = \frac{2F\exp(-k_A x)}{\frac{-k_A}{Re_A}(\exp(k_B\ell)+\exp(-k_B\ell)) + \frac{k_B}{Re_B}(\exp(-k_B\ell)-\exp(k_B\ell))} \tag{5.15}$$

where, $k_B = \sqrt{\frac{pRe_B}{2}}$, $k_A = \sqrt{\frac{pRe_A}{2}}$.

If there is no surface film, i.e. $\ell = 0$, then equation (5.15) would be the solution of equation (5.11) with the boundary condition

$$\frac{2}{Re_A}\frac{\partial u_A(0,t)}{\partial x} = F$$

The expression given in (5.15) can be expanded in powers of ℓ. If the surface film was thin, i.e. $\ell \neq 0$ but $\ell^2 \ll \ell$, then (5.15) would give (neglecting terms $O(\ell^2)$).

$$\overline{u_A} = \frac{F\exp(-k_A x)}{\frac{-2k_A}{Re_A} - \frac{2k_B^2\ell}{Re_B}} \tag{5.16}$$

this is a solution of (5.11) with the boundary condition

$$\frac{2}{Re_A}\frac{\partial u_A(0,t)}{\partial x} - \ell\frac{\partial u_A(0,t)}{\partial t} = F \tag{5.17}$$

[4] $\overline{u}(p,x)$ is the transform of $u(t,x)$

since

$$\frac{\partial u_A}{\partial t} = \frac{2}{Re_A}\frac{\partial^2 u_A}{\partial x^2} \tag{5.18}$$

equation (5.17) becomes

$$\underbrace{\frac{2}{Re_A}\frac{\partial u_2(0,t)}{\partial x}}_{\tau_A(0,t)=F} = F + \underbrace{\frac{2\ell}{Re_A}\frac{\partial^2 u_2(0,t)}{\partial x^2}}_{\text{'extra' term}} \tag{5.19}$$

This is the type of alternative boundary condition that is being sought, the 'extra' term represents the approximate effect a thin cooled layer would have on the bulk flow.

The Laplace transform method can only be applied in very simple cases, however, a more physical argument can be developed which gives results consistent with those obtained above but is readily extended to a more general case.

Physical Argument Considering the one dimensional situation described in the previous section by equations (5.6)-(5.9). The stress is a continuous function and if it is assumed that it is sufficiently differential then it can be expanded. For example

$$\tau(0,t) = \tau(-\ell,t) - \sum_{i=1}^{\infty}\frac{(-\ell)^i}{i!}\frac{\partial^i \tau(0,t)}{\partial x^i} \tag{5.20}$$

The free surface stress $\tau(-\ell, t)$ is known, giving a boundary condition of

$$\tau(0,t) = F - \sum_{i=1}^{\infty} \frac{(-\ell)^i}{i!} \frac{\partial^i \tau(0,t)}{\partial x^i} \tag{5.21}$$

This is a more general form of the boundary condition (5.19) obtained using the Laplace transform method; (5.19) can be obtained from (5.21) by curtailing the series and substituting in the assumed forms of the stresses.

This physical argument is more readily extended to the 3-d case where the viscosity varies near the surface.

5.4.3 3-d Case

The 3-d system used is axi-symmetric and expressed in terms of cylindrical polar co-ordinates, so only the components in the r and z direction need be considered.

The situation under consideration, illustrated in figure (5.1), is where there is a thin cooled layer, thickness ℓ, surrounding a larger area of isothermal liquid. In the bulk of the liquid, $n < a$, the Reynolds number is Re_2. At $n = b$ the Reynolds number is Re_2 but at the free surface, $n = c$, it is Re_1. The stress conditions are now in terms of the normal stress, τ_n. At the internal boundary between the isothermal area and the non isothermal

area the normal stress is continuous, i.e.

$$\tau_n(a) = \tau_n(b) \tag{5.22}$$

At the free surface the normal stress depends on the surface configuration and surface tension, i.e..

$$\tau_n(c) = F \tag{5.23}$$

The stress now needs to be expanded, there are two obvious expansions

$$\tau_n(c) = \tau_n(a+\ell) = \tau_n(a) + \ell\tau_n'(a) + \ldots$$

and

$$\tau_n(a) = \tau_n(c-\ell) = \tau_n(c) - \ell\tau_n'(c) + \ldots$$

These two expansions can be rearranged to give

$$\tau_n(a) = F + \sum_{i=1}^{\infty} \frac{(-\ell)^i}{i!} \frac{\partial^i \tau_n(c)}{\partial n^i} \tag{5.24}$$

$$\tau_n(a) = F - \sum_{i=1}^{\infty} \frac{(\ell)^i}{i!} \frac{\partial^i \tau_n(a)}{\partial n^i} \tag{5.25}$$

The normal stress is given by

$$\tau_n = \mathbf{n}^T \begin{bmatrix} -p + \frac{2}{Re}\frac{\partial u}{\partial r} & , & \frac{1}{Re}\left(\frac{\partial u}{\partial z} + \frac{\partial w}{\partial r}\right) \\ \frac{1}{Re}\left(\frac{\partial v}{\partial r} + \frac{\partial u}{\partial z}\right) & , & -p + \frac{2}{Re}\frac{\partial w}{\partial z} \end{bmatrix} \mathbf{n}$$

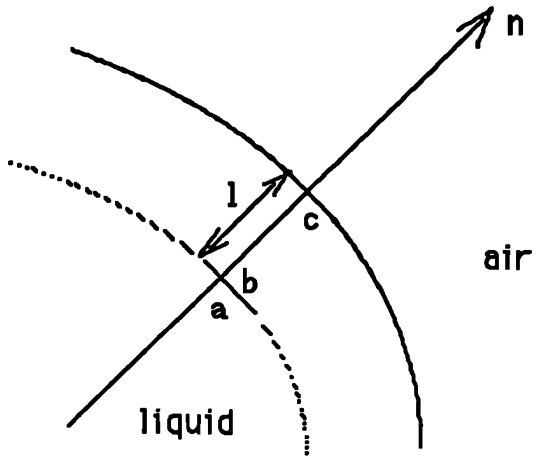

Figure 5.1 Fluid near the Free Surface

If the boundary layer is thin and it is known that the viscosity varies rapidly across it, then it is not unreasonable to assume

$$\frac{\partial Re}{\partial n} >> \frac{\partial u}{\partial n}, \frac{\partial w}{\partial n}, \frac{\partial p}{\partial n} \tag{5.26}$$

This together with the simplifying assumption that the variation in the Reynolds number across the boundary layer is linear, implies

$$\frac{\partial \tau_n}{\partial n} \approx \frac{(-1)^i i!}{Re^{i+1}} \left(\frac{\partial Re}{\partial n}\right)^i H(u, w, r, z) \tag{5.27}$$

where

$$H(u, w, r, z) = \mathbf{n}^T \begin{bmatrix} 2\frac{\partial u}{\partial r} & , & \frac{\partial u}{\partial z} + \frac{\partial w}{\partial r} \\ \frac{\partial w}{\partial r} + \frac{\partial u}{\partial z} & , & \frac{\partial w}{\partial z} \end{bmatrix} \mathbf{n}$$

This together with an approximation for the derivative gives

$$\frac{\partial \tau_n(a)}{\partial n} = \frac{(-1)^i i!}{Re_2^{i+1}} \left(\frac{Re_1 - Re_2}{-\ell} \right)^i H(u, w, r, z)$$
$$\frac{\partial \tau_n(c)}{\partial n} = \frac{(-1)^i i!}{Re_1^{i+1}} \left(\frac{Re_2 - Re_1}{\ell} \right)^i H(u, w, r, z) \qquad (5.28)$$

Substituting these back into (5.24) and (5.25) gives two possible forms of alternative boundary condition

$$\tau_n(a) = F - \frac{1}{Re_2} \sum_{i=1}^{\infty} \left(1 - \frac{Re_1}{Re_2} \right)^i H(u, w, r, z) \qquad (5.29)$$

$$\tau_n(a) = F + \frac{1}{Re_1} \sum_{i=1}^{\infty} \left(1 - \frac{Re_2}{Re_1} \right)^i H(u, w, r, z) \qquad (5.30)$$

These sums converge for $Re_1 < Re_2$ and $Re_1 > Re_2$ respectively. It can be shown [5] that both these sums have the limit

$$\tau_n(a) = F + \left(\frac{Re_1 - Re_2}{Re_1 Re_2} \right) H(u, w, r, z) \qquad (5.31)$$

This is essentially the geometric mean. Hence the alternative boundary condition (5.31) can be adopted, it will be valid for both cooling and heating of the surface.

5.4.4 Surface Temperature Approximation

For the alternative boundary condition outlined previously to be of use some method for finding the approximate temperature and hence Reynolds num-

[5] using $\sum_{i=1}^{\infty} x^i = \frac{x}{1-x}$ for $|x| < 1$

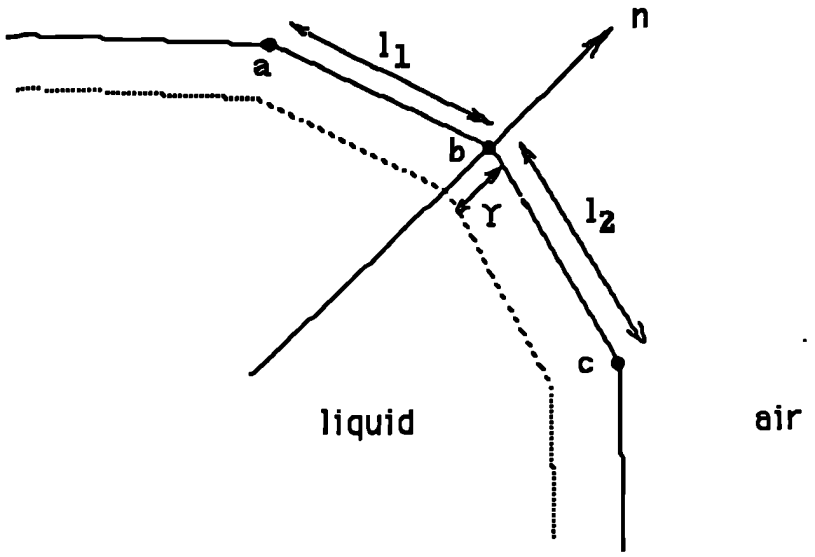

Figure 5.2

ber difference across the free surface is needed.

The simplest approximation would be to assume that the glass which was in contact with the mould is at the same temperature as the metal whereas there is no cooling across the free surface. This is only reasonable if the metal/glass heat transfer coefficient is large and the glass/air one is negligible which is not the case. Hence a simple approximation was used that calculated the surface temperature from the previous surface temperature, the position and step length. Consider the situation shown in figure (5.2).

The heat flow is governed by the equation

$$\frac{\partial T}{\partial t} = \frac{1}{Pe}\left(\frac{\partial^2 T}{\partial z^2} + \frac{\partial^2 T}{\partial r^2} + \frac{1}{r}\frac{\partial T}{\partial r}\right) \tag{5.32}$$

with the boundary condition at the surface of

$$\begin{aligned}\frac{\partial T}{\partial n} = & - \epsilon^* \left[(T + \frac{T_0 + 273}{T_{max} - T_{min}})^4 - (T_{am} + \frac{T_0 + 273}{T_{max} - T_{min}})^4\right] \\ & + H^*(T_{am} - T)\end{aligned} \tag{5.33}$$

The derivatives can be approximated to give

$$\begin{aligned}\frac{T_b^{i+1} - T_b^i}{\delta t} = \frac{1}{Pe}\Bigg(\frac{T_b^i - 1}{2\Upsilon} + \frac{T_a^i - 2T_b^i + T_c^i}{l_1 + l_2} & + \\ \frac{cos\phi}{r}\frac{T_b^i - 1}{\Upsilon} & + \frac{sin\phi}{r}\frac{T_a^i - T_c^i}{l_1 + l_2}\Bigg)\end{aligned} \tag{5.34}$$

and

$$\begin{aligned}\frac{T_b^i - 1}{\Upsilon} = & - \epsilon^* \left[(T_b^i + \frac{T_0 + 273}{T_{max} - T_{min}})^4 - (T_{am} + \frac{T_0 + 273}{T_{max} - T_{min}})^4\right] \\ & + H^*(T_{am} - T_b^i)\end{aligned} \tag{5.35}$$

Here subscripts refer to position superscripts to time and ϕ is the angle between the outward normal and the r direction, T_{am} is the temperature of the adjacent medium. These two equations contain two unknowns, Υ the thickness of the cooled film and T_b^{i+1} the new surface temperature, simple manipulation eliminates Υ to leave an approximation for the new surface

temperature.

$$
\begin{aligned}
T_b^{i+1} &= T_b^i - \frac{H^* \delta t}{Pe}\left(\frac{1}{2} + \frac{cos\phi}{r}\right)\left[T_{am} - T_b^i\right] \\
&- \frac{\epsilon^* \delta t}{Pe}\left(\frac{1}{2} + \frac{cos\phi}{r}\right)\left[(T_b^i + \frac{T_0 + 273}{T_{max} - T_{min}})^4 - (T_{am} + \frac{T_0 + 273}{T_{max} - T_{min}})^4\right] \\
&+ \frac{\delta t}{Pe}\left(\frac{T_a^i - 2T_b^i + T_c^i}{l_1 + l_2} + \frac{sin\phi}{r}\frac{T_a^i - T_c^i}{l_1 + l_2}\right) \qquad (5.36)
\end{aligned}
$$

The terms represent the heat lost from the glass via conduction, radiation and the internal transport of heat respectively.

This approximation was used as it can incorporate heat loss by radiation and variable heat transfer coefficients.

Chapter 6

Results Including Temperature Variations

6.1 Introduction

In this chapter, temperature variations across the boundary were introduced via the augmented boundary condition described in the preceding chapter. The model was used to ascertain whether or not the cooling of a thin surface layer of liquid has a significant effect on the flow of molten glass during a pressing operation.

Note that unless otherwise stated, all times and temperatures quoted in

this chapter are dimensionless.

6.2 A Partially Cooled Free Surface

Under normal conditions molten glass in contact with the metal plunger or mould cools faster than the portion of the glass open to the air. Therefore, it might be expected that the glass around the contact point[1] would be cooler than that of the rest of the free surface. The model was used to predict the behaviour of the flow in such a situation. A twenty element grid was used to simulate a simple pressing operation, with the plunger moving at a constant downward velocity and with $Re = 1.0$, $Fr = 5.0$, $Wb = 0.1$. It was assumed that the glass had an even temperature, $T = 1.0$, except in the area immediately adjacent to the mould where it was cooler. The situation is shown schematically in figure (6.2), together with the node numbering referred to later in this section. The temperature of the glass is fixed thoughout the pressing, i.e. there is no heat flow within or from the glass.

[1] where the free surface of the glass touches the metal

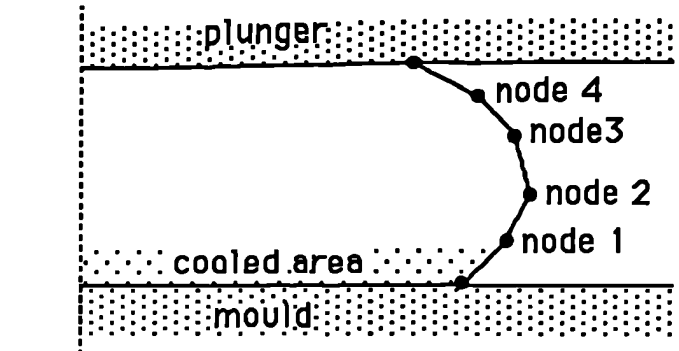

figure 6.2

figure	surface temperature
6.2.1	T=1.0 over all surface
6.2.2	T=0.8 at bottom plate, T=1.0 elsewhere
6.2.3	T=0.6 at bottom plate, T=1.0 elsewhere
6.2.4	T=0.4 at bottom plate, T=1.0 elsewhere

The figures (6.2.1)-(6.2.4) show snapshots of the flow, the area of interest around the contact point has been enlarged for clarity. In figure (6.2.1), as in all previous isothermal cases, the glass advances in a 'rolling' manner with

the nodes of the grid touching the plate in order. However, when the liquid adjacent to the mould is cooled it slows the flow in the immediate vicinity of the contact point.

Figure (6.2.5) shows the velocity of node 1 at time=0.35 plotted against the temperature of the corner node. As the temperature of the corner node is decreased the first node is slowed.

Figure (6.2.6) shows the average velocity of nodes 2,3 and 4 at time=0.35 plotted against the temperature of the corner node. The average velocity of the rest of the free surface increases as the temperature of the corner node is decreased. The plunger is moving at the same constant rate in all four cases hence the rest of the free surface, (nodes 2,3 and 4), has to move more to compensate for the bottom node moving less.

The differences in velocity along the free surface become more pronounced the larger the temperature difference, until the flow near the plate is slowed to such an extent that the hotter glass 'flows over' to touch the plate first leaving an air gap. This gives rise to a rippled effect of the free surface. This can be seen in figure (6.2.4) and to a lesser extent in figure (6.2.3).

This phenomenon is observed in real life when molten glass in poured on to a cold plate, or glass in pressed in too cool a mould. Rippling often

occurs when a production line has just been started and the moulds, though preheated, are not yet up to the correct temperature. Therefore, any stoppages of the continuous manufactoring process, for example to replace a worn mould, are costly in terms of lost production.

To predict the size and study the nature of these 'ripples' the elements would need to be very small. However, if the model was being used to assess the likely outcome of pressing under a particular set of circumstances, the appearance of this 'overlap effect' could be used as a warning that the mould or plunger are too cold to produce a high quality surface finish.

Figure (6.2.1)

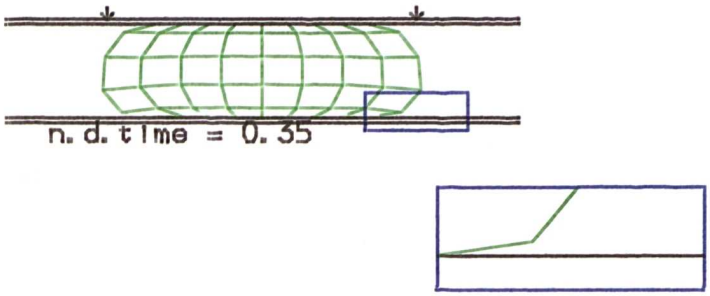

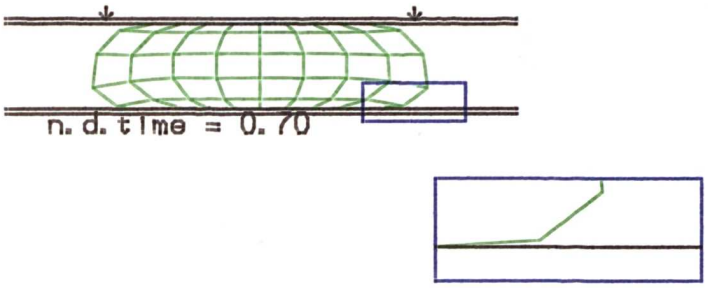

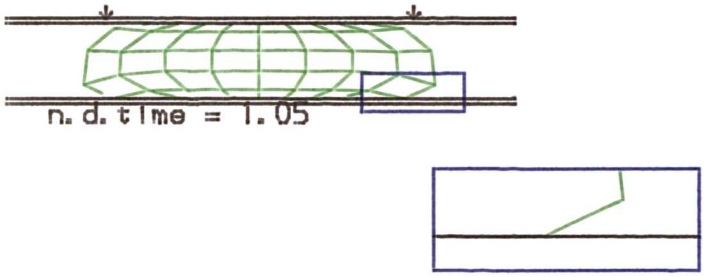

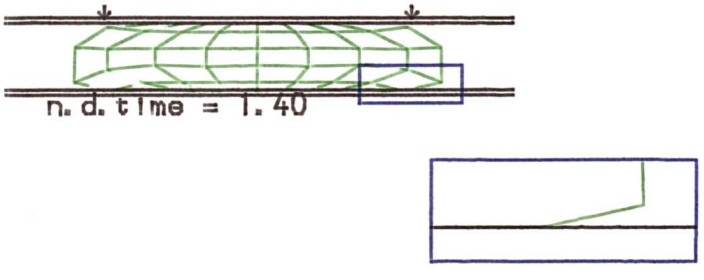

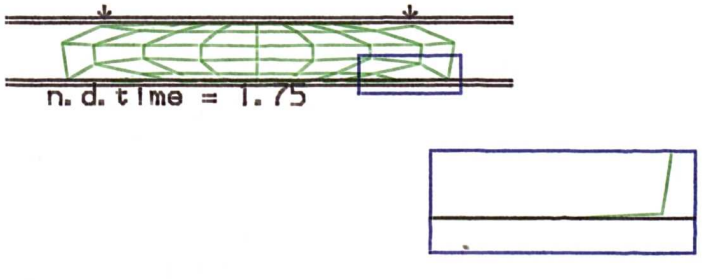

Figure (6.2.2)

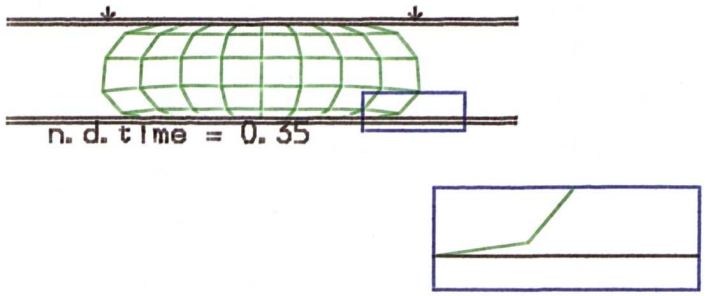

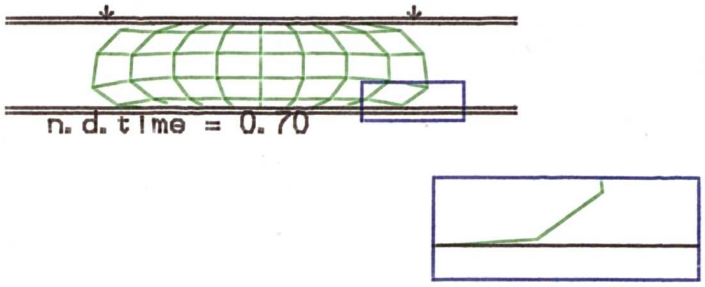

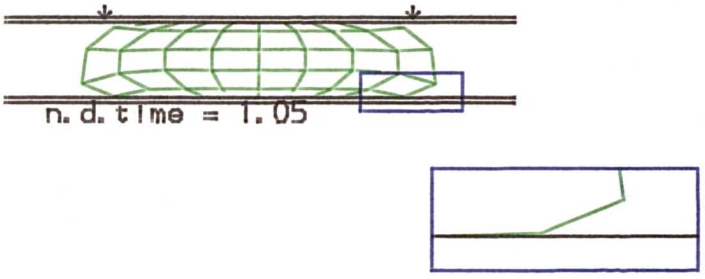

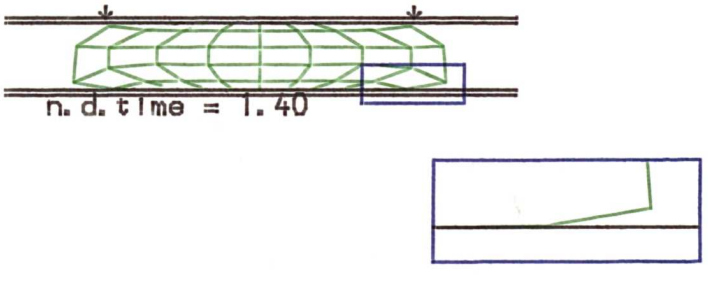

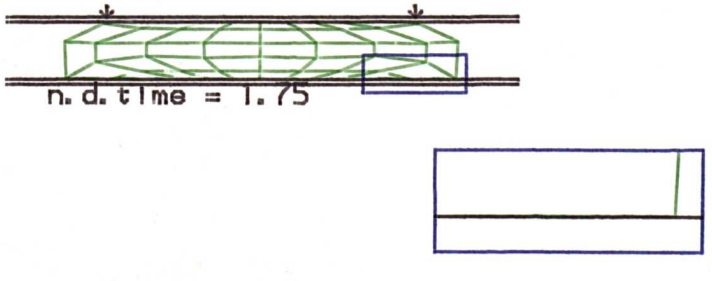

Figure (6.2.3)

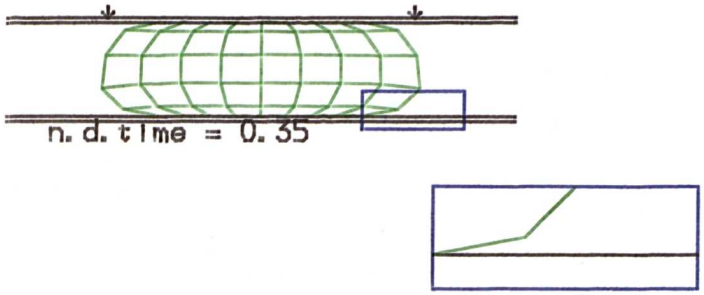

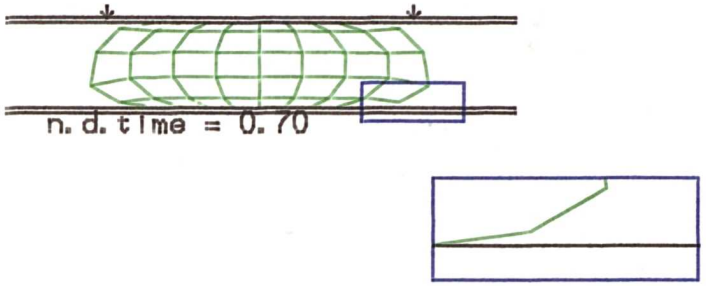

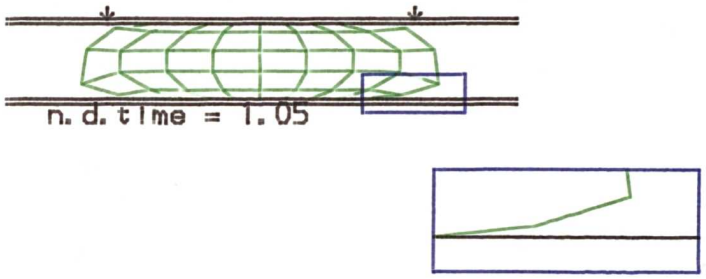

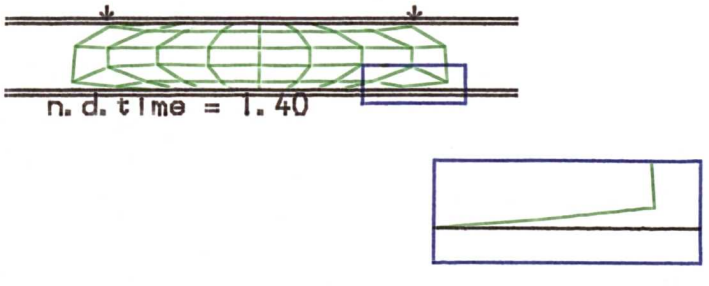

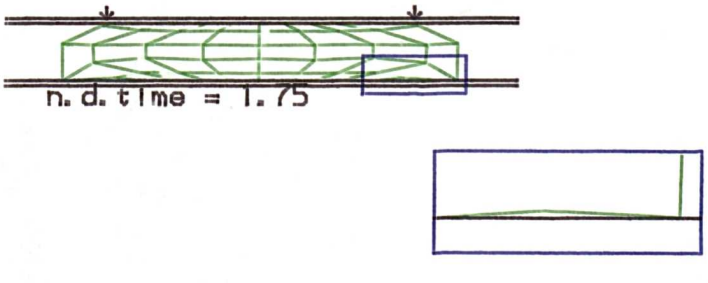

Figure (6.2.4)

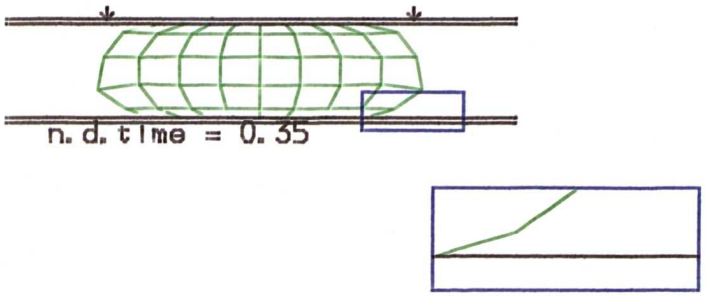

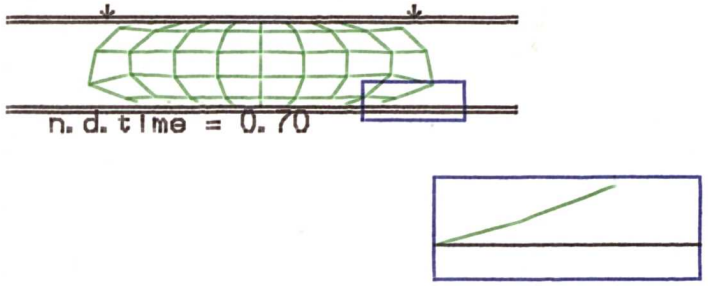

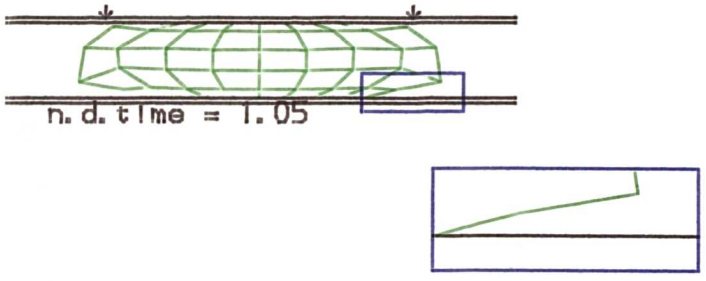

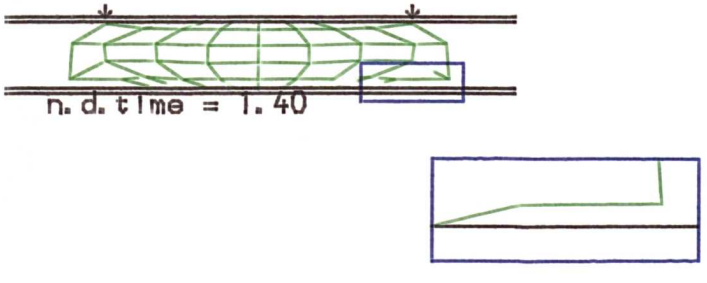

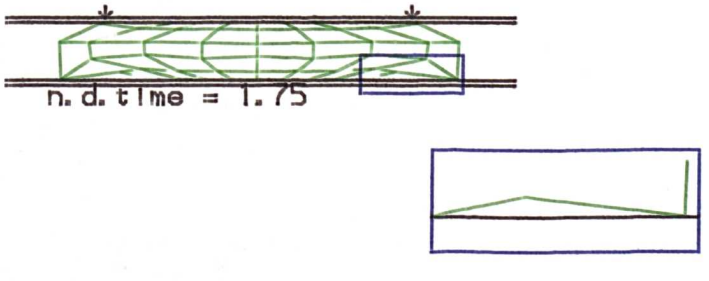

Figure 6.2.5 Velocity of First node

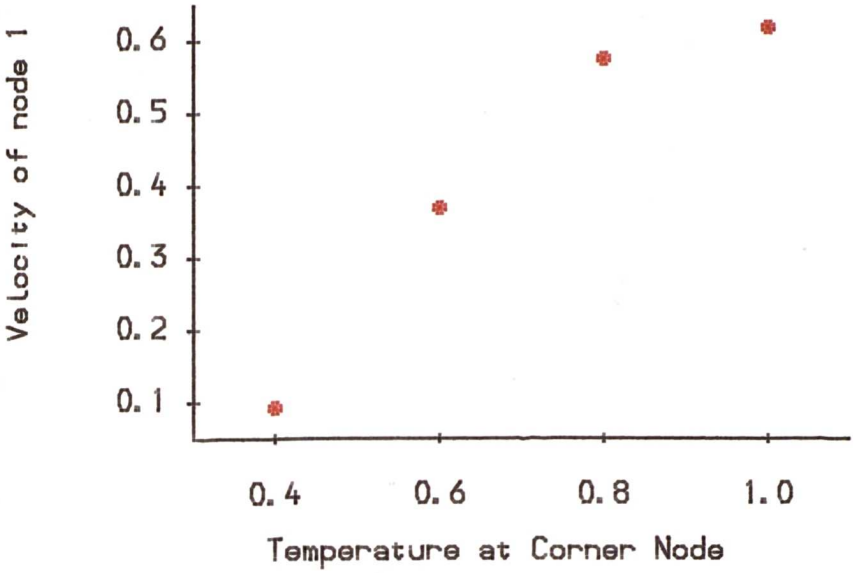

Figure 6.2.6 Average velocity

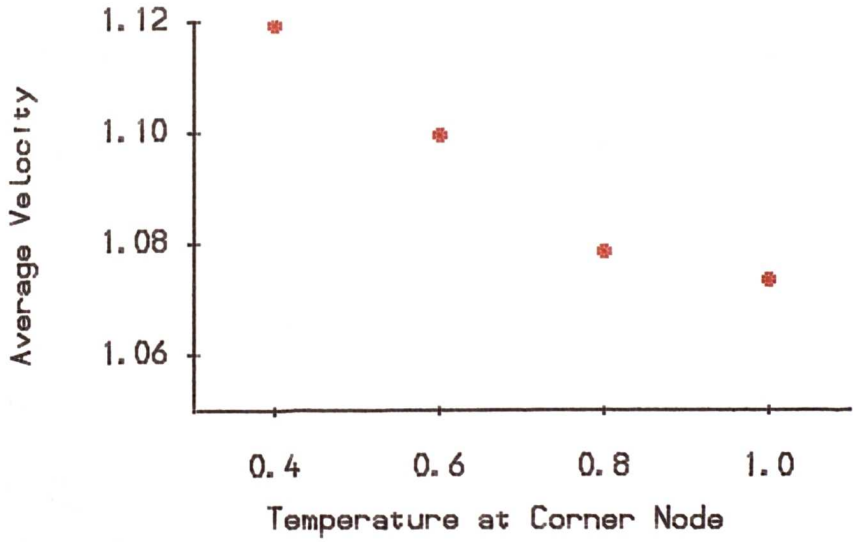

6.3 Overall Surface Cooling

In this section the model was used to predict what would happen if the gob being pressed was still hot on the inside, but all of the free surface was cooler, again there is no transport of heat during the pressing.

The set up is the same as that in (6.2), a twenty element grid was pressed by a plunger moving at a constant downward speed, with $Re = 1.0$, $Fr = 5.0$, $Wb = 0.1$.

figure	surface temperature
6.3.1	T=1.0
6.3.2	T=0.6

Figure (6.3.1) is the isothermal situation, it was calculated as a control.

The even surface cooling has no effect on the order of node crossing so the rippling effect, seen in the previous section, is more dependent on there being a temperature gradient along a surface rather than just across it. However, even after a short time it can be seen that the cooled layer affects the pressure field within the glass. The pressures inside the cooled glass, seen in figure (6.3.2), are larger, but perhaps more significantly, the

configuration of the pressure contours has been altered from those in the isothermal situation shown in figure (6.3.1), again showing that cooling, even when confined to a thin surface film, has a noticeable effect.

The drop of temperature at the surface also affects the numerical stability, for example in (6.3.1) when the surface temperature is 1.0 a timestep of 0.001 can be used, but when the temperature has dropped to 0.6 at the surface as in (6.3.2) the timestep has to be reduced to 0.0001 to eliminate the characteristic pressure oscillations first observed in section (4.2).

Figure 6.3.1 No Cooling

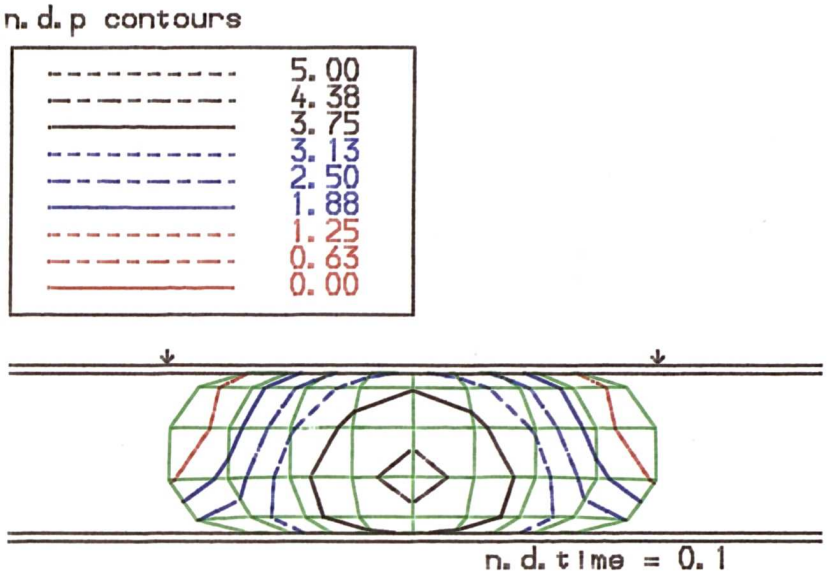

Figure 6.3.2 Cooled Surface

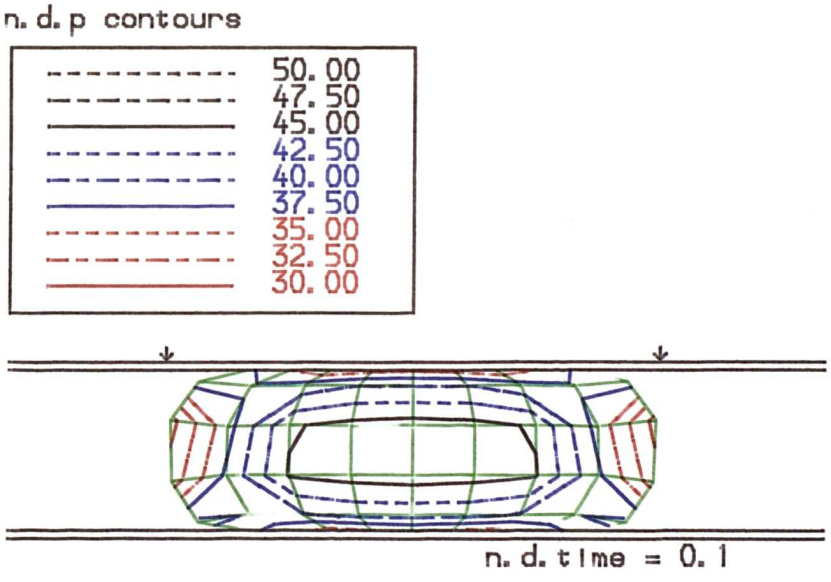

6.4 The Surface Temperature

The surface temperature was calculated using the simple algorithm described in section (5.4.4), and recalled here.

$$
\begin{aligned}
T_b^{i+1} &= T_b^i - \frac{H^* \delta t}{Pe}\left(\frac{1}{2} + \frac{cos\phi}{r}\right)\left[T_{am} - T_b^i\right] \\
&- \frac{\epsilon^* \delta t}{Pe}\left(\frac{1}{2} + \frac{cos\phi}{r}\right)\left[(T_b^i + \frac{T_0 + 273}{T_{max} - T_{min}})^4 - (T_{am} + \frac{T_0 + 273}{T_{max} - T_{min}})^4\right] \\
&+ \frac{\delta t}{Pe}\left(\frac{T_a^i - 2T_b^i + T_c^i}{\ell_1 + \ell_2} + \frac{sin\phi}{r}\frac{T_a^i - T_c^i}{\ell_1 + \ell_2}\right)
\end{aligned}
$$

where the new temperature at a node, T_b^{i+1}, depends on its old temperature, T_b^i, the temperature at the neighbouring nodes, T_a^i and T_c^i, distances ℓ_1 and ℓ_2 away and the temperature of the adjacent medium T_{am}. ϕ is the angle between the outward normal of the surface and the r direction, all other symbols have their usual meanings.

There are two separate sorts of interface to be considered.

Glass touching a solid boundary The majority of the heat flow between glass and the metal is by conduction because the metal is opaque to radiation. The rate of cooling depends on the n.d.heat transfer coefficient, H^* and the temperature difference between the glass and the adjacent metal. Figure (6.4.1) shows the temperature of a point[2] on the curved surface of

[2] $r = 2.0, z = 2.0$

a stationary cylinder[3] which is cooled by conduction only, plotted against time for various constant heat transfer co-efficients. The initial temperature of the cylinder is 1.0. The curved surface of the cylinder is in contact with a mould. The mould is assumed to be maintained at a constant temperature of 0.0.

Free Surface Here the heat flow is by conduction and radiation, the amount of radiation depends on the emissivity, ϵ^*. Figure (6.4.2) shows the temperature of a point on a cylinder initially at 1.0, where heat is lost by radiation into a medium of temperature 0.0, conduction is taken to be negligible. The different curves are for different values of emissivity.

The cooling by radiation is proportional to T^4, hence the curves in (6.4.2) are steeper than those when the cooling is by conduction only (6.4.1) which depends on T.

These results are consistent with the variations in surface temperature of a solid which can be calculated analytically, Carslaw and Jaeger [10] provide an overview of the available analytical solutions.

[3] $r \leq 2, 0 \leq z \leq 4$

Figure (6.4.1) Surface Temperature

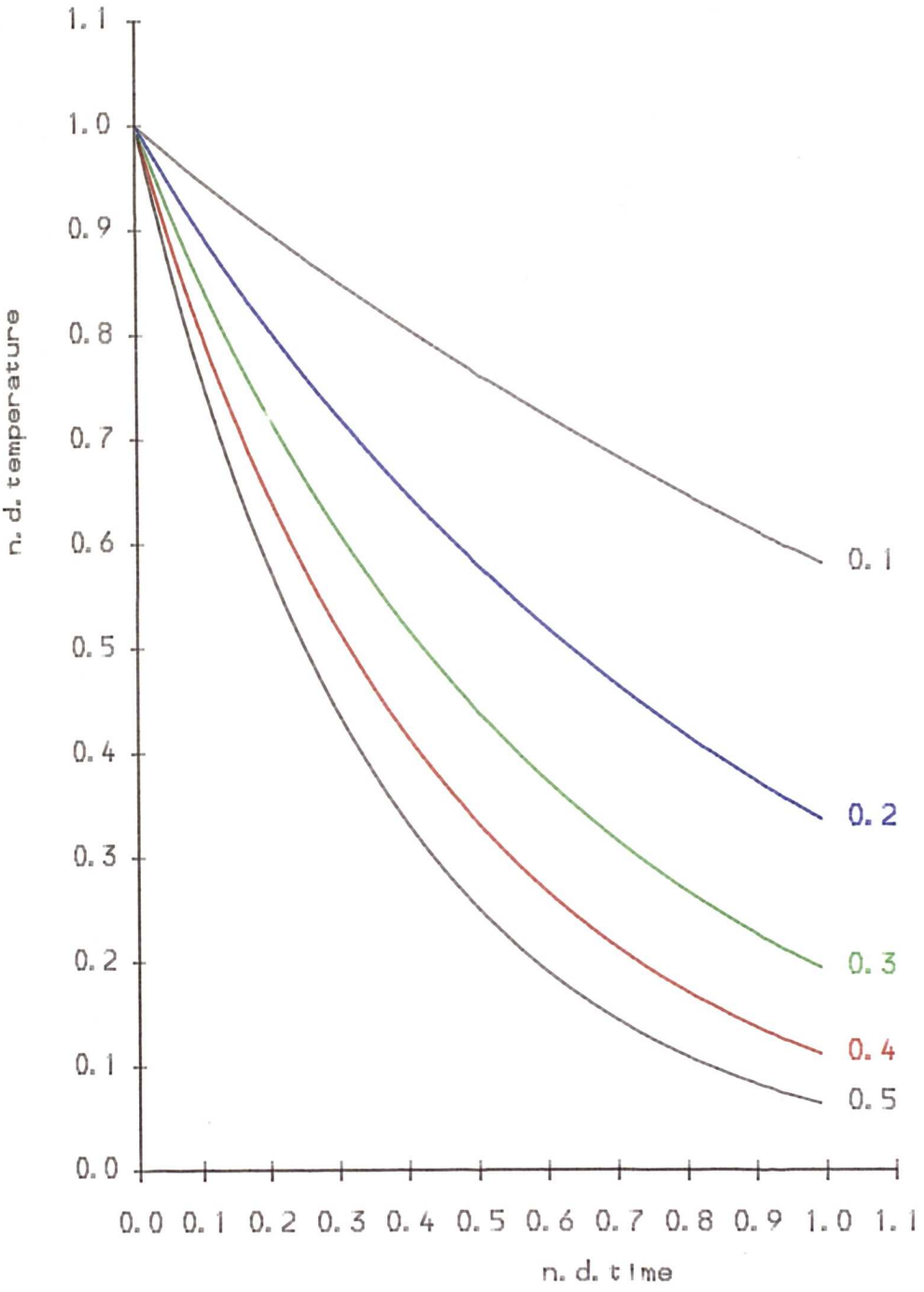

Figure (6.4.2) Surface Temperature

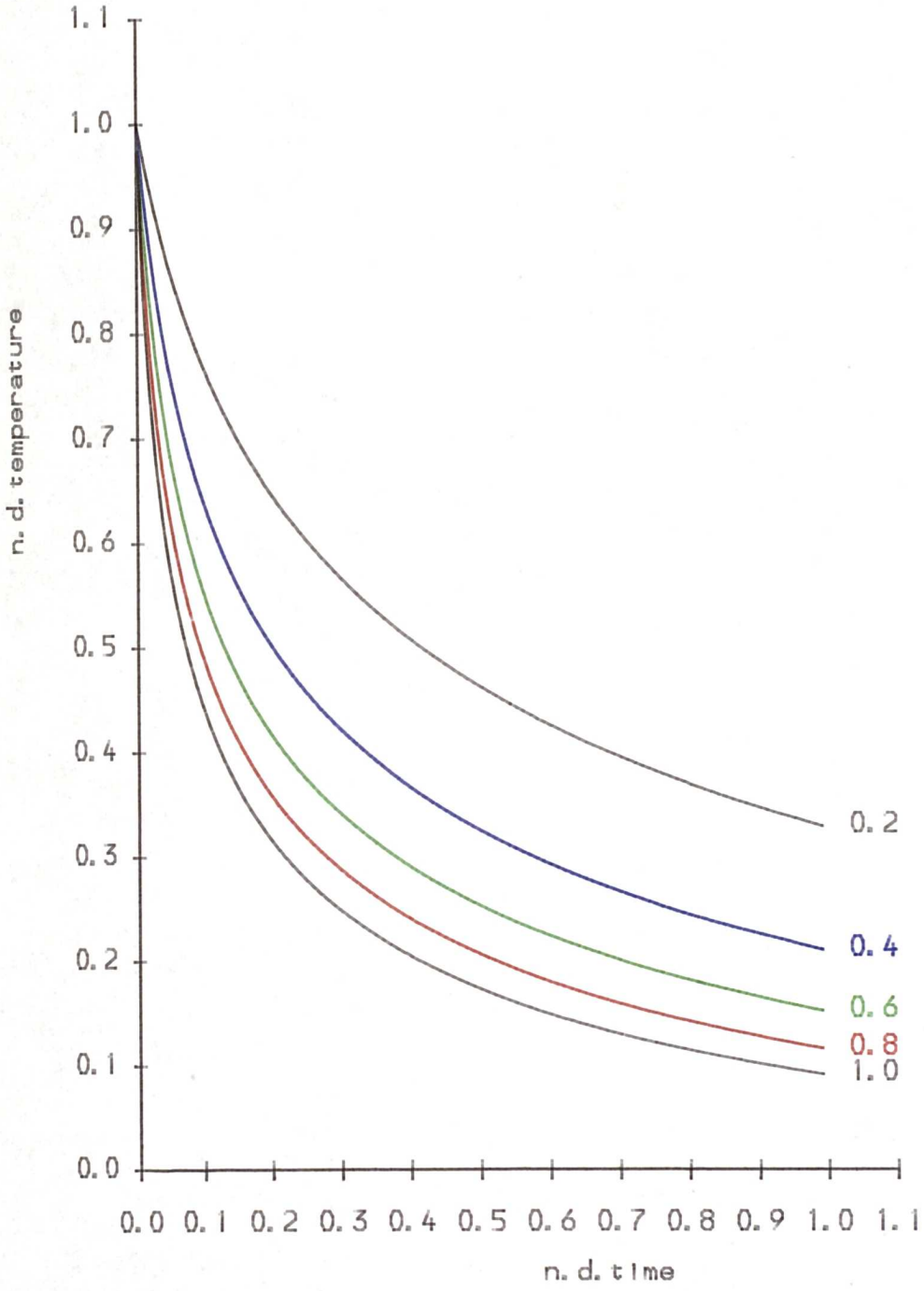

6.5 Combined Model

The surface temperatures calculated in the previous section were for a stationary fluid. In actuality, the free surface is moving and new areas of glass are coming into contact with the solid boundaries. The changing situation of the surface will be reflected in the calculated surface temperatures. This is best illustrated by an example.

The model was used to predict the flow of glass immediately after a roughly spherical gob was dropped onto a shaped plate. The parameters were $Re = 1.0$, $Fr = 10.0$, $Wb = 0.01$. The surface temperature was calculated using $H_m^* = 4.0$, $H_a^* = 0.0$, $\epsilon^* = 0.0$, i.e. no heat lost directly from the free surface. The initial temperature of the glass was 1.0 with the plate at temperature of 0.6. A grid identical to the one in section (4.3) was used.

Figure (6.5.1) shows snapshots of the flow with the associated pressure field at various times. The deformed outline of the grid is given in green, the internal element boundaries having been omitted. The gob hits the plate with a uniform downward velocity of $5U_0$, then flows down over the mould, the small gap left between the mould and the fluid is due to the fact that the mould is curved but the grid is polyhedral, a problem first noted in Chapter

4. The 'fit' can be improved by using smaller elements.

Figure (6.5.3) shows the temperature history of four of the nodes used in the calculation. The initial position of these nodes can be seen in figure (6.5.2). The cooling at node 1 is smooth because it is in contact with the plate for the whole of the time. A marked change in the cooling of nodes 2 and 3 can be seen when they touch the bottom plate. Node 4 does not touch the plate at any time but there is a slight amount of cooling; this is due to the flow of heat from the hotter glass to the cooled area[4], when the Peclet number is large this is only a minor effect.

[4]this is due to the $\nabla^2 T$ term in the energy equation

Figure 6.5.1

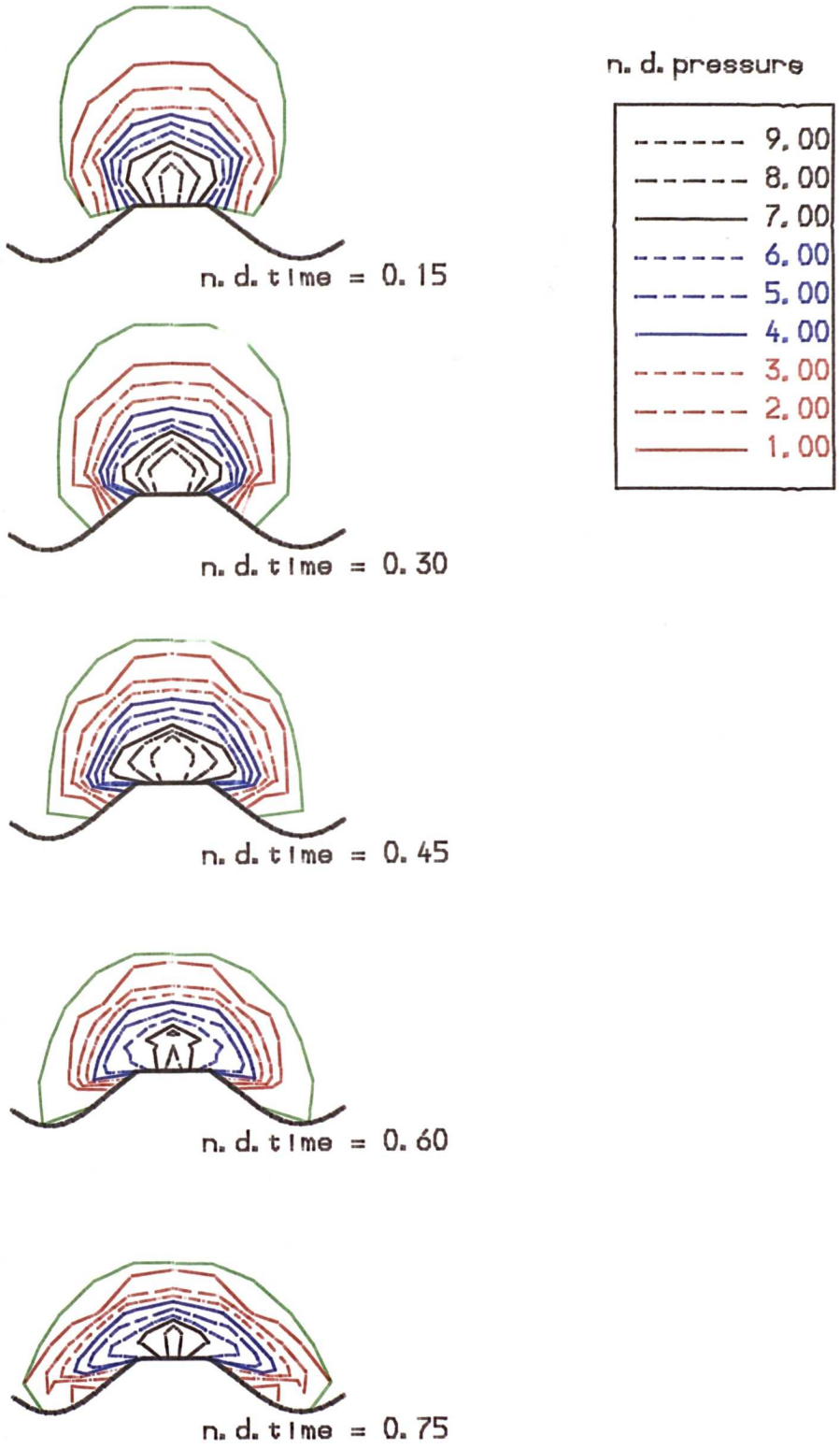
n. d. pressure
9.00
8.00
7.00
6.00
5.00
4.00
3.00
2.00
1.00
n. d. time = 0.15
n. d. time = 0.30
n. d. time = 0.45
n. d. time = 0.60
n. d. time = 0.75

Figure 6.5.2 Node numbers

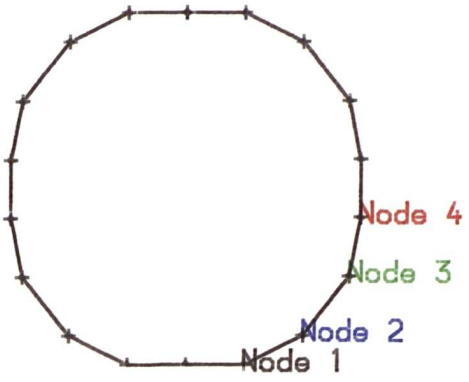

Figure 6.5.3 Surface Temperature

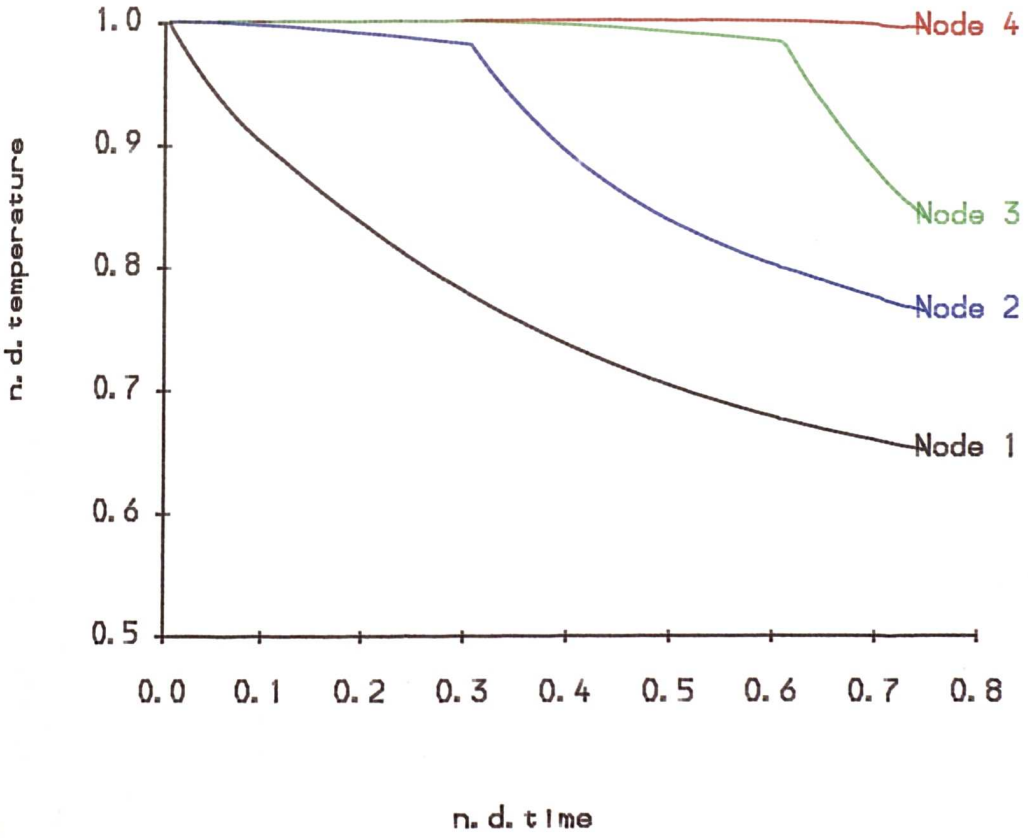

6.6 Surface Smoothing

The model incorporating the alternative boundary condition, though developed with the pressing operation in mind, could be used to assess the effects of a thin cooled layer in other situations.

In this section, the model is used to predict the movement of a free surface as it is smoothed by the action of surface tension and gravity, after being slightly perturbed from its horizontal equilibrium position.

The situation under consideration is that of a viscous liquid in an open topped cylindrical container. The no-slip boundary condition is applied where the fluid touched the base and side of the container. Figure (6.6.1) shows the grid and the node numbers which are referred to in later diagrams, node 1, which is initially the top of the 'blip', is on the axis of symmetry. The initial perturbation of the free surface, shown in figure (6.6.2)[5], is small 0.026 units, compared to the equilibrium height of 3 units. Initially, the fluid is at rest, it then is allowed to flow, the flow parameters were $Re = 1.0$, $Wb = 0.5$ and $Fr = 100.0$.

Results To compare the effects of differing surface temperatures on the rate at which the surface perturbation was smoothed out, some sort of bench

[5]note the different scales in the horizontal and vertical directions

mark is needed. Here it was taken to be the 'half life' i.e. the amount of time it takes for the maximum surface height variation to fall to 50% of its initial value.

First, the isothermal case was considered, where the bulk temperature was the same as the free boundary temperature (b.t), both having a value of 1.0. Figure (6.6.3) shows the heights variations of four surface nodes plotted against time. Figure (6.6.4) gives the maximum height variation across the free surface at any given time as a percentage of the original perturbation. It can be seen that as time progresses the variations are smoothed out. It takes ≈ 13 units of time for the variation to fall to 50% of its original value. The first couple of steps in the calculation produce a slightly anomalous result this is due to the grid being released from rest, hence the small deviations from a smooth curve at very small times in the figures.

Figures (6.6.5) and (6.6.6) show the corresponding results, from a calculation where the bulk temperature was 1.0 but the surface was cooled to a temperature of 0.9, this represents an approximate doubling of the viscosity. In this case it takes ≈ 25 units of time for the variations across the surface to halve.

Figures (6.6.7) and (6.6.8) are the results when the boundary temperature (b.t), was 0.8. Here the smoothing effect is further slowed, in fact the

perturbation grows slightly before it begins to fall. The time taken for the surface variation to halve is $\approx$ 36 units.

The augmented boundary condition is valid for surface temperatures higher as well as lower than the bulk temperature[6]. Figures (6.6.9) and (6.6.10) show the results of smoothing when the surface has been heated to a temperature of 1.1. The smoothing is more rapid than the isothermal case with it only taking $\approx$ 2 time units for the perturbation to fall to 50% of its initial value.

Comments The calculations in this section have been on a very simple grid but they illustrate the possibilities of using this model to study the formation and behaviour of surface waves.

The formation and decay of surface irregularities is particularly important in the float glass process. The decay of surface waves are considered by Woo[46] and Cassidy & Gjostein [11].There have been some attempts to produce analytical solutions, for example, Woo presents an analytical solution describing the decay of an isolated axi-symmetric perturbation, using various simplifictions[7]. However, none of these solutions allow for variations

[6] see section (5.4.3)

[7] prescribed perturbation profile, infinite deep liquid and simplified free surface stress boundary condition

of viscosity in the glass.

The augmented boundary condition is valid for a 'surface viscosity' either higher than the bulk viscosity or lower which occurs when the surface is heated, therefore, operations such as fire polishing could be investigated. The model could also be used to predict flows in other situations where there is a different 'surface viscosity', such as a thin film of liquid floating on another, or where a liquid absorbs or reacts with another at its surface.

6.7 Remarks

From a computational point of view, the assumption that the glass is isothermal makes things easier, but, it can be seen from these results that the effects of cooling, even if confined to a thin film, cannot be ignored.

The conclusion, that even small areas of cooling can be influential, is not altogether unexpected. The importance of heat transfer in glass fabrication is mentioned by many of the referenced workers including Rawson [38] and Bonacina et al.[7].

Figure 6.6.1 Grid and Node numbers

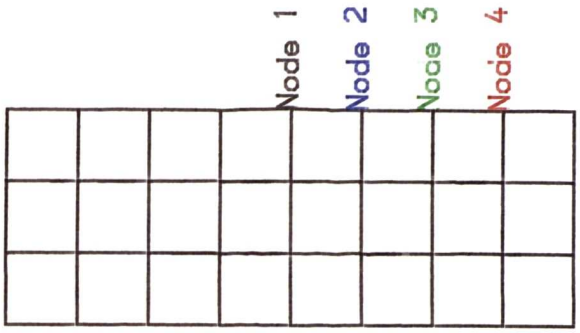

Figure 6.6.2 Surface Perturbation

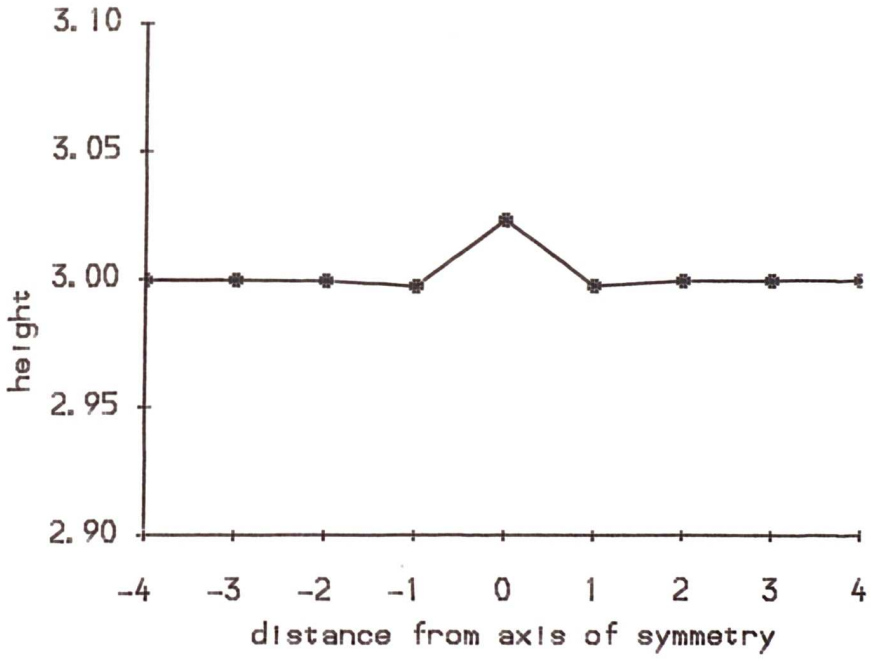

Figure 6.6.3 Vertical movement of nodes (bt=1.0)

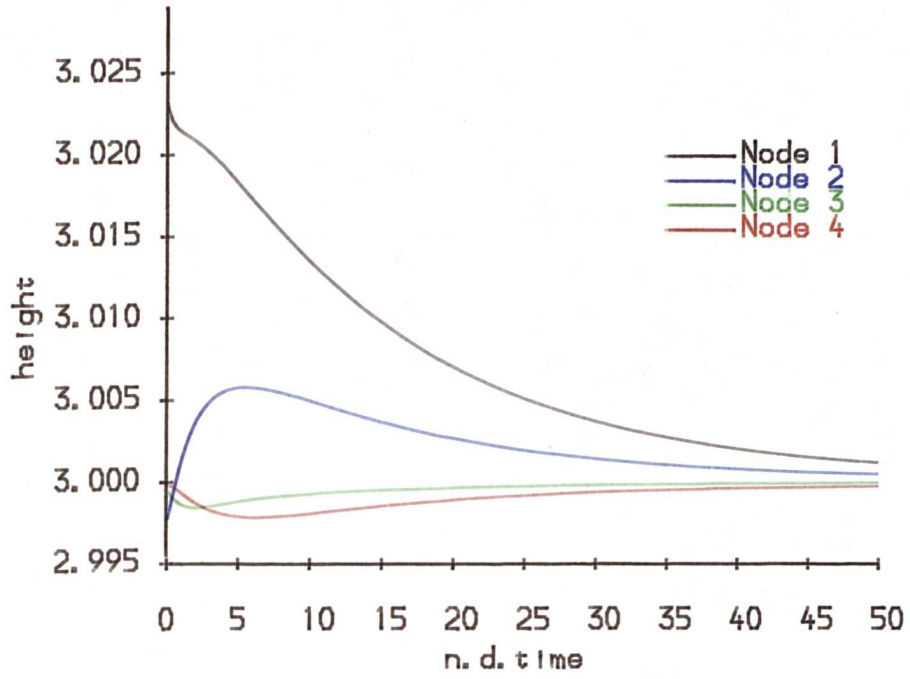

Figure 6.6.4 Maximum Height Variation (bt=1.0)

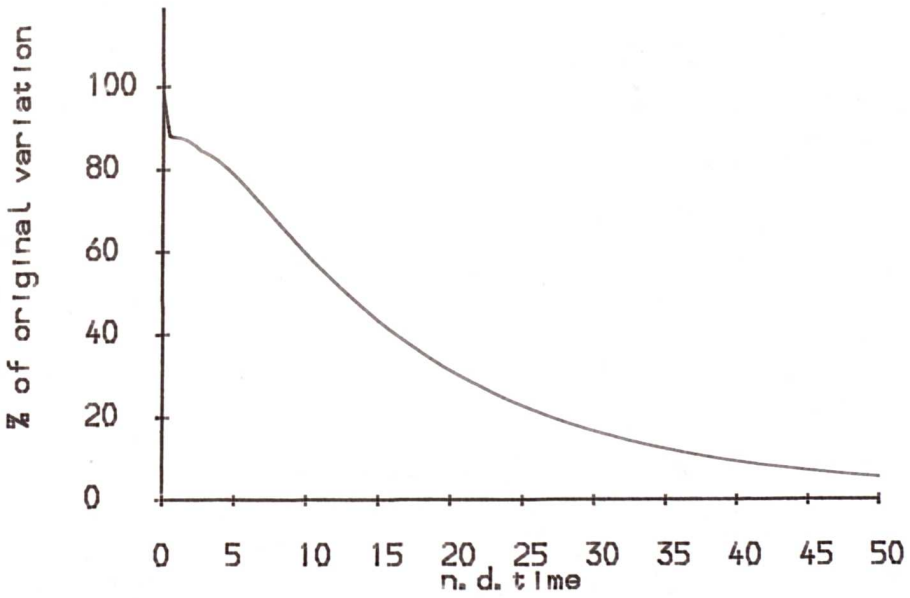

Figure 6.6.5 Vertical movement of nodes (bt=0.9)

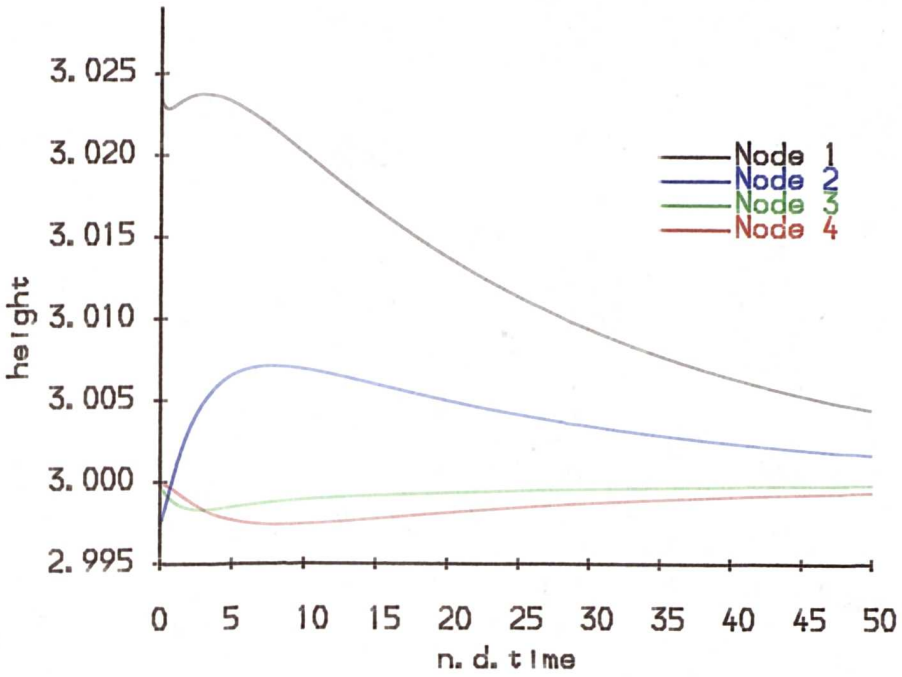

Figure 6.6.6 Maximum Height Variation (bt=0.9)

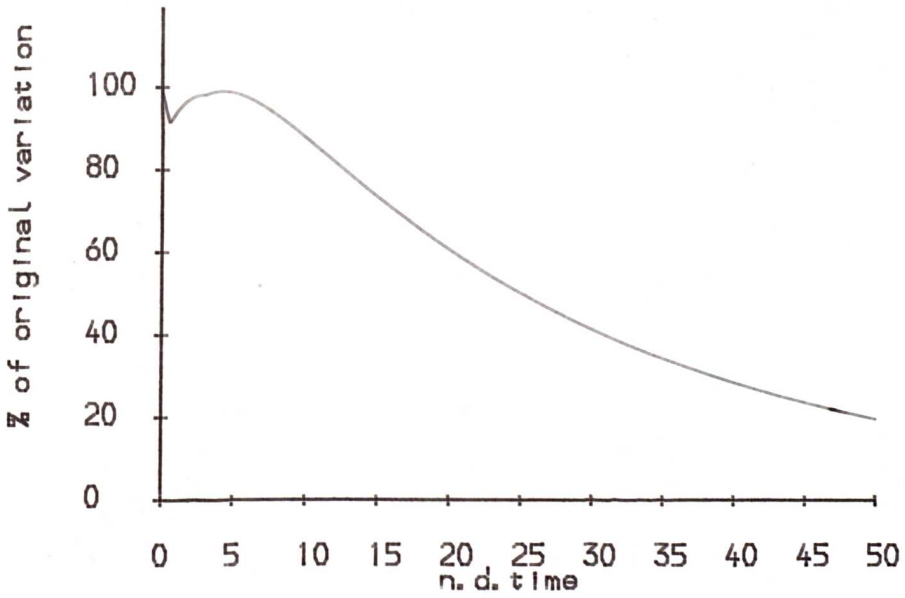

Figure 6.6.7 Vertical movement of nodes (bt=0.8)

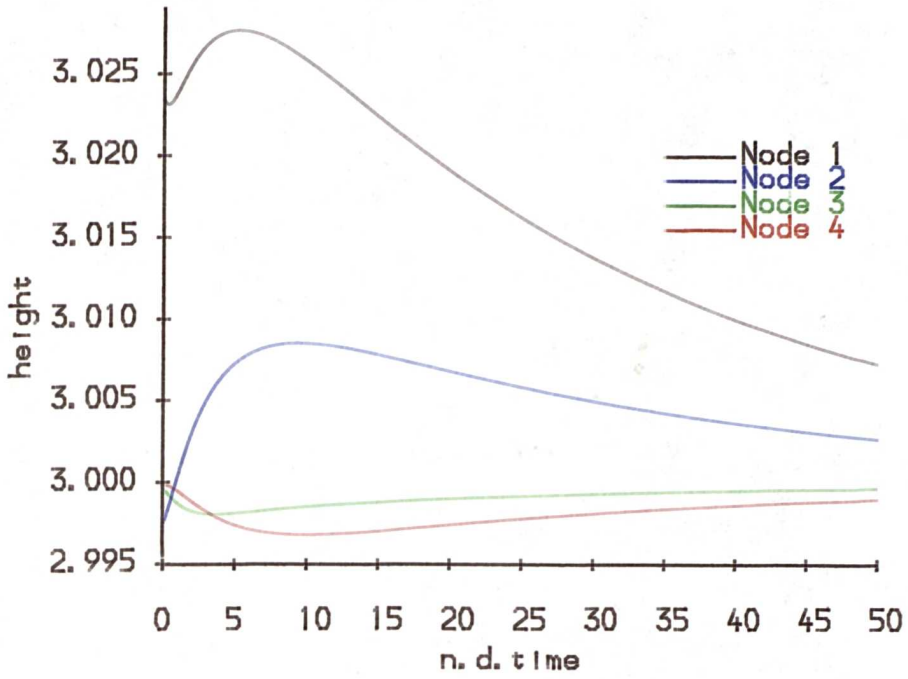

Figure 6.6.8 Maximum Height Variation (bt=0.8)

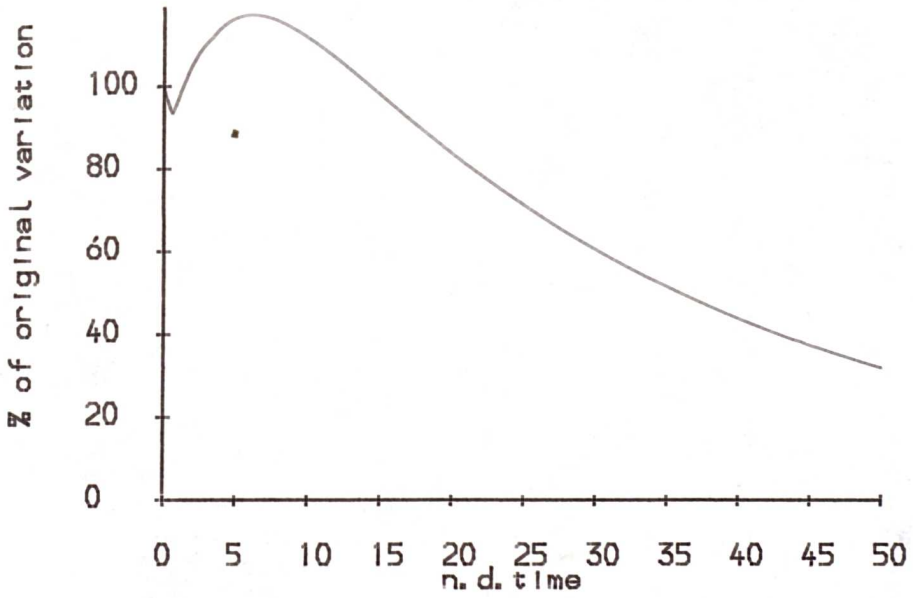

Figure 6.6.9 Vertical movement of nodes (bt=1.1)

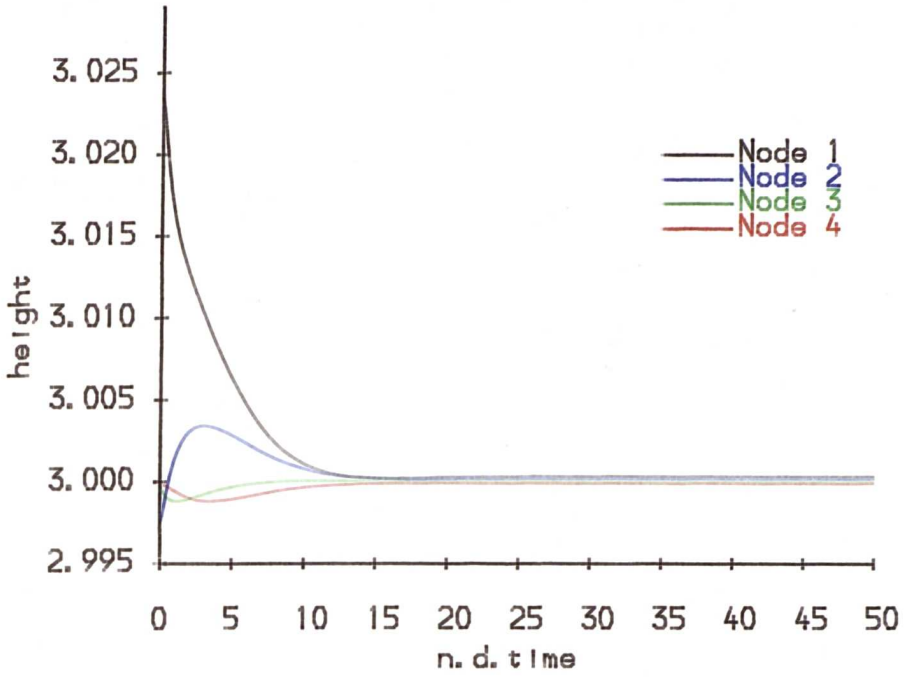

Figure 6.6.10 Maximum Height Variation (bt=1.1)

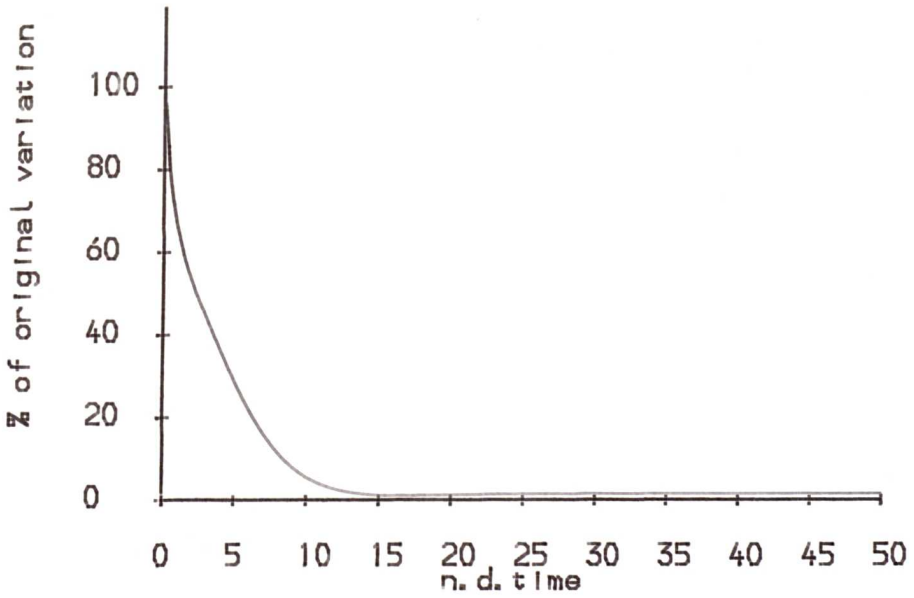

Chapter 7

Modelling Real Life Situations

7.1 Introduction

Up to now the results presented have been of a simple nature, used to illustrate various aspects of the computer model, and no attempt has been made to equate non-dimensional values to real ones. In this chapter, realistic value for the various physical parameters are considered and some attempt is made at modelling a real situation.

7.2 Physical Parameters

Description	Symbol	value	source
surface tension	σ	$0.3Nm^{-1}$	[1]
density	ρ	$2500kgm^{-1}$	[35]
Fulcher equation	A	-3.0	[14]
constants[a]	B	4500	"
	T_0	242^oC	"
Heat Transfer Co-efficient			
air/glass	H_a	$20-40Wm^{-2}\,^oC^{-1}$	[22]
mould/glass[b]	H_m	$11000e^{-0.9t}Wm^{-2}\,^oC^{-1}$	[19]
Stefan Constant	σ_s	$5.57 \times 10^{-8}Wm^{-2}\,^oK^{-4}$	[4]
Heat capacity	c	$1339JKg^{-1}\,^oC^{-1}$	[40]
thermal conductivity[c]	k	$2.50Wm^{-2}\,^oC^{-1}$	[33]

[a]The form of the equation is given in 2.3.2.
[b]this varies with the time of contact because the glass shrinks from the metal
[c]an average value, it varies with temp. e.g. $k = 2.03$ at 670^oC, $k = 2.70$ at 1100^oC

These are the values which determine the physical properties of the glass. They are normally dependent on the composition of the particular glass being considered, the values used in the section are for that of a typical soda-lime-silica glass.

7.3 Situation Specific Parameters

As well as the composition of the glass which determines its properties the treatment of the glass can be varied, these variables are, to some extent, controllable. Here is a list of these factors with some indication as to their order.

- The geometry of the mould and plunger can be altered, though these are restricted by the need to remove the finished article.
- The size and intial shape of the gob of glass can be varied by the feeder mechanism.
- The height from which it is dropped into the mould can be varied and hence, the velocity of the glass when it hits the mould, normally it is between 1 and 5 ms^{-1}.
- The initial viscosity of the gob, around $10^3 Nsm^{-1}$, is controlled by controlling its temperature, i.e. $\approx 1000°C$.
- The dwell time is variable, i.e. the length of time the gob is allowed to settle in the mould before it is hit by the plunger, is about a second.
- The initial temperatures of the mould and plunger can be altered, usually they are at $\approx 400°C$. Sometimes the mould and plunger are

cooled externally, often the plunger is hollow allowing water to be circulated.

- The initial velocity of the plunger is usually $\approx 0.1ms^{-1}$. The motion of the plunger during the pressing process depends on the driving mechanism of the machine and the power available.

These values were obtained from Rawson[38], McGraw[33] or from observations of a pressing machine at Waterstone Glassware Ltd. a small glass maker at Wath-upon-Dearne.

For the non-dimensional scheme values for T_{max},T_{min}, L and U_0 are needed. T_{max} is the maximum temperature encountered and as chosen as $1150°C$; T_{min}, the minimum value for the temperature used in the calculation, was set at $50°C$ to allow for any possible air temperature. L is the length scaling factor. Setting L to 0.01 means that a unit length is $1cm$. U_0 is probably the most difficult to set because of the wide range of velocities in a pressing operation, a value of 1 was taken for convenience so the units of velocity are metres per second. These value with those in the table give

$$Re = \frac{25.0}{\mu(T^*)}$$

$$Fr = 10.2$$

$$Wb = 0.01$$

$$H_a^* = 0.12$$

$$H_m^* = 40.0e^{-9\times10^{-3}t^*}$$

$$\epsilon^* = 30.0\epsilon$$

$$Pe = 15000 \tag{7.1}$$

where t^* is the non-dimensional time; T^* the non-dimensional temperature and

$$\mu(T^*) = 10^{-3.0+\frac{4500}{1100T^*-192}} \tag{7.2}$$

For a glass temperature of less than $1100°C$

$$Re < 0.01$$

so the assumption that viscous forces dominate made in chapter 2 is reasonable. The Peclet number is large which confirms the assertion, made in chapter 5, that heat flows only slowly within the fluid.

7.4 Stability Problems

For the parameterization quoted in the previous section, the maximum Reynolds number is 0.01, this means that the maximum stepsize is of the order[1] $\delta t = 0.0005$. If the operation to be studied took 1 second in real

[1] see section (4.2), there is also a dependence on the element sizes

time, this would correspond to 100 units n.d.time[2]. Hence the number of timesteps needed would be

$$\frac{100.0}{0.0005} = 2.0 \times 10^5$$

For a twenty element grid, such as the one used in (5.3), each time step takes $\approx$ 5 seconds CPU time on the IBM Mainframe, so the CPU time need to complete the above calculation would be

$$1 \times 10^6 sec \approx 11 days$$

Clearly, this problem is mainly due to lack of computing power. Predicting the flow in a detailed real life situation is therefore impractical on the IBM, but on a Cray or other powerful machine the speed the calculations would take a more manageable amount of time, also with the introduction of increasingly powerful work stations and the advent of parallel processors this size of calculation is becoming more amenable.

If, as in this case, the computing power is unavailable there are two basic approaches that can be adopted to try to overcome these timing problems;

Numerical Approach This would be to look at the nature of the numerical instability and to try to combat it without affecting the accuracy.

[2]using the relation $(n.d.time) = \frac{U_0}{L}$(real time)

One possibility would be to solve the equations of flow implicitly. Implicit schemes are far more stable but not necessarily[3] more accurate, accuracy can be increased by using a mixed implicit/explicit scheme. Both these options require substantial program alterations which would lengthen of the calculation because the matrix equations (3.40) in section (3.3.3) for the r and z direction acceleration would no longer be separate; Golafshini considers an implicit method for calculating flows[26].

Another option would to introduce a smoothing scheme to try to control the pressure oscillations, but care would need to be taken so that the smoothing does not mask any important features, the problems with some smoothing schemes are considered by Gresho and Lee[25].

Physical Approach In the pressing situation considered where the plunger is moving at a prescribed known velocity, it seems that it is the differences in viscosity that has most effect on the flow, rather that the actual viscosity that only seems to effects the internal pressure. Therefore, it could be assumed that the Reynolds number is one, except at the surface where it is allowed to alter. It is important to calculate the surface temperature even if its effect on the flow is not included, because it will be critical in determining

[3] see appendix A

the behaviour of the article once it is removed from the mould, i.e. if it is not cool enough it will collapse under gravity. The surface temperature also influences whether the glass sticks in the mould, a potentially disastrous fault on a continuous production line.

The physical approach is adopted here. It is envisaged that in a practical situation calculations would be performed with the maximum Reynolds number of one using larger steps for an over view, enabling the user to identify conditions or areas of flow that needed more detailed investigation which could then be undertaken using the actual parameters.

Though no actual 'true-to-life' situations are calculated here, a couple more examples are included.

7.5 Example 1 - Pressing a Beaker

This example was included because it deals with a more realistic geometry and shows that with repeated remeshing a relatively small number of elements, in this case twenty, can be used.

The model predicted the flow for the isothermal case with $Re = 1.0$, this was chosen to maximize the step size. The other parameters were $Fr = 10.0$ and $Wb = 0.01$. Initially, the gob of glass was assumed to have a

uniform downward velocity of 1 ms^{-1}. It hits the mould at n.d.time= 0.0, at n.d.time= 2.5 the glass was touched by a plunger travelling downwards at a constant speed of 1 ms^{-1}. Figure (7.5.1) shows the resulting deformations of the glass and how the grid alters to follow the deformed shape.

A single step in the calculation takes $\approx$ 4.7 seconds CPU time; compared to this, the time for remeshing, $\approx$ 0.2 seconds, is small. The total calculation of over 3000 steps took $\approx$ 4 hours of CPU time.

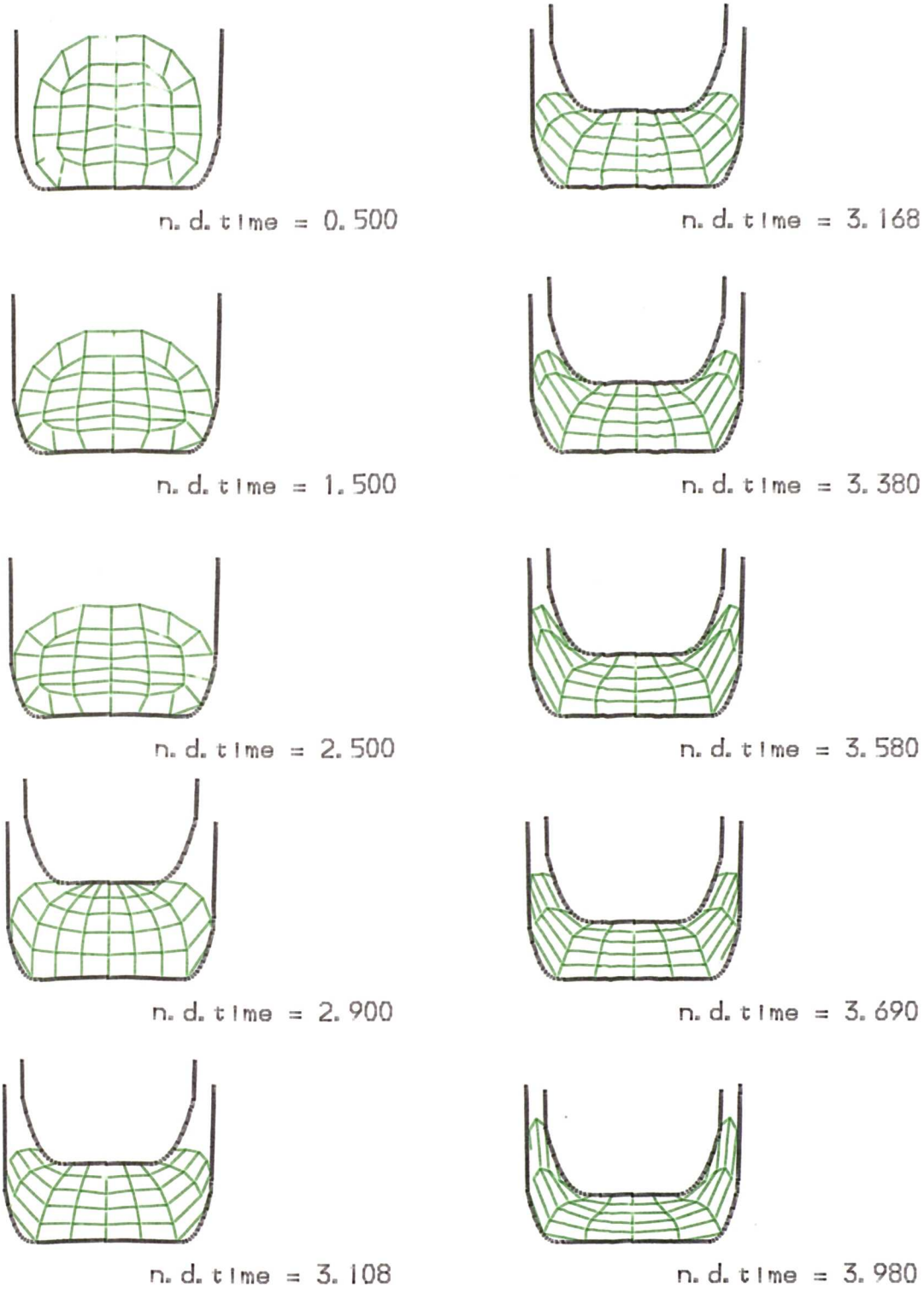

Figure 7.5.1 Pressing of a small beaker

7.6 Example 2 - Stretching

The model was originally developed for pressing but can be used for any axi-symmetric operation. In this example the model is used to predict the behaviour of a cylinder of moulten glass when it is stretched.

The parameters used where $Re = 1.0$, $Fr = 10.0$ and $Wb = 0.01$, the glass was pulled upwards at a constant rate of 2 ms^{-1}.

Figure (7.6.1) shows the result of stretching the cylinder at various times; as expected the cylinder 'necks'. Each element in the grid has its volume conserved from one step to the next, unless remeshing occurs. Since there is no remeshing in this calculation, the shapes of the elements in the deformed grid give a good indication of the amount of deformation undergone by that area of glass. For example, in figure (7.6.1) at n.d.time= 5.0 the grid is still regular reflecting the relatively even distortion of the glass. This even distortion can be contrasted with the situation illustrated in figure (7.6.2). Figure (7.6.2) shows the stretching of a cylinder of glass under similar conditions the only difference being the the lower half of the free surface has been cooled to a n.d.temperature of 0.8. This distorts the flow making it more uneven with more 'necking', this fact is reflected in the distortion of the grid.

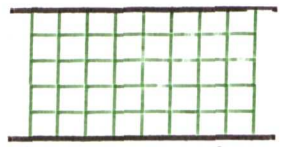

n. d. time = 0.0

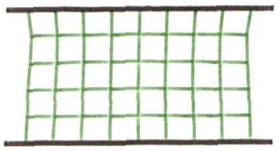

n. d. time = 0.2

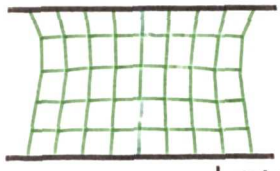

n. d. time = 0.8

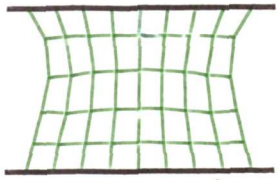

n. d. time = 1.4

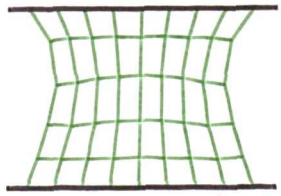

n. d. time = 2.0

n. d. time = 2.6

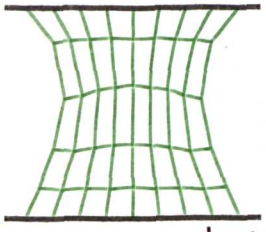

n. d. time = 3.2

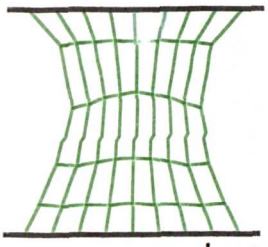

n. d. time = 3.8

n. d. time = 4.4

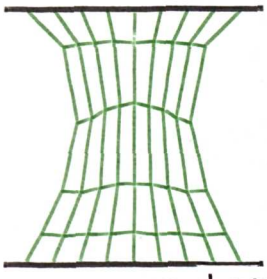

n. d. time = 5.0

Figure 7.6.1 Stretching

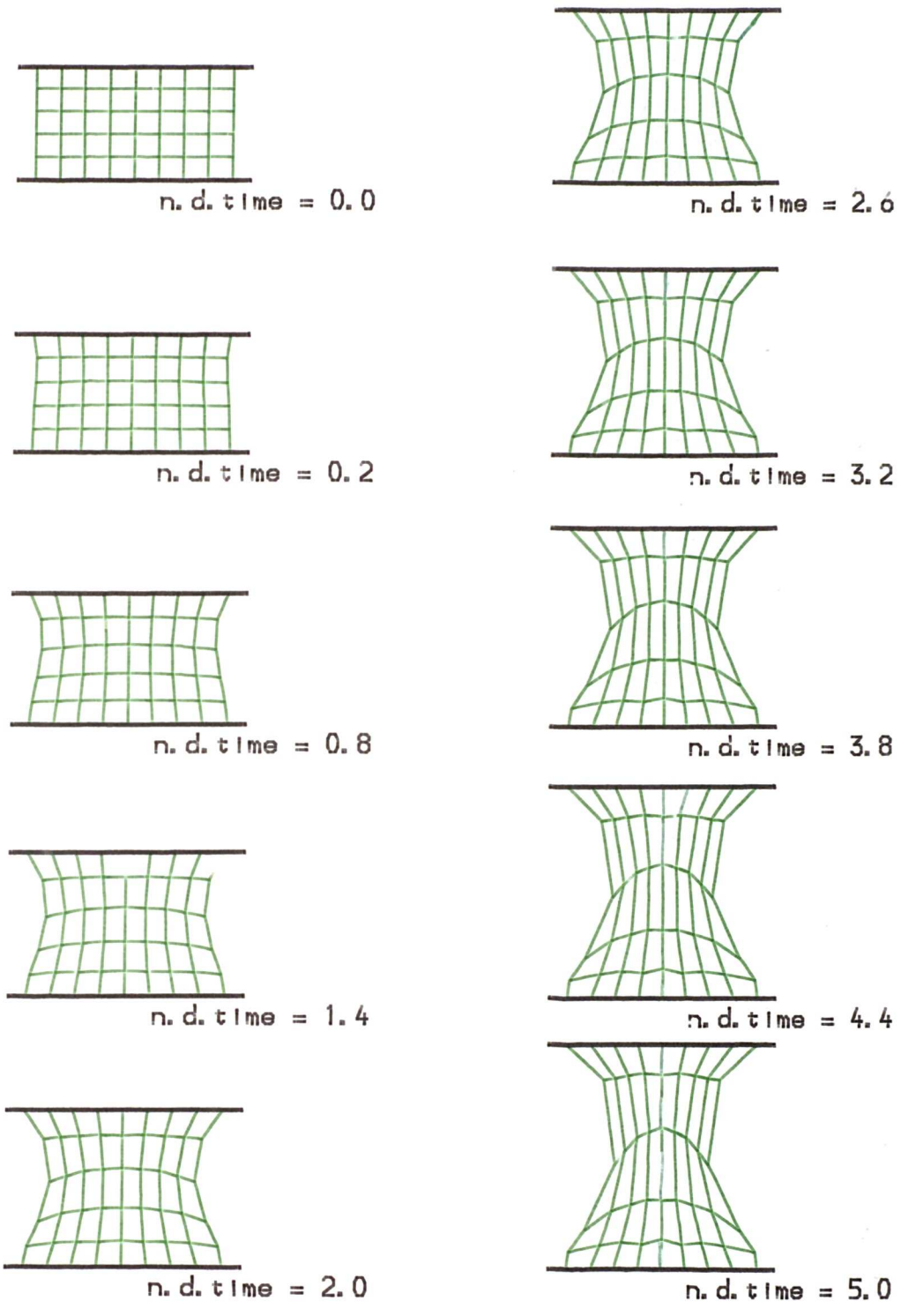

Figure 7.6.2 Stretching - with partially cooled surface

7.7 Example 3 - Elongation under Gravity

A thin cooled layer of glass surrounding an article, as well as affecting the finished shape can also affect the time it takes to reach that shape. This was shown to some extent in section (6.5) where the effect of a different surface viscosity on the smoothing of a surface was considered, it is further illustrated by this example.

A gob of glass in hung[4] from a plate and its rate of elongation is studied. The final shape will depend on the balance between gravity 'pulling it down' and surface tension 'holding it up' but the cooled layer acts as a retarding force, slowing the motion of the free surface.

The parameters used are $Re = 1.0$, $Fr = 10.0$ and $Wb = 0.01$. The resistance to motion comes via the alternative boundary condition, discussed in chapter 5.

Figure (7.7.1) shows how an isothermal lump of glass elongates under gravity. Similar calculations were performed with different surface temperatures, the overall shape was very similar but the rate at which they were achieved differed. Figure (7.7.2) shows the lengthening of an isothermal gob (boundary temperature[5] = 1.0) compared to one with a cooled surface

[4] how is not considered

[5] non-dimensional temperature and non-dimensional time are used

(boundary temperature = 0.9). Figure (7.7.3) shows how the time for a 5% elongation varies over a range of surface temperatures.

The rate of elongation is important if an article is not to deform too much under gravity when removed from a machine, or transferred between machines[6]. This is the sort of calculation, with more realistic parameters and geometry, which could be undertaken if only a small amount of stretching could be tolerated in the transfer of a parison.

[6]for example in the press and blow bottle manufacture

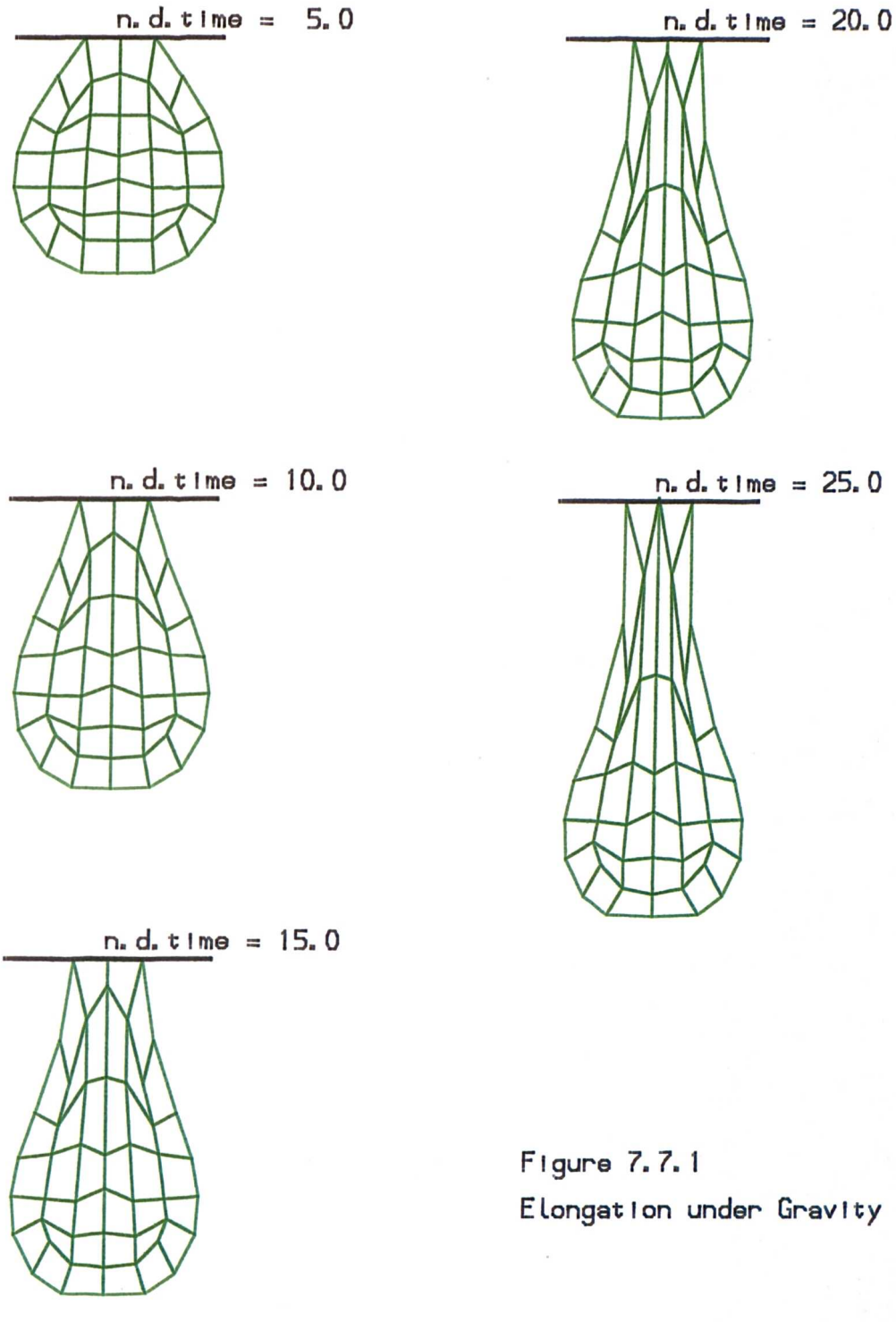

Figure 7.7.1
Elongation under Gravity

Figure 7.7.2 % Elongation v Time

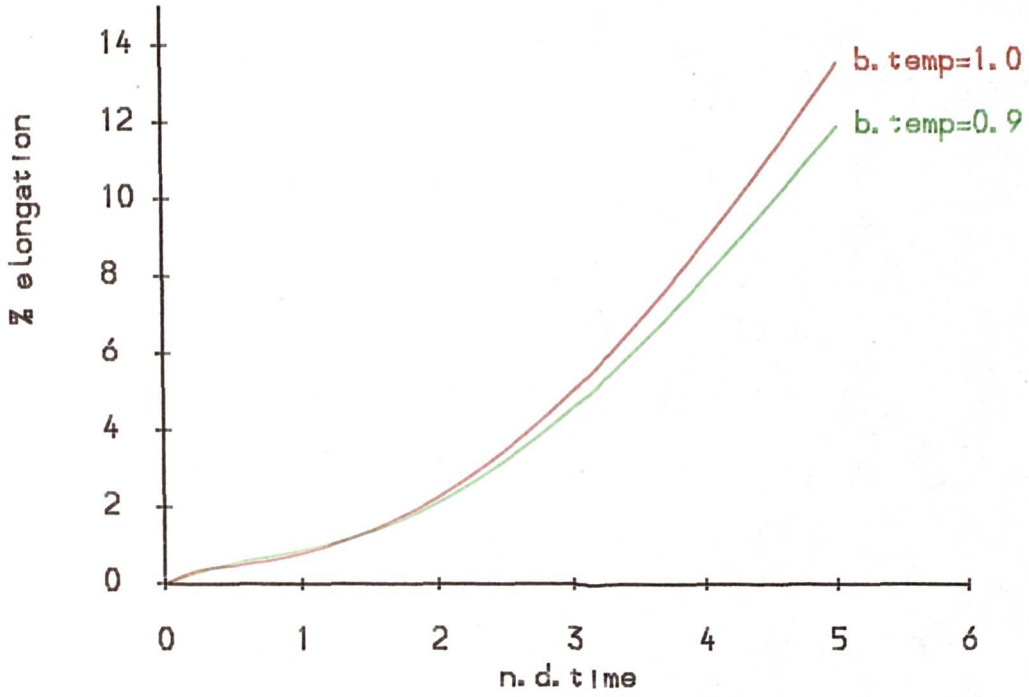

Figure 7.7.3 Time taken for 5% Lengthening

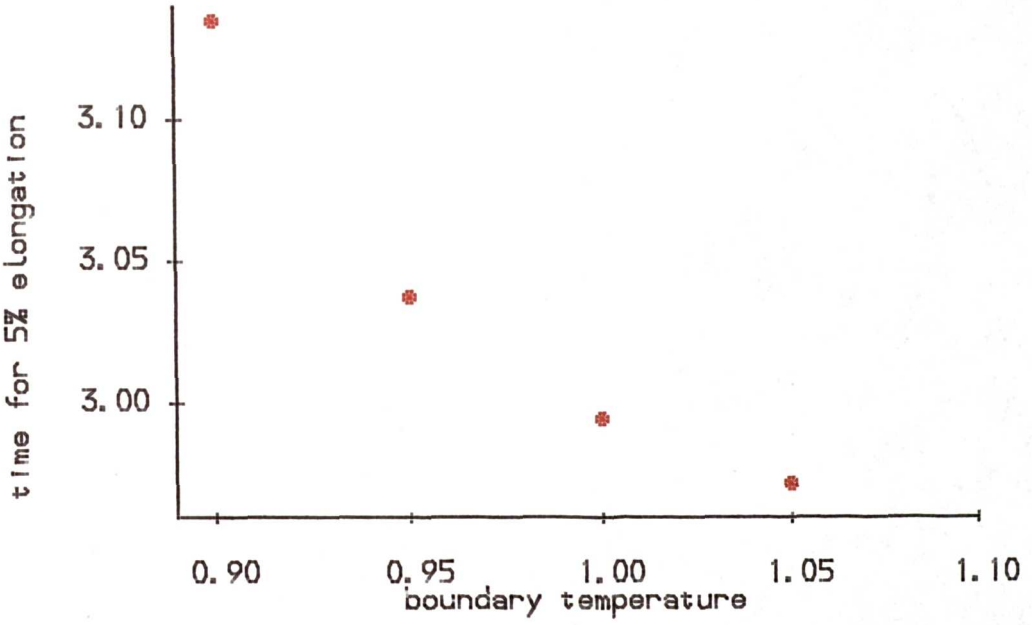

Chapter 8

Concluding Remarks

In this final chapter an overview of the project is given along with suggestions for further work.

8.1 Overview

The aim of this project was to produce a mathematical model that would predict the heat transfer and flow of molten glass during a pressing operation.

A summary of the glass production methods are given in Chapter 1, and the advantages of using a computer based mathematical model over more interventionist methods are discussed.

In order to be able to use mathematical techniques, the situation has to be described in a mathematical manner. The partial differential equations governing the flow of fluid and heat were introduced, simplified and non-dimensionalized in Chapter 2. The final forms of the equations, summarized in section (2.5), are those describing an axi-symmetric, incompressible, Newtonian, creeping flow partially surrounded by a free surface.

Before a solely numerical solution was implemented, the analytical and approximate solutions to the governing equations were surveyed, in section (3.1), but these were unable to describe satisfactorily the flow in anything other than the simplest situations. Hence the finite element method, a numerical technique that gives approximate solutions to systems governed by differential equations, was used. The finite element method is a well established technique, an outline of its basic principles together with more specific details to its application to this particular problem are given in section (3.3). The f.e.m works by overlaying the fluid with a grid, dividing it up into elements over which approximations can be made, allowing approximate solutions to the whole flow to be constructed. In this problem the grid was allowed to move with the flow, so that the free surface could be accurately tracked.

Chapter 4 shows results generated by using the finite element method to

model an isothermal flow field. It shows that it is feasible to predict the flow of glass in a simple pressing operation. There is no difficulty incorporating different mould and plunger shapes. However moving the grid to track the free surface does mean that the elements shear and distort. This can be successfully combatted by introducing an automatic remeshing scheme that periodically redraws the grid. There are various schemes available which do this process, the simple one chosen, based on Caswell's fourth order operator is outlined in appendix A. The other problem is that the calculation times can become prohibitively large, for anything but the most powerful machines. Large calculation times arise from two sources-

- Large numbers of elements. It is far more economic to use a smaller number of elements and remesh more often than to have a larger number of elements. If, as in the centre of a pressed disc, there is an approximate analytical solution available it can be 'patched together' with a finite element flow model. The example given in section (4.4) shows a large saving of CPU time ($\approx$ 90%), with only a small loss in accuracy (at worst 13%). Hence for large grids it is always worth investigating whether an approximate analytic solution exists for any areas of the flow.

- Numerical Instabilities. These limit the size of δt, the time step length used to advance the position of the grid. Its size is approximately governed by the formula

$$\delta t < c \times Re$$

where c depends on the grid and Re is the Reynolds Number which is greatly influenced by the viscosity of the liquid, hence the time for the calculations is strongly dependent on the physical properties of the liquid in question.

Any variations in the temperature within the molten glass affect the flow field and the numerical stability of the finite element model for the flow field because the viscosity is strongly temperature dependent. These were introduced in Chapter 5. Due to the physical properties of molten glass the temperature field consisted of a thin cooled area near the glass surface. It was computationally unsatisfactory to model these temperature variations accurately using the finite element method, because to model this type of temperature field realistically the element sizes would need to be very small and thus very time consuming. The approach used was to try to capitalize on the known form of the temperature field and to introduce an augmented boundary condition, recalled here, which incorporated extra

terms encapsulating the effects of the cooled layer near the interfaces.

The Augmented Boundary Condition, derived in chapter 5, is

$$\tau_n = F + \left(\frac{Re_1 - Re_2}{Re_1 Re_2}\right) H(u, w, r, z)$$

where τ_n is the normal component of the stress at the surface, F depends on the surface tension and surface configuration, $H(u, w, r, z)$ depends on the local velocity gradients, and $Re_1 - Re_2$ is the change in Reynolds number near the surface. The 'alternative' boundary condition with the approximation for the surface temperature introduced in Chapter 5 are easily combined with the finite element model for the flow field. The combined model was shown to generate qualitatively correct results in Chapter 6. A difference in viscosity along the free surface leads to differing rates of movement, so altering the shape of that surface. Complete cooling of a free surface, though not having a dramatic effect on the final shape, alters the internal pressure in the glass, potentially influencing the movement of a gravity driven plunger. The augmented boundary condition is equally applicable to decreases in surface viscosity as well as increases, i.e. heating as well as cooling, opening possibilities of studying other processes, such as fire polishing.

The actual physical properties of a typical soda-lime glass were surveyed in Chapter 7. Unfortunately the size of the Reynolds number means that a

very small step size has to be used, hence a large amount of computer time is needed. This would be less of a problem with a more powerful computer. However, the results in Chapter 6 suggest that the differences in viscosity rather then its actual value are the most important factors influencing the flow patterns. Therefore, if the computing time was unavailable some sort of estimations of the likely behaviour could still be undertaken.

This project although hampered by the lack of computing power available, has demonstrated that it is feasible to simulate both the heat transfer and fluid flow occurring in a glass pressing operation by numerical techniques. The model was developed specifically with the pressing operation in mind but could be used to model other axi-symmetric operations, such as stretching or elongation under gravity.

8.2 Further Work

To develop the present model into a fully realistic model further work in several areas would be beneficial.

- Linking the fluid and heat flow model to outside conditions. For example, no account is taken of the temperature variations in the mould or plunger. A finite element model, such as the one proposed by Bonocina

et al.[7], of the temperature flow in the mould could be coupled with the flow model.

- Extension from axi-symmetric to fully three dimensional. This would involve a large expansion in the number of variables, increasing the computer time as well as the storage space needed; enough to tax the fastest of machines. Remeshing and visualization of the results would also be more complicated.

- Even with the advent of more powerful computers any techniques for reducing the numbers of calculations would be welcome. Investigations into the effects of using implicit or semi-implicit methods to combat the numerical instabilities would be worth while.

As well as improving the mathematical model, it would be useful if a parallel path of experimental work was followed, to provide an accurate indication as to the values and variations of the physical parameters involved. For example, there is little data on the values of the heat transfer coefficient between the glass and the mould. The work that has been done[1] only serves to illustrate that its complex dependence on contact time, pressure and temperature. Such variations, provided they can be accurately described,

[1] e.g. by Fellows and Shaw[19]

can easily be handled in a numerical model.

Appendix A

Remeshing

A.1 Introduction

Many remeshing schemes have been developed often tailored to various situations, the most common are those which generate two dimensional triangular grids, see for example the paper by Jin[31]. In this work quadrilateral elements have been used, again there are a variety of schemes to choose from, for example the automatic scheme proposed by Talbert[41], the relatively simple scheme opted for is described in a paper by Wang[43] hence only a brief outline is given.

1. Grid distortion triggers automatic remeshing

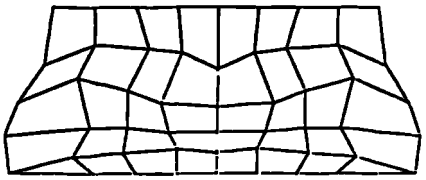

2. New boundary nodes are placed

either

equidistant or weighted

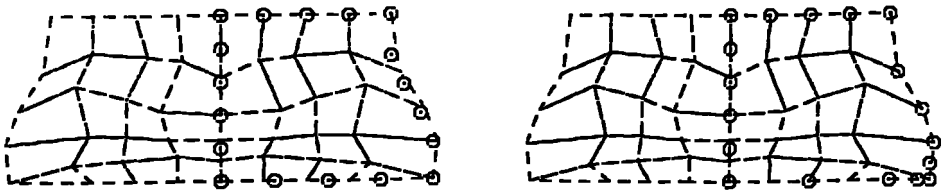

3. New internal nodes positioned to give a new grid

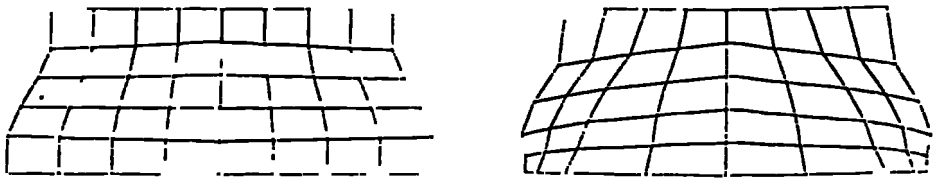

4. Interpolation to find velocities at the new node points

Figure A.1: Remeshing

A.2 Scheme

Remeshing is introduced to combat the grid distortion caused by the node movement and to stop the 'loss' of the free surface nodes[1]. The scheme chosen, shown schematically in figure (A.1), is relatively simple, when triggered by, for example, a node touching a boundary, it fits an $n \times m$ grid[2] over the area of the fluid. The new exterior mesh points are placed around the boundary. Normally, these nodes are placed equidistant along each boundary, but they can be weighted to increase the concentration in a certain area. The x and y co-ordinate[3] of the (i,j) th node[4] is calculated from the positions of the eight surrounding nodes using

$$f_{i+1,j+1} + f_{i-1,j+1} + f_{i-1,j-1} + f_{i+1,j-1}$$
$$-2(f_{i,j-1} + f_{i-1,j} + f_{i,j+1} + f_{i+1,j}) + 4f_{i,j} = 0 \qquad \text{(A.1)}$$

where f is the position of the x or y co-ordinate of this node. This equation, based on Caswell's fourth order operator approach, is the central difference solution of

$$\frac{\partial^4 f}{\partial i^2 \partial j^2} = 0 \qquad \text{(A.2)}$$

[1] see section (4.4)
[2] $n \times m$ nodes, $(n-1) \times (m-1)$ elements
[3] or the r and z co-ordinates if an axi-symmetric grid is being generated
[4] i nodes from the left, j nodes from the bottom of the grid

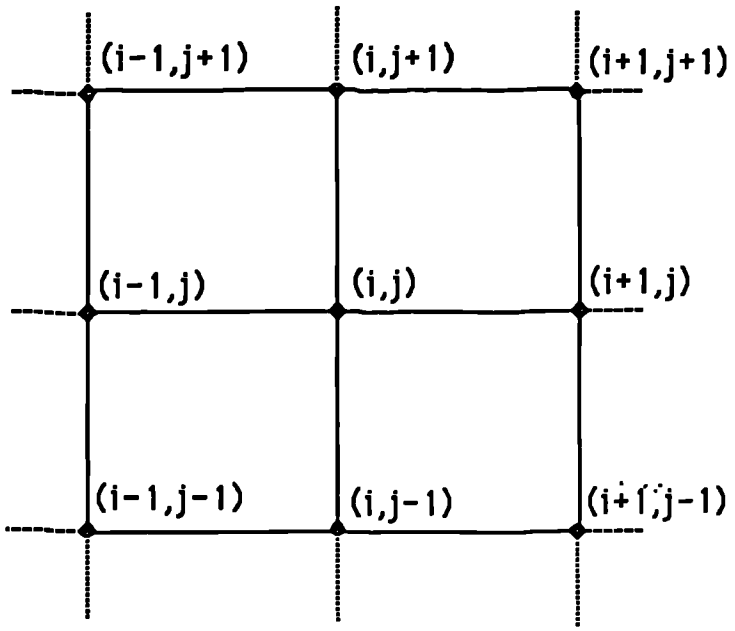

Figure A.2: Local Node Numbering

The positions of the surrounding nodes will not all be known, some will also be interior nodes. Hence, the remeshing scheme solves the $(n-2)(m-2)$ simultaneous linear equations for the $(n-2)(m-2)$ unknowns.

To continue the computation the values of the velocity at the new node points need to be calculated. This is done by finding which old element each of the new node points lies in, then interpolating to find the velocity at this point. To check if a point lies in an element the number of intersections of a line drawn horizontally from that point with the sides of the element is counted; an odd number means the point is contained within the element;

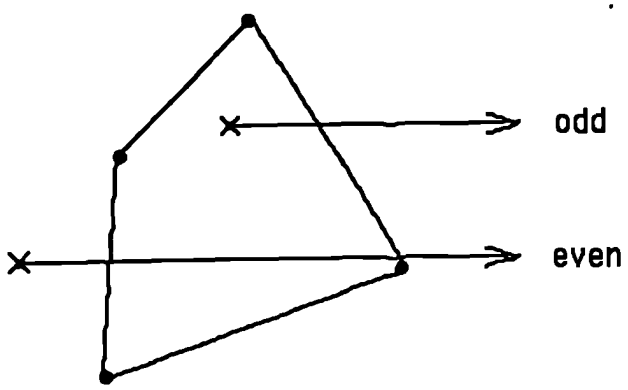

Figure A.3: Searching Scheme

an even number means that it is outside.

Appendix B

Instabilities

These arise due to the use of an explicit method. The nature of the instabilities can best be illustrated by considering a simple one dimensional problem which has an analytical solution. Consider the system given by

$$\frac{\partial x}{\partial t} = -k\, x$$

$$\text{with } x = A \text{ at } t = 0$$

$$\text{and } k > 0 \qquad \text{(B.1)}$$

this has analytical solution

$$x = Ae^{-kt} \qquad \text{(B.2)}$$

if this were solved using the numerical scheme

$$x_{n+1} = x_n + \delta t(\lambda \left(\frac{\partial x}{\partial t}\right)_n + (1-\lambda)\left(\frac{\partial x}{\partial t}\right)_{n+1}) \tag{B.3}$$

with δt as the time step and λ is a constant between[1] 0 and 1, $\lambda = 0$ corresponds to an implicit scheme and $\lambda = 1$ corresponds to an explicit scheme. This gives a numerical approximation to the analytic solution of

$$x_n = A\left(\frac{1-k\delta t\lambda}{1+k\delta t(1-\lambda)}\right)^n \tag{B.4}$$

where x_n is the x value at $t = n\delta t$. For this to tend to zero smoothly as n gets large and to agree with the limit of the analytical solution then it is reqired that

$$0 < \frac{1-k\delta t\lambda}{1+k\delta t(1-\lambda)} < 1 \tag{B.5}$$

This limits the size of the step length. For an explicit scheme, $\lambda = 1$, the limit is

$$\delta t < \frac{1}{k} \tag{B.6}$$

Hence if k is large then δt has to be small otherwise the scheme does not converge. A larger region of convergence can be obtained by the introduction

[1] it can be outside these limits if under or over relaxation is used

of an implicit or partially explicit scheme, i.e. one in which $\lambda \neq 1$. Now the region of convergence can be increased to

$$\delta t < \frac{1}{k\lambda} \tag{B.7}$$

The situation considered in this appendix is far simpler than that in the project but is analogous[2], so it is reasonable to assume that a partially or fully implicit scheme would allow a larger step size to be used in the f.e. glass pressing model.

[2]compare equation (B.6) with the stability condition given in section (4.2)

Bibliography

[1] Badger A.E., Parmelee C.W. and Williams A.E.,'Surface Tension of various Molten Glasses',*J. Amer. Ceramic Soc.*, **20** pp 325-329 (1937)

[2] Bartell and Bjorjlund,'Hystersis of Contact Angles. A Study of Interfacial Contact Angles in the Mercury-Benzene-Water System',*J. Physical Chem.*, **56** pp 453-457 (1952)

[3] Batchelor G.K.,*An Introduction to Fluid Dynamics*, Cambridge University Press, (1967)

[4] Beek W.J. and Muttzall K.M.K.,*Transport Phenomena*, Wiley, (1975)

[5] Bird R.B., Stewart W.E. and Lightfoot E.N.,*Transport Phenomena*, Wiley, (1960)

[6] Bockris J.O'M., White J.L. and Mackenizie J.D.,*Physico-Chemical Measurements at High Temperatures*, Butterworths Scientific Publications, (1959)

[7] Bonacina C., Strada M. and Gottardi V.,'Finite Element Analysis of the Temperature Fields in Glass Moulds',*Glass Tech.*, **23** No 4 pp 172-176 (1982)

[8] Cameron A.,*Basic Lubrication Theory*, Longman, (1971)

[9] Carling J.C.,'Two and Three Dimensional Mathematical Models of Flow and Heat Transfer in Forehearths'*Glasstech. Ber.*, **49** pp 269-277 (1976)

[10] Carslaw H.S. and Jaeger J.C.,*Conduction of Heat in Solids*, Clarendon Press, (1959)

[11] Cassidy D.C. and Gjostein N.A.,'Capillarity-Induced Smoothing of Glass Surfaces by Viscous Flow',*J. of Am. Cerm. Soc.* **53** pp 161-168 (1970)

[12] Chung T.J.,*Finite Element Analysis in Fluid Dynamics*, McGraw-Hill, (1978)

[13] Clough R.W.,'The Finite Element Method in Plane Stress Analysis',*Proc. 2nd A.S.C.E. Conf. on Electronic Computation,* Pittsburgh (1960)

[14] Doremus R.H.,*Glass Science*, Wiley, (1973)

[15] Douglas R.W.,Frank S.,*A History of Glassmaking*, Foulis, (1972)

[16] Dussan E.B,'on the Spreading of Liquids on Solid Surfaces: Static and Dynamic Contact Lines', *Ann. Rev. Fluid Mech.*, 11 pp 371-400 (1979)

[17] Dussan E.B. and Ngan C.G,'On the Dynamics of Liquid Spreading on Solid Surfaces', *J. Fluid Mech.*, **209** pp 191-266 (1989)

[18] Elliot G.E.P. and Riddiford A.C.,'Dynamic Contact Angles',*J. Colliod Science and Interface Science,* **23** pp 389-398 (1967)

[19] Fellows C.J. and Shaw F.,'A Laboratory Investigation of Glass to Mould Heat Transfer during Pressing',*Glass Techn.*,**19** pp 4-9 (1978)

[20] Fulcher G.S.,'Analysis of Recent Measurements of Viscosity of Glasses',*J. Am. Ceramic Soc.*,**8** pp 339-355, (1925)

[21] Gardon R.,'The Emissivity of Transparent Materials', *J. Am. Ceramic Soc.*, **39** pp 278-287 (1956)

[22] Gardon R.,'Calculation of Temperature Distributions in Glass Plates Undergoing Heat-Treatment',*J. Am. Ceramic Soc.*,41 pp 200-209 (1958)

[23] Genzel L.,'On the Calculation of the Radiation Conductivity of Glasses',*Glasstech. Ber.*, 26 pp 69-71 (1953)

[24] Graham S.J.,'Mathematical Modelling of Glass Flow in Container Manufacture', *Ph.D Thesis University of Sheffield* (1987)

[25] Gresho P. M. and Lee R. L.,'Don't Suppress the Wiggles- They're Telling You Something',*Computers and Fluids*, 9 pp223-253 (1981)

[26] Golafshani M.,'A Simple Technique for Transient Creep Flows with Free Surfaces',*Int. Jor. for Num. Meth. in Fluids*, 8 pp 897-912 (1988)

[27] Hirt C.W. and Shannon J.P.,'Free-Surface Stress Conditons for Incompressible Flow Calculations',*J. Comp. Phys.*, 2 pp 403-411 (1968)

[28] Hirt C.W., Cook J.L. and Bulter T.D.,'A Langrangian Method for Calculating the Dynamics of an Incompressible Fluid with a Free Surface',*J. Comp. Phys.*,5 pp 103-124 (1970)

[29] Huh C. and Scriven L.E.,'Hydrodynamic Model of Steady Movement of a Solid/Liquid/Fluid Contact Line', *J. Colloid and Interface Science*, **35** pp 85-101 (1971)

[30] Ikegawa M. and Washizu K.,'Finite Element Method Applied to Analysis of Flow over a Spillway Crest', *Int. J. Numer. Meths. in Eng.*, **6** no 4 pp 179-189 (1973)

[31] Jin H. and Wieberg N.-E.,'Two-Dimensional Mesh Generation, Adaptive Remeshing and Refinement.',*Int. J. Numer. Meths. in Eng.*,**29** pp 1501-1526 (1990)

[32] Maloney F.J.T.,*Glass in the Modern World*, Aldus Books, (1967)

[33] McGraw D.A.,'Transfer of Heat in Glass During Forming',*J. Am. Ceramic Soc.*,**44** pp 353-363 (1964)

[34] Meissner U.,'A Mixed Finite Element Model for use in Potential Flow Problems', *Int. J. Numer. Meth. in Eng.*, **6** no 4 pp 467-474 (1973)

[35] Morey G.W. and Merlin H.E.,'The Relation Between the Composition and the Density and Optical Properties of Glass. I. The soda-lime-silica Glasses.'*J. Optical Soc. Amer.*, **22** pp 632-662 (1932)

[36] Physical Properties Commitee,*J. Soc. Glass Techn.*, **40** pp 83-104 (1956)

[37] Rawson H.,'Physics of Glass Manufacturing Processes', *Phys. and Techn.*, **2** pp 91-114 (1974)

[38] Rawson H.,'Mathematical and Physical Models of Glass Making Processes',*XIth Int. Congr. Glass*, **2** pp3-25 (1977)

[39] Reddy J.N.,*An Introduction to the Finite Element Method*, McGraw-Hill, (1984)

[40] Rekhson S. M., Wang Y. and Wang H. P.,'Computer Modelling of Glass Flow in Ribbon Process',*Proc. 50th Glass Problems Conference.*, University of Illinois, (1989)

[41] Talbert J. A. and Parkinson A. R.,'Development of an Automatic, Two-dimesional Finite Element Mesh Generator using Quadrilateral Elements and Bezier Curve Boundary Definition',*In. J. for Numer. Meths. in Eng.*, **29** pp 1551-1567 (1990)

[42] Tayler A.B., *Mathematical Models in Applied Mechanics*, Clarendon, (1986)

[43] Wang H. P. and McLay R. T.,'Automatic Remeshing Scheme for Modeling Hot Forming Processes.',*Advances in Grid Generation -FED (ASME)*,**5** pp 151-158

[44] Whiteman J.R.,'The Mathematical Modelling of Forehearths',*Glass* **57** pp 19-20 (1980)

[45] Wilkinson J.H. and Reinsch C.,*Handbook for Automatic Computation. Volume II, Linear Algebra*, Springer-Verlag, pp 93-110 (1971)

[46] Woo T.C.,'Wave Decay on Glass Surface at High Temperatures',*J. Appl. Physics*, **40** pp 3140-3143 (1969)

[47] Zienkiewicz O.C.,*The Finite Element Method*, McGraw-Hill, (1977)